FABRICATION AND CHARACTERIZATION OF NOVEL TRANSPARENT LAMINATED GLASS-COMPOSITE PANELS FOR DYNAMIC LOAD MITIGATION

A Dissertation

Presented to

the Faculty of the Graduate School

University of Missouri

In Partial Fulfillment

of the Requirements for the Degree

Doctor of Philosophy

---

by

HUA ZHU

Dr. Sanjeev K. Khanna, Dissertation Supervisor

MAY 2014

The undersigned, appointed by the dean of the Graduate School, have examined the dissertation entitled

FABRICATION AND CHARACTERIZATION OF NOVEL TRANSPARENT LAMINATED GLASS-COMPOSITE PANELS FOR DYNAMIC LOAD MITIGATION

presented by Hua Zhu,

a candidate for the degree of Doctor of Philosophy,

and hereby certify that, in their opinion, it is worthy of acceptance.

Professor Sanjeev K. Khanna

Professor Robert A. Winholtz

Professor Qingsong Yu

Professor Raghuraman Kannan

Dedication

This dissertation is dedicated to my beloved mother

Shan Wang (1953-2008)

You are profoundly appreciated for your

support of my academic pursuits.

ACKNOWLEDGEMENTS

I would like to take this opportunity to express my sincere gratitude to my advisor Dr. Sanjeev K. Khanna for his continuous guidance and support during my Ph. D. study.

Besides my advisor, I also would like to express my sincere gratitude to the rest of my advisory committee members: Dr. Robert A. Winholtz, Dr. Qingsong Yu and Dr. Raghuraman Kannan, for their insightful comments and suggestions.

I would like to give my special thanks to my father, Chunqing Zhu, and my wife, Tianyi Qiu for their consistent love, understanding, and support during my study.

I am grateful to my colleagues, Ajit Tambvekar and Ha T. T. Phan for their help in the experiments.

I am also grateful to the technical staff of Engineering Technical Services (ETS): O.S. "Rex" Gish, Brian Samuels and Rich Oberto, for their assistance in sample machining and equipment repairing.

Financial support from U.S. Department of Homeland Security is gratefully acknowledged.

TABLE OF CONTENTS

LIST OF FIGURES

Figure Page

LIST OF TABLES

ABSTRACT

Bomb threats and attacks are common in many parts of the world today. One of the significant effects of a blast is damage to the glass windows in nearby buildings. The debris produced from the damaged windows, especially the sharp glass fragments produced, can lead to severe injuries and even casualties. One way to mitigate the damage is to use blast-resistant laminated glass, which is conventionally made of one or more polyvinyl butyral (PVB) interlayer sandwiched between two or more glass sheets, for windows. Although the PVB interlayer is widely used in the world, it still has some disadvantages, such as low strength to weight ratio which results in large thickness and increased weight of the laminated glass. The low strength to weight ratio problem can be solved by replacing the PVB interlayer with a transparent glass fiber-reinforced polymer composite interlayer, because glass fiber-reinforced composites have high strength to weight ratio and potentially higher fracture toughness. By using the glass fiber-reinforced composite interlayer, the thickness and weight of the laminated glass can be potentially reduced.

A laminated glass panel utilizing a newly developed transparent glass fiber-reinforced composite interlayer has been fabricated in this study. The transparent composite interlayer was obtained by matching the refractive index of the polyester resin matrix with that of E-glass fibers. The light transmittance of the fabricated laminated glass is above 60% over the light wavelength range of 482 nm to 700 nm with the highest transmittance is 84.4% when the light wavelength is 577 nm. The composite interlayer's mechanical properties under both quasi-static and dynamic loading conditions have been

characterized. In addition, the fabricated glass panels were tested under various blast loading conditions. The panels perform well under U.S. General Services Administration (GSA) specified C, D and E blast loading levels.

In this research, the dynamic response, in terms of the midpoint deflection, of the fabricated laminated glass under blast loading has been analytically investigated using model-based method and finite element method. Failure analysis of the laminated glass was performed using the stress analysis approach.

CHAPTER 1 INTRODUCTION

1.1 Problem statement

Bomb threats and attacks are now common in many parts of the world. One of the significant effects of a blast is damage to the glass windows in nearby buildings. The sharp glass fragments produced from the damaged windows can lead to large casualties. And blast pressure entering buildings through the damaged windows can cause additional injuries to the occupants. So the need of mitigating the hazards caused by windows failure is essential.

One way to mitigate the damage is to use blast-resistant laminated glass, which is conventionally made of one or more polyvinyl butyral (PVB) interlayer sandwiched between two or more glass sheets, for windows. PVB is chosen as the interlayer material mainly due to its optical transparency. Although laminated glass with PVB interlayer is widely used in the world, it still has some disadvantages, such as large thickness requirement for blast resistance, which increases the production cost and installation cost. The thickness and weight can be potentially reduced by replacing the PVB interlayer with a glass fiber-reinforced polymer composite interlayer, because glass fiber-reinforced polymer composites have high strength to weight ratio.

Typically glass fiber-reinforced polymer composites are opaque. The low transparency (light transmittance) is due to the refractive index mismatch between glass fibers and the polymer matrix. The transparency increases with the decrease of the refractive index difference. However, only a basic understanding of the relationship

between the transparency and the refractive index difference is available. A quantitative understanding of the relationship is needed.

A study of the dynamic response of a blast-resistant laminated glass under blast loading is important for understanding the effect of blast loading on the laminated glass. Although the dynamic response of the laminated glass with PVB interlayer under blast loading has been widely studied, the dynamic response of the laminated glass with glass fiber-reinforced polymer composite interlayer under blast loading has not been studied yet. So, such a study is needed.

This research focuses on fabricating a laminated glass panel utilizing a transparent glass fiber-reinforced polymer composite interlayer. The transparency of the composite interlayer is achieved by matching the refractive index of the polymer matrix with that of glass fibers. The relationship between the transparency and the refractive index difference is quantitatively studied. The dynamic response of the fabricated laminated glass under blast loading is also investigated.

1.2 Literature review-blast and its hazards

1.2.1 Blast and blast effect on structures

A blast is a sudden release of stored energy. When a blast happens, rapid expansion of energy resulting from the blast gives rise to a wave of compressed air which is called shock front. The shock front travels radially in air in all directions. As the shock front moves, the shock front releases energy to surrounding air and the overpressure of the shock front decreases. When the pressure of the shock front drops below the atmospheric

pressure, surrounding air gives energy to the shock front and the pressure of the shock front finally returns to the atmospheric pressure [1]. The whole process is shown in Fig. 1.1 [2].

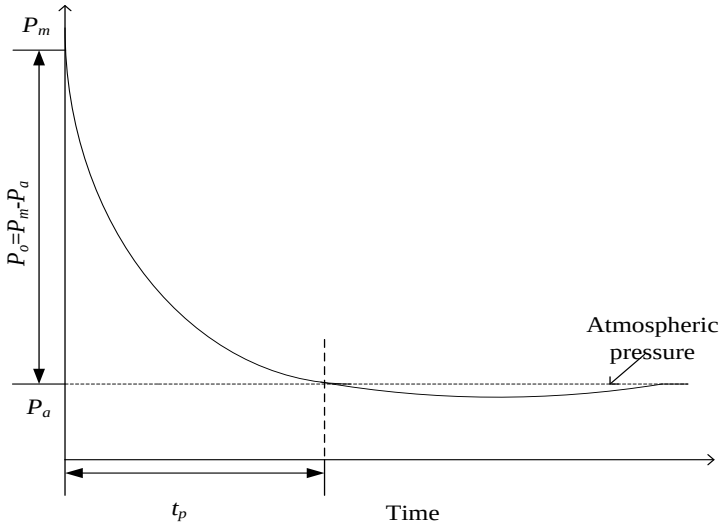

Figure 1.1 Shock front expanding process

The pressure-time curve shown in Fig. 1.1 can be described using the following equation [3]

$$P(t)=P_o\left(1-t/t_p\right)e^{-\alpha t/t_p} \tag{1.1}$$

where $P(t)$ is the blast pressure at time t, P_o is the peak pressure, α is a constant and t_p is the positive pressure duration time. According to references [3, 4], the key parameters of a blast are: peak pressure P_o, constant α and positive pressure duration time t_p.

Blast effect on structures can be divided into three types. In the first type, the shock front is stopped by a relatively small structure. In this case, blast wave simultaneously

acts on the entire structure and the structure is massive enough to resist translation. In the second type, the shock front is stopped by a structure which is much smaller than the structure in the first case. In this case, blast wave also simultaneously acts on the entire structure but the structure is small enough to be moved by the blast wave. In the final type, the shock front is stopped by a big structure. The shock front is too small to act on the whole structure simultaneously. Instead of simultaneously loading, the structure is affected in succession [5].

1.2.2 Blast hazards

Every year, numerous blast events take place in the United States. These blasts are usually small blast events (explosive weights are equal or less than 10 lb (4.53 kg) TNT (2, 4, 6-trinitrotoluene)) [6]. The damage caused by such blasts is small. However, large blasts occur infrequently, such as bombing in Oklahoma City, Oklahoma [7], the first bomb attack on the World Trade Center, New York City, New York [8], bombing in Manchester City, England [9] and attack on Embassy of Australia in Jakarta, Indonesia [10]. For those blasts, 1000 lb (453 kg) or more explosives were used. Under such blast loadings, experience shows that the most damage occurs to the windows of surrounding buildings [11]. Windows, which are made of ordinary glass, usually break into pieces in such situations (Fig. 1.2). The broken pieces can travel at a speed up to 200 ft/sec (61 m/s) [12], which can cause great injuries and even deaths [7, 13]. In the Oklahoma City bombing, 508 persons suffered injuries outside the Alfred P. Murrah building (the attacked building) [6]. Of these, 200 injuries were directly related to the broken glass

fragments. In addition to glass fragments, blast pressure passing through the broken windows may cause additional injuries because it only needs 15 psi (~100 kPa) pressure to rupture eardrums and cause lung damage and pressure created by an explosion can be very high (higher than 15 psi) [14]. Hence, the need of mitigating the hazards caused by windows failure is essential. One way to mitigate the damage is to use laminated glass for windows. Using laminated glass can significantly reduce the possibility of generating fragments during a blast loading (Fig. 1.3).

Figure 1.2 Glass fragments produced in Oklahoma City bombing (Reprinted with permission from "Survey of window glass broken by Oklahoma City bomb on April 19, 1995, revised", copyright belongs to Glass Research and Testing Laboratory, Texas Tech University).

Figure 1.3 Laminated glass window and door fractured but remaining in frame in Oklahoma City bombing (Reprinted with permission from "Survey of window glass broken by Oklahoma City bomb on April 19, 1995, revised", copyright belong to Glass Research and Testing Laboratory, Texas Tech University).

1.3 Literature review-laminated glass

Laminated glass, which is normally used in the places where human injury may happen [2, 15, 16] or where glass may fall if shattered [17], was invented in 1910 by a French chemist Edouard Benedictus [18], who first patented the use of gelatin as the interlayer between glass sheets. Gelatin interlayer binds two normal glass sheets together and this glass "sandwich" looks like normal glass and behaves as a single unit.

The glass sheets used to make laminated glass are usually tempered glass sheets. Tempered glass is produced by first heating annealed glass (the most common glazing material used in residential windows) and then rapidly cooling the glass. This treatment gives additional strength to the glass. So, tempered glass is stronger than annealed glass

of the same dimension. The typical tensile strength of tempered glass (more than 175 MPa) is much higher than that of annealed glass (around 40 MPa) [15, 19]. Another advantage of tempered glass is that tempered glass tends to break into relatively small and blunt edges fragments under external loading. This reduces the possibility of injury to people. Therefore, instead of annealed glass, tempered glass is chosen to make the laminated glass in this study.

With the development of technique, instead of gelatin, the interlayer of modern laminated glass is made of polyvinyl butyral (PVB). Polyvinyl butyral (PVB) is a resin used for applications that require optical transparency, strong binding, high toughness and high flexibility [20]. PVB is prepared by reacting polyvinyl alcohol with butyraldehyde. The synthesis process of PVB is shown in Fig. 1.4.

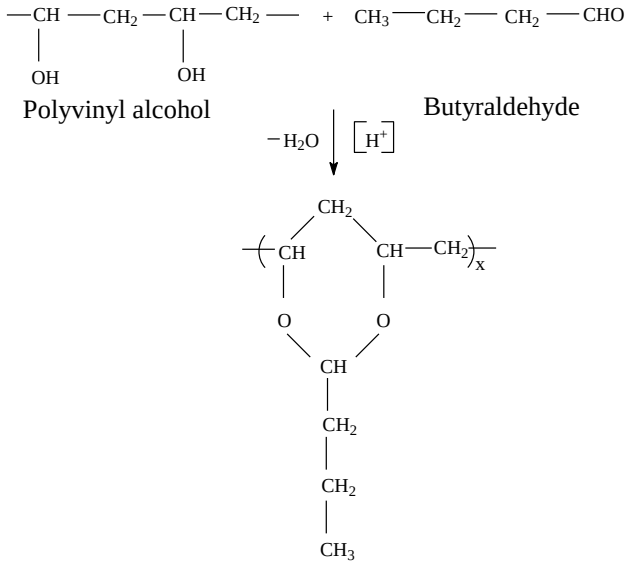

Figure 1.4 Synthesis process of polyvinyl butyral (PVB)

PVB has many applications, such as solar modules [21] and ceramic binders [22]. The major application of PVB is for fabricating the interlayer of laminated glass. The reason for using PVB as the interlayer is: firstly, PVB is colorless; secondly, PVB interlayer can bind the resulting glass fragments when the outer layer glass sheets are broken; Last but not least, PVB has good energy absorption ability which is due to its plastic deformation after impacting.

Currently, PVB is a mature product and is provided by a number of companies, including Chung Petrochemicals ("WINLITE" brand PVB, Taiwan), Sekisui ("S-Lec" brand PVB, Japan), DuPont ("Butacite" brand PVB, United States), Eastman ("Saflex" brand PVB, United States) and Kuraray Europe GmbH ("Trosifol" brand PVB and "Mowital/Pioloform" brand PVB, Germany) [20].

Besides PVB, there are other types of interlayer materials in use, including transparent thermoplastic polyurethane (TPU) [23] and transparent polycarbonate (PC) [24].

Transparent TPU is a kind of polyurethane which has high optical clarity and excellent adhesion property to glass. TPU also offers excellent resistance to hydrocarbon oil, chemicals and moisture [25]. The combination of these features enables the laminated glass designers to use it as the interlayer of laminated glass. The shortcoming of TPU is its low mechanical properties. For example, the Young's modulus of TPU is around 60 MPa (at room temperature (~20 ℃)) [26], which is much lower than that of PVB (~100 MPa at room temperature (~20 ℃)) [27]. Because of its low mechanical properties, the

impact resistance of the laminated glass with TPU interlayer is lower than that of the laminated glass with PVB interlayer.

PC is a thermoplastic polymer. Compared with other transparent polymers, the advantage of PC is that it is very tough [24, 28]. If a blast happens near a laminated glass with PC interlayer and the outer layer glass sheets of the laminated glass shatter, the PC interlayer may be able to prevent the penetration of debris by bulging plastically [29]. The main problem for PC, which is not a big problem for PVB, is that it embrittles with age. The embrittlement is due to 1) physical aging (thermodynamic equilibrium) [30], 2) chemical changes due to exposure to ultraviolet (UV) light, ozone, nitrogen oxides, moisture, etc. [31-35], 3) physical damage, e.g. surface microcracks introduced by solar radiation [36].

Compared with TPU (low mechanical properties) and PC (aging problem), it can be noted that PVB is a better interlayer material for laminated glass. But PVB is not the perfect interlayer material, it has some drawbacks, such as relatively low strength to weight ratio. According to literatures [37-40], glass fiber-reinforced polymer composite materials possess high strength to weight ratio. Therefore glass fiber-reinforced polymer composite is a potential replacement for PVB.

1.4 Literature review-glass fiber-reinforced polymer composite

1.4.1 Polymer composite

Polymer composite materials are engineering materials made from two or more materials. The major advantages of polymer composite materials are that they have high

strength to weight ratio, are economical, light in weight, weather resistant, chemical resistant and corrosion resistant. A polymer composite is composed of reinforcement and polymer matrix. The matrix holds the reinforcement to form a material with better properties. Based on the form of reinforcement, polymer composites can be classified as fiber-reinforced composite, particle-reinforced composite, flake-reinforced composite and filler-reinforced composite (Fig. 1.5). Compared with other composites, fiber-reinforced polymer composite, especially woven fiber-reinforced composite, doesn't have the reinforcement agglomeration problem which may lead to the decrease of strength [41-43]. So, fiber-reinforced composite is the most widely used polymer composite.

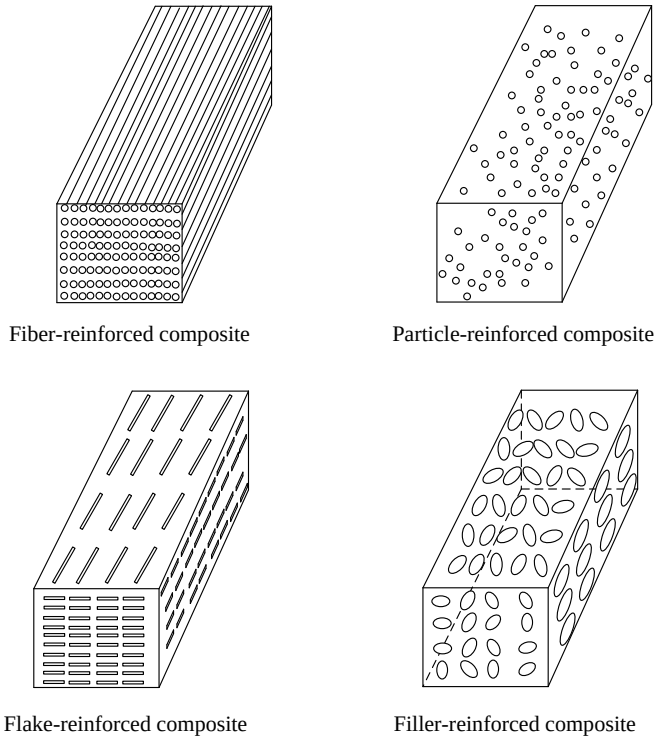

Figure 1.5 Polymer composites classification

For fiber-reinforced composite, the most commonly used fibers are glass fibers, aramid fibers and carbon fibers. The properties and cost of these fibers are listed in Table 1.1 and Table 1.2 respectively. From Table 1.1, it can be observed that all these fibers have good mechanical properties. From Table 1.2, it can be noted that the price of aramid fibers and carbon fibers is much higher than that of glass fibers. Because of the price advantage, glass fiber is the most widely used reinforcement material.

Table 1.1 Properties of fibers [44]

Material	E, GPa	σ_b, GPa	ρ, 10^3 kg/m^3	E/ρ, MJ/kg	σ_b/ρ, MJ/kg
E-glass	70	2.4	2.54	28.5	0.95
S-glass	85	4.5	2.49	34.3	1.8
Aramid	124	3.6	1.44	86	2.5
HS carbon	253	4.5	1.8	140	2.5
HM carbon	520	2.4	1.85	281	1.3

E is Young's modulus, σ_b is tensile strength, ρ is density, HS carbon is the high strength carbon and HM carbon is the high modulus carbon.

Table 1.2 Cost of fibers [15, 45]

Material	Cost, $/kg
E-glass	~2.2
S-glass	~20
Aramid	~50
HS carbon	70-200
HM carbon	150-600

1.4.2 Glass fiber-reinforced polymer composite

Glass fiber-reinforced polymer composite is a composite made of polymer matrix and glass fibers reinforcement. Incorporation of glass fibers into polymer matrix can greatly improve the mechanical properties of the polymer matrix.

Abdulmajeed et al. [46] found the mechanical properties of glass fiber-reinforced poly(triethyleneglycol dimethacrylate (TEGDMA)) could be enhanced by increasing the volume fraction of glass fibers. By increasing the volume fraction of glass fibers from 51.7% to 61.7%, there was an increase of 27% in Young's modulus, 34% in toughness, 15% in load bearing capacity and 8% in flexural strength.

Akkapeddi reported [47] that by incorporating 15 wt% of glass fibers in a polyamide nanocomposite, flexural modulus of the composite was increased by 49%, flexural strength was increased by 18%, tensile strength was increased by 30% and impact toughness was increased by 100%.

Iba et al. [48] fabricated a glass fiber-reinforced epoxy matrix polymer composite. They found Young's modulus of the composite increased with the increase of the fiber

volume fraction. Young's modulus increased linearly from about 4 GPa to 36 GPa with the fiber volume fraction increasing from 0% to 50%. They also found that the tensile strength of the composite increased linearly with the increase of the fiber volume fraction. They concluded that incorporation of glass fibers into the epoxy matrix could improve the mechanical properties of the epoxy matrix. Although adding glass fibers could improve the mechanical properties of the epoxy matrix, the authors reported that adding glass fibers decreased the transparency (light transmittance) of the epoxy matrix. They believed this is caused by the refractive index mismatch between glass fibers and the polymer matrix.

To sum up, adding glass fibers into a polymer matrix can greatly improve its mechanical properties, but the transparency of the glass fiber-reinforced polymer composite decreases due to the refractive index mismatch between glass fibers and the polymer matrix.

Iba et al. [49] reported that when glass fiber volume fraction was 10%, with the refractive index difference increased from 0.0005 to 0.0015, the light transmittance, at the light wavelength of 589 nm, of a glass fiber reinforced epoxy composite decreased from 80% to 10%.

Olson et al. [37] tested the optical transparency of a glass fiber-reinforced poly (methyl methacrylate) (PMMA) composite. They found that the light transmittance of the composite decreased with the increase of the volume percentage of glass fibers. They stated that the reason for the reduction in the transmittance is due to the presence of more reflection interfaces (introduced by the presence of glass fibers) in the composite. If the

refractive index of glass fibers approaches that of the polymer matrix, the reflection will decrease. If glass fibers' refractive index is the same as the polymer matrix's refractive index, the reflection will be eliminated. In this situation, the number of fibers cannot affect the light transmittance of the composite and the composite will behave as an optically transparent material. Authors believed that good refractive index match between glass fibers and the PMMA matrix could increase the light transmittance (transparency) of the fiber-reinforced PMMA composite.

Lin et al. [50] thought the light transmittance of a glass fiber-reinforced composite depends upon the light extinction coefficient of the composite. The coefficient is a function of several factors: (a) the ratio of the refractive indices of glass fibers and polymer matrix; (b) the fiber content; (c) the distribution in the refractive index of fibers; (d) the fiber diameter; and (e) the amount of fibers not wetted by the polymer matrix. To achieve the highest light transmittance, glass fibers' refractive index should match the matrix's refractive index. They found the refractive index of glass fibers could be changed by annealing. According to this discovery, they fabricated a transparent glass fiber-reinforced PMMA composite by matching the refractive index of glass fibers with that of the PMMA matrix through changing the annealing condition of glass fibers.

1.4.2.1 Polymer matrix

Plastic resins are commonly used as the matrix of glass fiber-reinforced polymer composites [51-54]. According to property differences, plastic resins can be divided into two groups, one is thermosetting plastic resins, and the other is thermoplastic plastic

resins. Thermosetting resin is the resin which is liquid before curing and is solid after curing. The cure can be done through heat, irradiation or chemical reactions [15]. Thermoplastic resin is the resin which is soft above a specific temperature and is hard below this temperature. Compared with thermoplastic resins, thermosetting resins, such as polyester, epoxy and vinyl ester, are more often used as the matrix materials. Because thermosetting resins are liquid at room temperature, this allows for convenient impregnation of glass fibers. Thermoplastic resins are usually solid at room temperature, so it is very difficult to impregnate glass fibers into thermoplastic resins. In order to make a thermoplastic fiber-reinforced composite, following procedures are used: 1) heat the matrix resin to its melting point; 2) impregnate fibers into the matrix; 3) cool the composite to room temperature (~20 ℃). This process is more complex and expensive than a thermosetting fiber-reinforced composite manufacturing process.

Polyester resin is the main matrix material for thermosetting fiber-reinforced polymer composite manufacture. It is a kind of polymer which contains ester functional group in the main chain. From Fig. 1.6, it can be seen that polyester resin holds 66% share of thermosetting resins used in composite industry [55]. Polyester is cheap, easy to use and compatible with glass fibers [15, 56].

Epoxy resin is another source for thermosetting fiber-reinforced polymer composite manufacture. Epoxy resin is a class of reactive polymers which contain epoxide groups. Epoxy resin contributes 23% share of thermosetting resins used in composite industry [55]. The annual output value of epoxy resin is very large. As of 2009, the output value of epoxy industry is more than 5 billion dollars in North America and about 15.8 billion

dollars worldwide [57]. The applications of epoxy resins are extensive and including adhesives, coatings and composite matrices. Epoxy has good mechanical properties, water resistance and high temperature resistance [58, 59].

Vinyl ester resin is the third often used matrix material for thermosetting fiber-reinforced polymer composite manufacture. Vinyl ester resin is manufactured by esterification of an epoxy resin with an unsaturated carboxylic acid. This resin is created like infusing epoxy molecules into polyester molecules. So, vinyl ester resin possesses both attributes of epoxy and polyester resins. Vinyl ester resin contributes around 5% share of thermosetting resins used in composites industry [55]. Vinyl ester resin has good water corrosion resistance, so it is the commonly used resin in marine industry.

From Fig. 1.7, it can be observed that among three resins, the properties of the epoxy resin are the best and the properties of the vinyl ester resin and the polyester resin are similar. From table 1.3, it can be observed that the price of polyester is the lowest. Consider cost-performance ratio, polyester is chosen as the matrix material in this research.

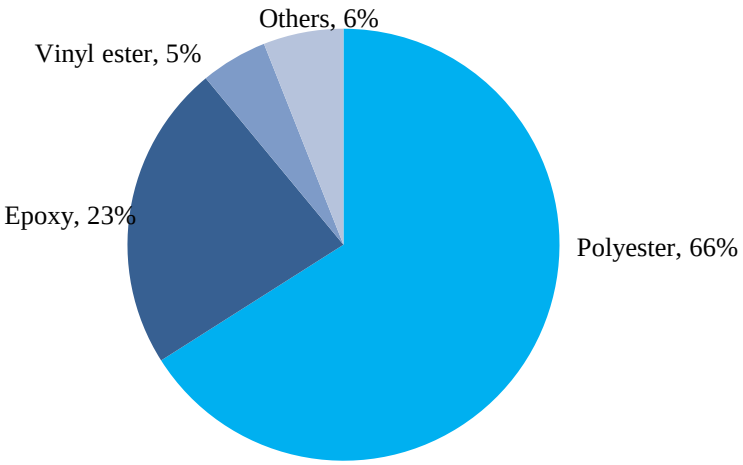

Figure 1.6 Thermosetting resins market share in composites industry (2007) [55]

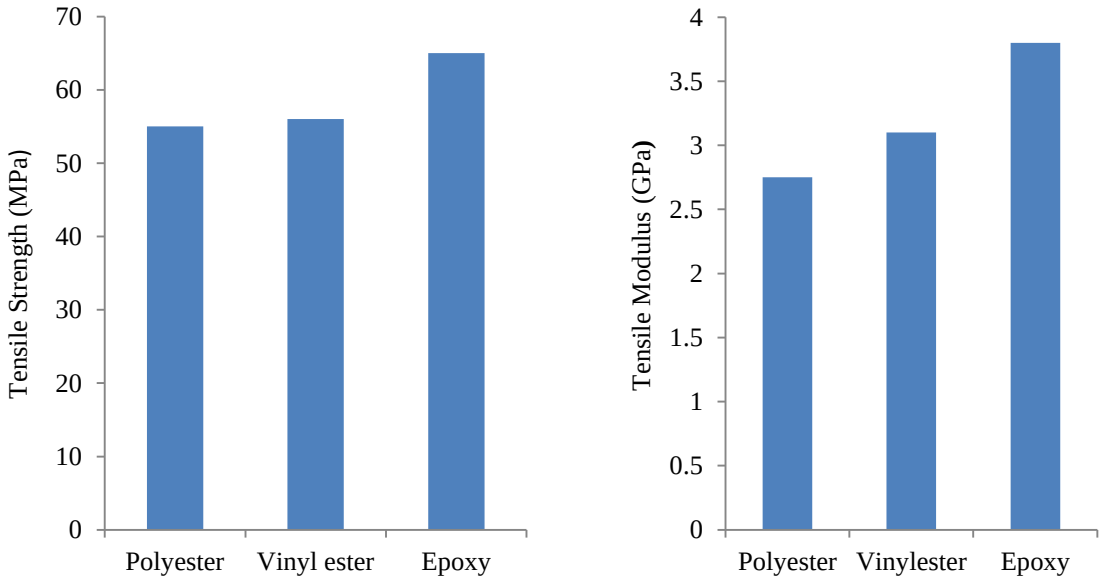

Figure 1.7 Tensile strength and modulus comparison among three resins [60]

Table 1.3 Price of resins

Resin Name	Price ($/Ton)
Polyester	~1800 (FOB)* [61]
Epoxy	~3000 (FOB) [62]
Vinyl ester	~2400 [63]

*FOB price: free on board price.

1.4.2.2 Glass fiber

S-glass fiber and E-glass fiber are the most commonly used glass fibers. E-glass fiber is a kind of glass fiber which has high strength, high stiffness, good chemical resistance and good electric insulation properties. Compared with E-glass fiber, S-glass fiber is a kind of glass fiber which has better mechanical properties (Table 1.1). But E-glass fiber is much cheaper than S-glass fiber (Table 1.2). By considering cost-performance ratio, E-glass fiber is chosen as the reinforcement in this research.

1.4.2.3 Summary

In this research, glass fiber-reinforced composite, which is intended to be used as the interlayer of a blast-resistant laminated glass panel, will be fabricated using polyester (matrix) and E-glass fibers (reinforcement). The outer layer glass sheets of the blast-resistant laminated glass panel are tempered glass sheets.

The primary use of blast-resistant laminated glass (or other laminated plates) is to protect people from injuries under blast/impact loading conditions. Therefore, the response of a laminated glass (or other laminated plates) under dynamic loading is a very

important criterion for measuring the suitability of the laminated glass (or other laminated plates).

1.5 Literature review-dynamic response of laminated plates under blast loading

Much work has been done to understand the effect of dynamic loading, such as small missile impact loading and blast loading, on laminated plates such as laminated glass and laminated polymer composite.

Ji et al. [64] studied the probability of damage at the impact site of laminated glass units under low velocity small missile impact loading. A numerical model was introduced to characterize the probability of damage. According to their report, the probability of damage at the impact site could be predicted by the developed numerical model. Calculated results were in good agreement with the experimental results.

Kaiser et al. [65] presented experimental results of low velocity, small steel ball impact tests on laminated glass plates with polyvinyl butyral (PVB) interlayer. Their results showed that increasing the interlayer thickness and increasing the inner glass sheet thickness could significantly increase the steel ball impact velocity required to break the inner glass sheet.

Larcher et al. [66] experimentally studied the response of impact-loaded laminated glass with PVB interlayer. They conducted their experiments at a shock tube facility. Besides experiments, they also used several numerical models, such as layered model and solid 3D model, to simulate the response of the impact-loaded laminated glass. They

found that the layered model could efficiently simulate the experimentally measured results, also in cases where the interlayer failed. The 3D solid model could also simulate the experimental results, though requiring larger computational power. Lusk et al. [67] also experimentally studied the response of impact-loaded laminated glass with PVB interlayer. Three samples were tested using a full-scale shock tube. Instead of numerical modelling, Lusk used the commercial finite element code LS-DYNA to simulate the dynamic response of the laminated glass. The results simulated by LS-DYNA agreed well the experimentally measured results. Lusk stated that the mechanical properties of the materials that were used to fabricate the laminated glass were the most important parameters for LS-DYNA inputs and should be tested before simulation.

Turkmen et al. [68] performed blast tests on a stiffened laminated plate (carbon fiber fabric) and measured blast pressures and strains at different points on the stiffened laminated plate and its stiffener. After analyzing the measured strain data, Turkmen stated that the peak strain of the laminated plate depended on the peak pressure value and the strain variation with time depended on the pressure variation with time. The authors also numerically modelled the response of the plate and reported the numerical results correlated well with the experimental results.

Wei et al. [2, 69, 70] investigated the dynamic response of laminated glazing with PVB interlayer subjected to blast loading through theoretical approaches. They presented two models, which are based on the classical small deflection plate theory and von Karman's large deflection plate theory, respectively, to characterize the response of the laminated glass under blast loading. For comparison, they also simulated the dynamic

response using a 3D finite element code LS-DYNA. The model-predicted results matched with the finite element analysis results. The authors also studied the damage probability of the laminated glass subjected to blast loading. Their results showed that newly fabricated laminated glass panel could withstand higher blast loading than old ones and decreasing outer glass sheet thickness and increasing inner glass sheet thickness while keeping the total thickness of the laminated glass constant is an economical way to increase the blast resistance of the laminated glass.

Amadio et al. [71] visited the problem of the behavior of a conventional glazing structure (glass curtain wall) subjected to high- and low-level air blast loading. The authors found that additional deformability and additional energy dissipation ability could be provided to the conventional glass curtain wall by adding viscoelastic (VE) devices at the frame corners of the glass curtain wall. The VE device was made of two metallic plates and a middle rubber (viscoelastic material) layer. VE devices were positioned between the frame of the glass curtain wall and the structural backup of it. The authors discovered that VE devices could reduce the maximum stresses in the glass curtain wall, reduce the deflection of the total structure and decrease the maximum reactions transmitted to the structural backup.

Birman et al. [72] studied the dynamic response of simply supported anti-symmetrically laminated angle-ply thick plates (graphite-epoxy plates) subjected to blast loading. A closed-form solution was proposed for describing the dynamic response of the plates. In their work, the effect of transverse shear deformations on the response of the plates was considered. Their analysis yielded a non-dimensional deflection versus time

relationship and this relationship was used to calculate the stresses and strains of the plates.

Kazancı et al. [73] addressed the problem of nonlinear dynamic response of a simply supported laminated plate (fiber-glass fabric) under blast loading. They derived equations of motion of the laminated plate, in the frame of von Karman's deflection theory with the consideration of geometric nonlinearity effects. The equations of motion were solved using finite difference method and the obtained results were compared with literature and finite element analysis results. Good agreement was reported for deflection and frequencies of vibrations.

1.6 Summary

There has been a lot of research on methods to mitigate the damage caused by windows failure under blast loading. Until today, the most effective method to mitigate the damage is use blast-resistant laminated glass for windows. Currently, the most widely used laminated glass is the laminated glass with polyvinyl butyral (PVB) interlayer. The reason for using PVB as the interlayer material has been mentioned previously: colorless; able to bind glass fragments after windows failure; good energy absorption ability. The disadvantage of the laminated glass with PVB interlayer is its large thickness and weight. This disadvantage can be overcome by replacing the PVB interlayer with a transparent glass fiber-reinforced polyester composite interlayer which has high strength to weight ratio. The transparency of the glass fiber-reinforced composite is achieved by matching the refractive index of the polymer matrix with that of glass fibers.

The dynamic response of the laminated glass with PVB interlayer under blast loading has been experimentally and analytically studied. Several numerical models have been developed to characterize the dynamic response of the laminated glass with PVB interlayer under blast/dynamic loading. But to the best of our knowledge, the dynamic response of the laminated glass with glass fiber-reinforced composite interlayer under blast loading has not been studied previously.

In this research, a novel blast-resistant laminated glass panel utilizing a transparent glass fiber-reinforced composite interlayer has been successfully fabricated. The dynamic response of the fabricated laminated glass under blast loading has been investigated experimentally and analytically.

The investigation in this research has been organized in three parts:

(1) Part I: this part is the introduction, which includes Chapter 1 titled "Introduction".

(2) Part II: this part focuses on fabricating the transparent glass fiber-reinforced composite interlayer and studying its optical properties and mechanical behavior, which includes Chapter 2 titled "A novel optically transparent woven glass fiber-reinforced polymer composite: fabrication and properties".

(3) Part III: this part reports studies of the dynamic response of the novel blast-resistant laminated glass under blast loading, which contains Chapter 3 titled "A study of the dynamic response of the novel laminated glass under blast loading" and Chapter 4 titled "Nonlinear dynamic analysis of the novel laminated glass under blast loading".

REFERENCES

[1] Smith, P.D., and Hetherington, J.G., 1994, "*Blast and ballistic loading of structures*", Oxford: Butterworth-Heinemann.

[2] Wei, J., and Dharani, L.R., 2006, "*Response of laminated architectural glazing subjected to blast loading*", International Journal of Impact Engineering, **32**, No.12, pp.2032-2047.

[3] Kinney, G.F., and Graham, K.J., 1985, "*Explosive shocks in air*", Berlin and New York: Springer-Verlag.

[4] Baker, W.E., 1973, "*Explosions in air*", Austin, TX: University of Texas Press.

[5] Forbes, D.J., 1999, "*Blast loading on petrochemical buildings*", Journal Energy Engineering, **125**, No.3, pp.94-102.

[6] Norville, H.S., and Conrath, E.J., 2006, "*Blast-resistant glazing design*", Journal of Architectural Engineering, **12**, No.3, pp.129-136.

[7] Norville, H.S., Smith, M.L., and King, K.W., 1995, "*Survey of window glass broken by the Oklahoma City bomb on April 19, 1995*", Lubbock, TX: Texas Tech University.

[8] Quenemoen, L.E., Davis, Y.M., Malilay, J., Sinks, T., Noji, E.K., and Klitzman, S., 1996, "*The World Trade Center bombing: injury prevention strategies for high-rise building fires*", Disasters, **20**, No.2, pp.125-132.

[9] Wikipedia, "*1996 Manchester bombing*", http://en.wikipedia.org/wiki/1996_ manchester_bombing.

[10] Wikipedia, "*2004 Australian Embassy bombing in Jakarta*", http://en.wikipedia.org/ wiki/2004_Australian_Embassy_bombing_in_Jakarta.

[11] Smith, D., 2001, "*Glazing for injury alleviation under blast loading—United Kingdom practice*", Glass Processing Days, pp.335-340.

[12] Graham, "*About blast mitigation*", http://www.grahamwindows.com/blast/ about_ blast.html.

[13] Brismar, B., and Bergenwald, L., 1982, "*The terrorist bomb explosion in Bologna, Italy, 1980: an analysis of the effects and injuries sustained*", The Journal of Trauma, **22**, No.3, pp.216-220.

[14] Katz, E., Ofek, B., Adler, J., Abramowitz, H.B. and Krausz, M.M., 1989, "*Primary blast injury after a bomb explosion in a civilian bus*", Annals of Surgery, **209**, No.4, pp.484-488.

[15] Shankar, K.R., 2007, "*Failure of transparent polymer composite laminated glass panels under impact loading*", Columbia, MO: University of Missouri.

[16] Xu, J., Li, Y., Liu, B., Zhu, M., and Ge, D., 2011, "*Experimental study on mechanical behavior of PVB laminated glass under quasi-static and dynamic loadings*", Composites Part B: Engineering, **42**, No.2, pp.302-308.

[17] Osborn, R.A., 1996, "*Shedding light on skylights*", Fine Homebuilding, **102**, No.5, pp.48-53.

[18] Wikipedia, "*Laminated glass*", http://en.wikipedia.org/wiki/Laminated_glass.

[19] Zang, M., and Chen, S., 2012, "*Laminated glass, Wiley Encyclopedia of Composites*", Hoboken , NJ: John Wiley & Sons.

[20] Wikipedia, "*Polyvinyl butyral*", http://en.wikipedia.org/wiki/Polyvinyl_butyral.

[21] Fonrodona, M., Santos, S., Mata, C., Vetter, M., and Andreu, J., 2010, "*Performance and productivity improvements in very large area amorphous silicon modules*", Proceedings of the 25th EU-PVSEC, pp.3661-3664.

[22] Su, B., and Button, T., 2009, "*A comparative study of viscous polymer processed ceramics based on aqueous and non-aqueous binder systems*", Journal of Materials Processing Technology, **209**, No.1, pp.153-157.

[23] Folgar, F., "*Advanced aliphatic polyurethane resins for high durability and superior ballistic performance laminated glass*", http://intermaterials-usa.com/images/FCKUploads/file/Advanced_AliphaticPolyurethanes_INTER_MaterialsLLC_1(2).pdf.

[24] Walley, S., Field, J., Blair, P., and Milford, A., 2004, "*The effect of temperature on the impact behaviour of glass/polycarbonate laminates*", International Journal of Impact Engineering, **30**, No.1, pp.31-53.

[25] Schollenberger, C., and Stewart, F., 1971, "*Thermoplastic polyurethane hydrolysis stability*", Journal of Elastomers and Plastics, **3**, No.1, pp.28-56.

[26] Promolding, "*TPU*", http://promolding.nl/materiaal-munt.php?lan=uk&c=125.

[27] Bennison, S.J., Qin, M.H., and Davies, P.S., 2008, "*High-performance laminated glass for structurally efficient glazing*", Innovative Light-Weight Structures and Sustainable Facades, pp.1-12.

[28] Rietsch, F., and Bouette, B., 1990, "*The compression yield behaviour of polycarbonate over a wide range of strain rates and temperatures*", European Polymer Journal, **26**, No.10, pp.1071-1075.

[29] Walley, S.M., Field, J.E., Blair, P.W., and Milford, A.J., 2004, "*The effect of temperature on the impact behaviour of glass/polycarbonate laminates*", International Journal of Impact Engineering, **30**, No.1, pp.31-53.

[30] Zurimendi, J., Biddlestone, F., Hay, J., and Haward, R., 1982, "*Physical factors affecting the impact strength of polycarbonate*", Journal of Materials Science, **17**, No.1, pp.199-203.

[31] Sherman, E., Ram, A., and Kenig, S., 1982, "*Tensile failure of weathered polycarbonate*", Polymer Engineering & Science, **22**, No.8, pp.457-465.

[32] Clark, D.T., and Munro, H.S., 1984, "*Surface and bulk aspects of the natural and artificial photo-ageing of Bisphenol A polycarbonate as revealed by ESCA and difference UV spectroscopy*", Polymer Degradation and Stability, **8**, No.4, pp.195-211.

[33] Turton, T., and White, J., 2001, "*Degradation depth profiles and fracture of UV exposed polycarbonate*", Plastics, Rubber and Composites, **30**, No.4, pp.175-182.

[34] Gardner, R.J., and Martin, J.R., 1979, "*Humid aging of plastics: effect of molecular weight on mechanical properties and fracture morphology of polycarbonate*", Journal of Applied Polymer Science, **24**, No.5, pp.1269-1280.

[35] Factor, A., and Chu, M., 1980, "*The role of oxygen in the photo-ageing of bisphenol-A polycarbonate*", Polymer Degradation and Stability, **2**, No.3, pp.203-223.

[36] Blaga, A., and Yamasaki, R., 1976, "*Surface microcracking induced by weathering of polycarbonate sheet*", Journal of Materials Science, **11**, No.8, pp.1513-1520.

[37] Olson, J.R., Day, D.E., and Stoffer, J.O., 1992, "*Fabrication and mechanical properties of an optically transparent glass fiber/polymer matrix composite*", Journal of Composite Materials, **26**, No.8, pp.1181-1192.

[38] Novak, B.M., 1993, "*Hybrid nanocomposite materials—between inorganic glasses and organic polymers*", Advanced Materials, **5**, No.6, pp.422-433.

[39] Mohd, I.Z., Leong, Y., Steeg, M., and Karger, K.J., 2007, "*Mechanical properties of woven glass fabric reinforced in situ polymerized poly (butylene terephthalate) composites*", Composites Science and Technology, **67**, No.3, pp.390-398.

[40] Malchev, P.G., David, C.T., Picken, S.J., and Gotsis, A.D., 2005, "*Mechanical properties of short fiber reinforced thermoplastic blends*", Polymer, **46**, No.11, pp.3895-3905.

[41] Mollazadeh, S., Javadpour, J., and Khavandi, A., 2007, "*Biomimetic synthesis and mechanical properties of hydroxyapatite/poly (vinyl alcohol) nanocomposites*", Advances in Applied Ceramics, **106**, No.4, pp.165-170.

[42] Karevan, M., Pucha, R.V., Bhuiyan, M.A., and Kalaitzidou, K., 2010, "*Effect of interphase modulus and nanofiller agglomeration on the tensile modulus of graphite nanoplatelets and carbon nanotube reinforced polypropylene nanocomposites*", Carbon Letters, **11**, No.4, pp.325-331.

[43] Gonçalves, G., Marques, P.A., Barros, T.A., Bdkin, I., Singh, M.K., and Emami, N., 2010, "*Graphene oxide modified with PMMA via ATRP as a reinforcement filler*", Journal of Materials Chemistry, **20**, No.44, pp.9927-9934.

[44] Gerstle, F.P., 1991, "*Composites, In: Encyclopedia of Polymer Science and Engineering*", New York, NY: John Wiley & Sons.

[45] CST, "*Fibers*", http://www.cstsales.com.

[46] Abdulmajeed, A.A., Närhi, T.O., Vallittu, P.K., and Lassila, L.V., 2011, "*The effect of high fiber fraction on some mechanical properties of unidirectional glass fiber-reinforced composite*", Dental Materials, **27**, No.4, pp.313-321.

[47] Akkapeddi, M., 2000, "*Glass fiber reinforced polyamide-6 nanocomposites*", Polymer Composites, **21**, No.4, pp.576-585.

[48] Iba, H., Chang, T., and Kagawa, Y., 2002, "*Optically transparent continuous glass fibre-reinforced epoxy matrix composite: fabrication, optical and mechanical properties*", Composites Science and Technology, **62**, No.15, pp.2043-2052.

[49] Iba, H., and Kagawa, Y., 1998, "*Light transmittance of continuous fibre-reinforced composites: analysis, model experiment and parametric study*", Philosophy Magazine B, **78**, No.1, pp.37-52.

[50] Lin, H., Kang, S.G., Day, D.E., and Stoffer, J.O., 1994, "*The effect of fiber annealing on the properties of an optically transparent PMMA composite*", Composites Science and Technology, **50**, No.3, pp.367-372.

[51] Kusano, Y., Norrman, K., Drews, J., Leipold, F., Singh, S.V., and Morgen, P., 2011, "*Gliding arc surface treatment of glass-fiber-reinforced polyester enhanced by ultrasonic irradiation*", Surface and Coatings Technology, **205**, No.7, pp.490-494.

[52] Ramesh, M., Palanikumar, K., and Hemachandra, R.K., 2012, "*Mechanical property evaluation of sisal-jute-glass fiber reinforced polyester composites*", Composites Part B: Engineering, **48**, No.5, pp.1-9.

[53] Rao, H.R., Rajulu, A.V., Reddy, G.R., and Reddy, K.H., 2010, "*Flexural and compressive properties of bamboo and glass fiber-reinforced epoxy hybrid composites*", Journal of Reinforced Plastics and Composites, **29**, No.10, pp.1446-1450.

[54] Manjunatha, C., Sprenger, S., Taylor, A., and Kinloch, A., 2010, "*The tensile fatigue behavior of a glass-fiber reinforced plastic composite using a hybrid-toughened epoxy matrix*", Journal of Composite Materials, **44**, No.17, pp.2095-2109.

[55] Mazumdar, S., "*Opportunities for thermoset resins in the composites industry*", http://www.trfa.org/erc/docretrieval/uploadedfiles/Technical%20Papers/2008%20Meeting/Mazumdar-Lucintel_paper-Composites_industry.pdf.

[56] Wikipedia, "*Polyester*", http://en.wikipedia.org/wiki/Polyester.

[57] Acmite Market Intellgence, "*World epoxy resin market*", http://www.acmite.com/market-reports/chemicals/world-epoxy-resin-market.html.

[58] Kuo, C.C., 2012, "*A simple and cost-effective method for fabricating epoxy-based composite mold inserts*", Materials and Manufacturing Processes, **27**, No.4, pp.383-388.

[59] Kim, J.K., Hu, C., Woo, R.S., and Sham, M.L., 2005, "*Moisture barrier characteristics of organoclay–epoxy nanocomposites*", Composites Science and Technology, **65**, No.5, pp.805-813.

[60] Azom, "*Resin properties for composite materials*", http://www.azom.com/article.aspx?ArticleID=997.

[61] Daeyang International Co. Ltd., http://www.alibaba.com/product-tp/139744747/UPR_191_196_Unsaturated_Polyester_Resin.html.

[62] Shanghai Shilei Chemical Co. Ltd., http://www.alibaba.com/product gs/555167436/epoxy_resin.html.

[63] Dalian CR Science Development Co. Ltd., http://www.alibaba.com/product-gs/698902977/vinyl_ester_resin.html.

[64] Ji, F., Dharani, L., and Behr, R., 1998, "*Damage probability in laminated glass subjected to low velocity small missile impacts*", Journal of Materials Science, **33**, No.19, pp.4775-4782.

[65] Kaiser, N.D., Behr, R.A., Minor, J.E., Dharani, L.R., Ji, F., and Kremer, P.A., 2000, "*Impact resistance of laminated glass using "sacrificial ply" design soncept*", Journal of Architecture Engineering, **6**, No.1, pp.24-34.

[66] Larcher, M., Solomos, G., Casadei, F., and Gebbeken, N., 2012, "*Experimental and numerical investigations of laminated glass subjected to blast loading*", International Journal of Impacting Engineering, **39**, No.1, pp.42-50.

[67] Lusk, B., Salim, H., Perry, K., Nawar, M., Wedding, W., and Kiger, S., 2011, "*Modeling and testing of laminated window systems under blast loading*", Structures Congress 2011: ASCE, pp.1552-1560.

[68] Türkmen, H., and Mecitoğlu, Z., 1999, "*Dynamic response of a stiffened laminated composite plate subjected to blast load*", Journal of Sound Vibration, **221**, No.3, pp.371-389.

[69] Wei, J., and Dharani, L., 2005, "*Fracture mechanics of laminated glass subjected to blast loading*", Theory of Applied Fracture Mechanics, **44**, No.2, pp.157-167.

[70] Wei J., 2004, "*Dynamics and failure analysis of architectural glazing subjected to blast loading*", Rolla, MO: University of Missouri.

[71] Amadio, C., and Bedon, C., 2012, "*Blast analysis of laminated glass curtain walls equipped by viscoelastic dissipative devices*", Buildings, **2**, No.3, pp.359-383.

[72] Birman, V., and Bert, C.W., 1987, "*Behaviour of laminated plates subjected to conventional blast*", International Journal of Impact Engineering, **6**, No.3, pp.145-155.

[73] Kazancı, Z., and Mecitoğlu, Z., 2008, "*Nonlinear dynamic behavior of simply supported laminated composite plates subjected to blast load*", Journal of Sound Vibration, **317**, No.3, 883-897.

CHAPTER 2 A NOVEL OPTICALLY TRANSPARENT WOVEN GLASS FIBER-REINFORCED POLYMER COMPOSITE: FABRICATION AND PROPERTIES

2.1 Introduction

Transparent engineering polymers are needed in various fields, including aerospace, military and automobile industries [1, 2]. Currently available transparent polymers have some drawbacks, such as low quasi-static and dynamic mechanical properties. Incorporation of glass fibers into a polymer matrix can greatly improve its mechanical properties [3-6], while reducing its transparency (light transmittance) to some extent. The transparency reduction is due to the refractive index mismatch between glass fibers and the polymer matrix [3, 7]. Iba and Kagawa [8] studied the relationship between the transparency and the refractive index difference and proposed an analytical model for predicting the transparency of unidirectional aligned continuous fiber-reinforced composite. Based on Iba's model, a new analytical model, which can be used to predict the light transmittance of $0/90^{o}$ woven glass fiber-reinforced composite, has been developed in this research.

Applications of optically transparent glass fiber-reinforced polymer composite, such as blast resistance screen and plane window, usually require high strength, good fracture toughness and good dynamic impacting resistance [3, 9-13]. Hence, quasi-static

mechanical properties, fracture toughness and dynamic mechanical properties of a transparent glass fiber-reinforced composite should be investigated before using it. Quasi-static mechanical properties and fracture toughness can be studied using an Instron universal testing machine. Dynamic mechanical properties can be studied using a split Hopkinson bar (SHB) [14-20]. A series of SHB tests on glass fiber-reinforced composite have been performed previously [21-25], reported results indicate that the dynamic mechanical properties of glass fiber-reinforced composite are dependent on strain rate.

In this study, an optically transparent woven (0/90 °) glass fiber-reinforced polyester composite has been fabricated. The composite has been used as an interlayer in a blast-resistant laminated glass panel fabrication. A model for predicting the light transmittance (transparency) of the composite has been proposed. According to the model, the light transmittance can be increased by reducing the refractive index difference between glass fibers and the polyester matrix. Since the refractive index of glass fibers is difficult to change, the refractive index of the polyester matrix was modified to reduce the difference. The modification was done by adjusting the concentrations of chemical additives, such as methyl ethyl ketone peroxide (MEKP), cobalt (II) 2-ethylhexanoate (CE), divinylbenzene (DV) and phenanthrene (PT). Besides the refractive index difference, the effect of fiber volume fraction on light transmittance was also studied. Properties of the composite, such as quasi-static mechanical properties, fracture toughness and dynamic mechanical properties, and viability of the fabricated laminated glass under blast loading were investigated.

2.2 Experimental methods

2.2.1 Polyester plate fabrication

Polyester (-(R'CH=CHCOOR)$_n$-, Ashland Specialty Co., USA) was mixed with 1.2 wt% methyl ethyl ketone peroxide (MEKP) ($C_8H_{18}O_6$, Sigma-Aldrich Co., USA), an initiator, 0.03 wt% cobalt (II) 2-ethylhexanoate (CE) ($C_{16}H_{30}CoO_4$, Sigma-Aldrich Co., USA), an accelerator and 4 wt% divinylbenzene (DV) ($C_{10}H_{10}$, Sigma-Aldrich Co., USA) or 1 wt% phenanthrene (PT) ($C_{14}H_{10}$, Sigma-Aldrich Co., USA), which are refractive index modifiers. All above mentioned components were thoroughly mixed for 3-4 min by hand in a plastic bucket. The mixture was set in a vacuum degassing chamber so as to allow air bubbles inside it to escape by creating vacuum inside the chamber. After degassing, the mixture was poured into a 3.2 mm deep mold which was made by placing aluminum frames on top of a polyvinyl chloride (PVC) plate with Mylar sheet (Fig. 2.1). After filling the mold, another PVC plate with Mylar sheet was laid on top of the mold, the top and bottom plates were clamped with C-clamps. The clamped plates were erected sideways to let entrapped air escape from the mold. The setup was left at room temperature (~20 ℃) for two days to ensure complete curing of the polyester.

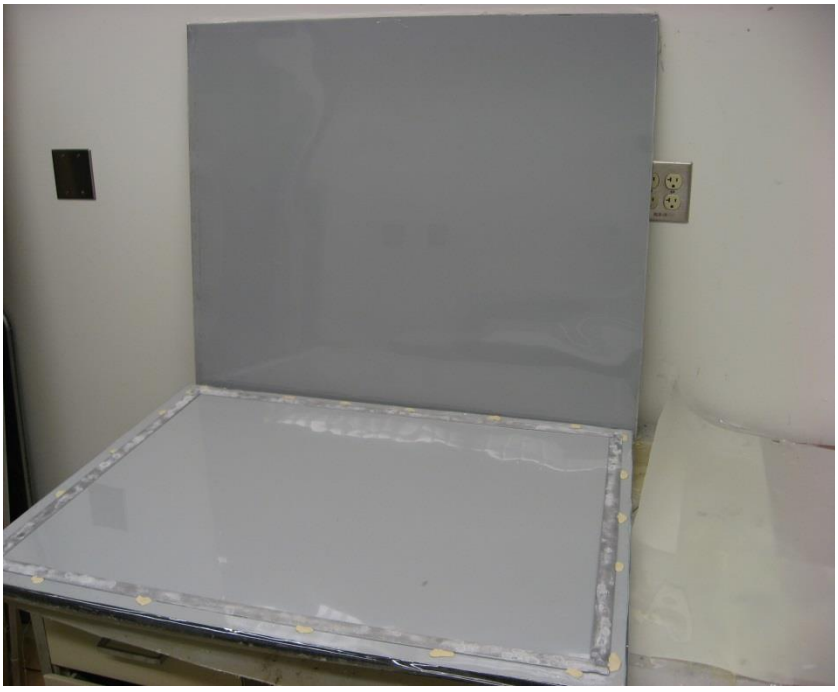

Figure 2.1 Mold for fabricating polyester and glass fiber-reinforced composite plates

2.2.2 Glass fiber-reinforced composite fabrication

Glass fiber-reinforced composite was prepared using a similar procedure as described above. The polyester was mixed with 1.2 wt% MEKP, 0.03 wt% CE and 4 wt% DV or 1 wt% PT. All components were thoroughly mixed for 2-3 min by hand in a plastic bucket. Then, the mixture was degassed in a vacuum chamber. But this time, after degassing, instead of pouring all mixture into the 3.2 mm deep mold, a small amount of the mixture was first poured into the mold so as to wet the base surface of the mold. Then a layer of glass fiber cloth (Aerospace Composite Products Co., USA) was put in the mold and some more polymer mixture was poured in the mold. This procedure was repeated 4 times, producing a composite of 3.2 mm thick with 5 layers of glass fiber

cloth. The setup was left at room temperature for two days to ensure complete curing of the composite. The cured composite had a fiber volume fraction of 12.3%.

Same procedure was also used to produce a composite of 1.6 mm thick with 5 layers of glass fiber cloth. The cured composite had a fiber volume fraction of 24.2%.

The properties of glass fibers and polyester are listed in Table 2.1.

Table 2.1 Some properties of glass fibers and polyester

	Glass fibers	Polyester
Density (g/cm^3)	2.54	1.05
Young's modulus (GPa)	70	3.25
Poisson's ratio	0.2	0.39
Refractive index at 589 nm at 20 ℃	1.5595	-
Fiber diameter (μm)	~10	-
Linear density* (fiber/mm)	~550	-

*transverse linear density and longitudinal linear density together.

2.2.3 Laminated glass panel fabrication

Laminated glass panel was fabricated by sandwiching the glass fiber-reinforced composite interlayer between two tempered glass sheets. The composite interlayer and glass sheets were bonded using a two part polyurethane resin (SP&S Co., USA). The procedure for fabricating a laminated glass is as follows: firstly, a glass sheet (Nashville Tempered Glass Co., USA) was placed on a table and a very thin layer of polyurethane resin was uniformly spread on the glass sheet. Secondly, the composite interlayer was placed on top of the glass sheet. Pressure was applied to spread the resin and remove any

entrapped air bubbles. Finally, a very thin layer of polyurethane resin was uniformly spread on the composite interlayer and the second glass sheet was placed on top of the composite interlayer. The setup was left at room temperature for at least one day to ensure complete curing of the polyurethane adhesive. The structure of the laminated glass is shown in Fig. 2.2.

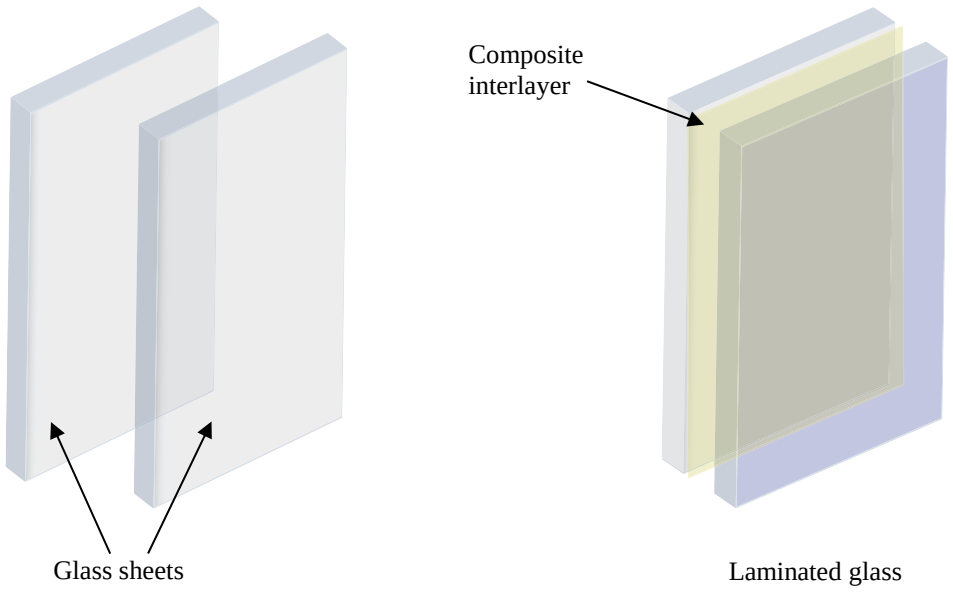

Figure 2.2 Laminated glass structure

2.2.4 Refractive index measurement

The refractive index of glass fibers (589 nm) was measured using the Central Illumination Method (Becke Line Method).

The refractive indices (589 nm) of polyester samples (25 mm × 8 mm ×3.2 mm) were measured using Abbe refractometer (NAR-3T, Atago Co., Japan, with a refractive index precision of 0.0001 in the range of 1.3 to 1.7) at room temperature.

2.2.5 Light transmittance measurement

The light transmittance of the composite, polyester matrix and fabricated laminated glass in the thickness direction was measured over a wavelength range of 190 to 900 nm using an ultraviolet-visible (UV-VIS) spectrometer (UV 2401 PC, Shimadzu Co., Japan). The resolution of the spectrometer is 1nm. All measurements were done at room temperature.

2.2.6 Composite interlayer's quasi-static mechanical properties testing

2.2.6.1 Young's modulus and Poisson's ratio

250 mm long and 25 mm wide strips were cut from the fabricated composite sheets (Fig. 2.3). The strips were machined to ensure that they were straight and had smooth edges. Aluminum tabs were attached to the gripped portions of the specimens to prevent any possible damage (the shadow area in Fig. 2.3). Tensile tests were performed at room temperature on a servo-hydraulic Instron 8800 universal testing machine with a 10 kN load cell, at a crosshead speed of 2mm/min. For the measurement of tensile strains, strain gages (CEA-13-240UZ-120, Vishary Precision Inc., USA) were attached on the specimens in both longitudinal (length direction) and lateral directions (width direction). During the test, loads and strains were recorded by computer. These data were used to

find tensile strength σ_T, failure strain ε_f, Young's modulus E and Poisson's ratio ν_{12}. ASTM D3039 [26] gives the following mathematical expression for calculating Young's modulus

$$E = \frac{\frac{\Delta P}{bd}}{\Delta \varepsilon} \tag{2.1}$$

where $\Delta\varepsilon$ is the strain difference between two strain points in the initial linear region of the stress-strain curve, ΔP is the load difference between the same two points, b is the specimen width, and d is the specimen thickness.

Poisson's ratio ν_{12} can be calculated using the following equation

$$\nu_{12} = -\frac{\Delta \varepsilon_{la}}{\Delta \varepsilon_{lo}} \tag{2.2}$$

where $\Delta\varepsilon_{la}$ is the lateral strain difference between two lateral strain points and $\Delta\varepsilon_{lo}$ is the longitudinal strain difference between two corresponding longitudinal strain points.

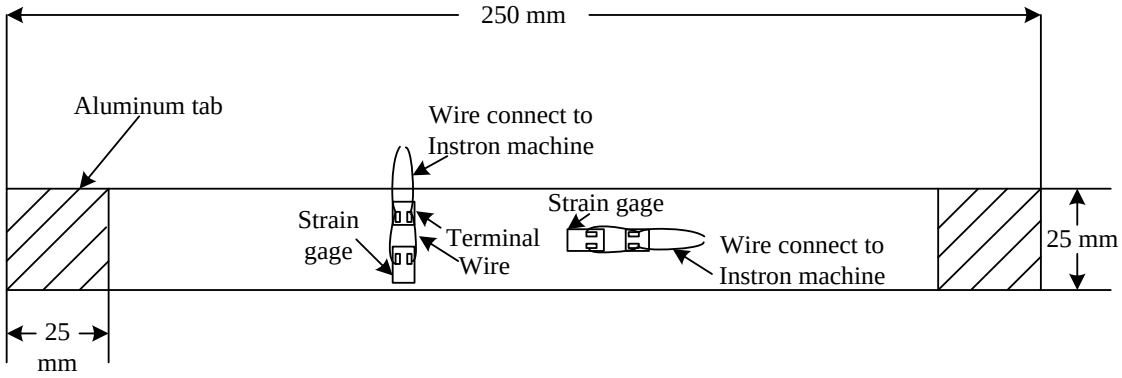

Figure 2.3 Shape and dimensions of tensile test specimens

2.2.6.2 Shear modulus

250 mm long and 25 mm wide $\pm 45^{o}$ fiber-reinforced strips were cut from the fabricated composite sheets. Strain gages were attached on the specimens in both longitudinal and lateral directions. The $\pm 45^{o}$ specimens were loaded in tension while recording loads and strains. According to the ASTM standard D3518 [27], shear modulus G can be calculated as

$$G = \frac{\Delta \tau}{\Delta \gamma} \tag{2.3}$$

where $\Delta \gamma$ is the shear strain difference between two shear strain points. $\Delta \tau$ is the shear stress difference between the same two shear strain points and is equal to $\Delta P / 2bd$. ΔP is the load difference between the two shear strain points, *b* is the specimen width and *d* is the specimen thickness.

2.2.7 Fracture toughness testing

The fracture toughness of the composite was investigated using J-integral method. J-integral method is a way to calculate the work energy per unit fracture surface area of a material. It has some advantages over the conventional stress intensity factor method, such as its result evaluation is easier and its result is more accurate [28]. So in this study, the J-integral method was used to study the fracture toughness of the composite.

J-integral method was developed by Cherepanov [29] and Jim Rice [30] independently. The theoretical concept of the J-integral method is that the energy integral

(called *J*) of a crack (notch) is independent of the path around it (Fig. 2.4). The J-integral value can be calculated using the following equation [30]

$$J = \int_{\Gamma} \left(W(x_1, x_2)\, dx_2 - \boldsymbol{t} \cdot \frac{\partial \boldsymbol{u}}{\partial x_1} ds \right) \tag{2.4}$$

$$\boldsymbol{t} = \boldsymbol{\sigma} \cdot \boldsymbol{n}$$

where Γ is a curve surrounding a crack (notch) tip. $W(x_1, x_2)$ is the strain energy density, x_1, x_2 are the coordinate directions, ds is the increment of the contour path, $\boldsymbol{u}$ is the displacement vector, $\boldsymbol{t}$ is the surface traction vector, $\boldsymbol{n}$ is the vector normal to the curve Γ and $\boldsymbol{\sigma}$ is the Cauchy stress tensor. Landes and Begley [31] reported that at a constant displacement, the J-integral value for a specimen can be defined as

$$J = -\frac{1}{t} \frac{\partial U}{\partial a}\Big|_{\text{constant displacement}} \tag{2.5}$$

where t is the thickness of the specimen, a is the crack length and U is the potential energy.

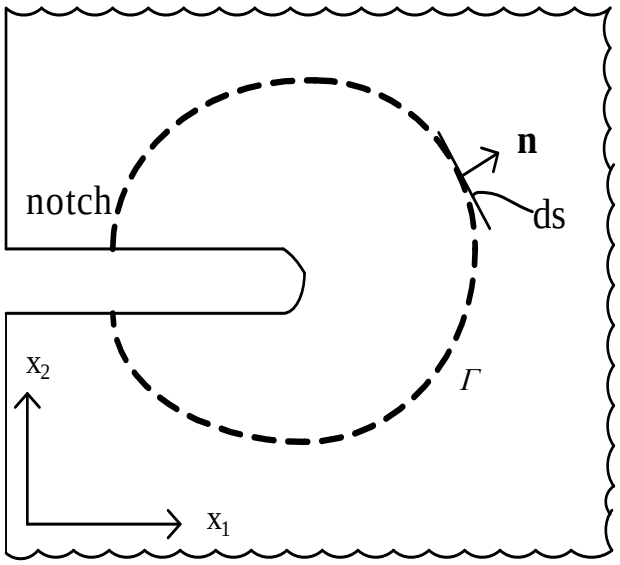

Figure 2.4 J-integral curve around a crack (notch)

In this research, J-integral tests were carried out using single-edge-notched-tension (SENT) specimens (Fig. 2.5) on the Instron 8800 universal testing machine with a 10 kN load cell, at a crosshead speed of 2 mm/min. The dimensions of SENT specimens were 165 mm × 38 mm × 1.6 mm. Aluminum tabs were affixed to the gripped portions (the shadow area in Fig. 2.5) of the specimens to prevent any possible damage. The total length between grips was 115 mm. The cracks (notches) on the specimens were made by first saw cutting and then sharpening with a diamond blade. The crack length (a) to specimen width (w) ratio (a/w) was varied from 0.1 to 0.75 using the following discrete ratios: 0.1, 0.15, 0.25, 0.35, 0.5, 0.6, 0.75. For every crack length, tests were conducted on three specimens.

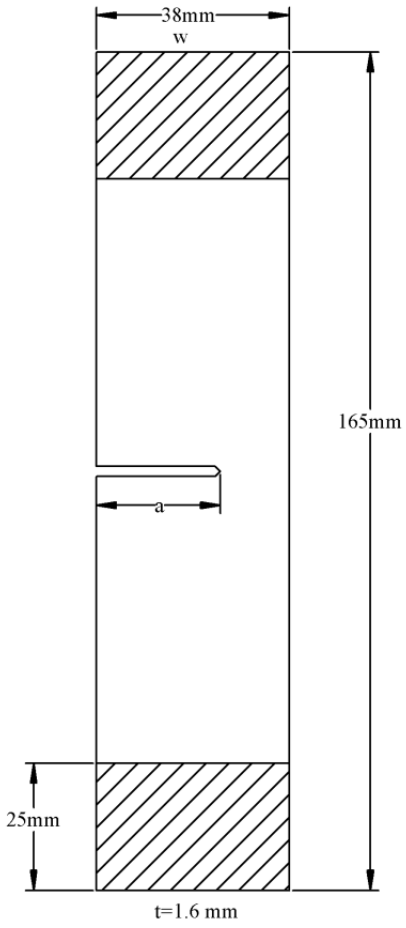

Figure 2.5 Dimensions of single-edge-notched-tension specimens

2.2.8 Dynamic mechanical properties testing

The dynamic mechanical properties of the composite were tested using the split Hopkonson bar (SHB). Classical SHB system (Fig. 2.6 and 2.7) consists of two elastic bars, called incident bar and transmitted bar, and a gas gun that can propel a striker bar. The mechanism of SHB technique is: upon firing the gas gun, the striker bar imparts a uniaxial stress pulse to the incident bar and a compressive stress wave generated in the

incident bar. This compressive stress wave travels in the incident bar and when this wave reaches a specimen, part of it is reflected back to the incident bar and part of it is transmitted through the specimen to the transmitted bar. The wave transmission in two bars can be captured using strain gages placed on bars (Fig. 2.7). It should be pointed out that before using SHB, it needs to be calibrated and the calibration procedures are outlined in reference [32]. By analyzing the captured strain signals, the stress $\sigma_s(t)$, strain $\varepsilon_s(t)$ and strain rate $\dot{\varepsilon}_s(t)$ of the specimen can be determined by the following equations [33]

$$\sigma_s(t) = \frac{EA}{A_s}\varepsilon_t(t) \tag{2.6}$$

$$\varepsilon_s(t) = \frac{-2c}{L}\int_0^t \varepsilon_r(t)\,dt \tag{2.7}$$

$$\dot{\varepsilon}_s(t) = \frac{-2c}{L}\varepsilon_r(t) \tag{2.8}$$

where E is Young's modulus of bars, A is the cross-sectional area of bars, A_s is the cross-sectional area of the specimen, c is the stress wave velocity in bars, L is the length of the specimen, $\varepsilon_r(t)$ is the reflected strain signal and $\varepsilon_t(t)$ is the transmitted strain signal.

Figure 2.6 Split Hopkinson bar (SHB) apparatus

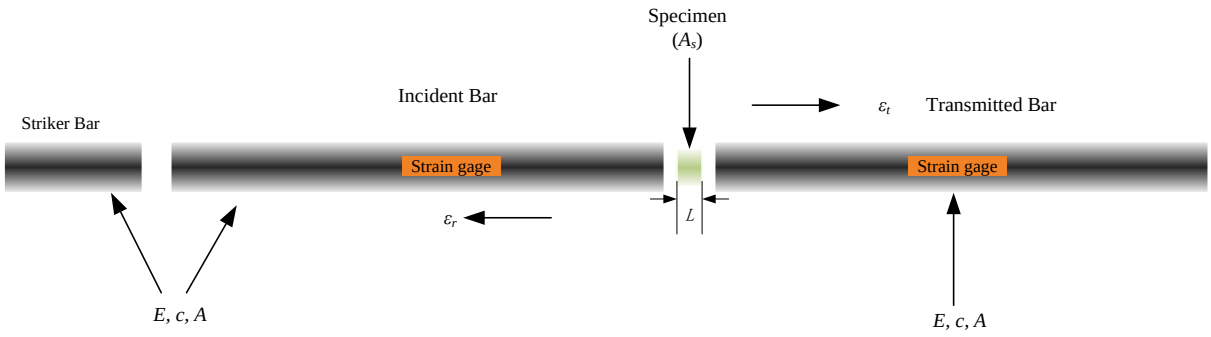

Figure 2.7 Schematic of main components of a SHB system

Usually cylindrical specimens are used in SHB tests. But according to the results reported by Woldesenbet et al. [34] and Phan [33], similar high strain rate mechanical properties can be obtained by either using square-shape specimens or cylindrical-shape specimens. Since cylindrical specimens are relatively difficult to produce, square specimens were used. The dimensions of test specimens were 6.4 mm × 6.4 mm × 3.2 mm

In this research, specimens were loaded in the thickness direction because in dynamic applications, composite is usually loaded in the thickness direction. Fiber orientation of specimens is 0/90 º.

2.2.9 Fiber volume fraction determination

The fiber volume fraction of the composite was determined according to ASTM D2584 [35]. A 25.4 mm × 25.4 mm × 1.6 mm composite specimen was weighed and burnt in an empty ceramic crucible. Once the matrix resin was completely removed, the residue was cooled to room temperature and weighted. The burn-off weight is the polyester matrix weight and the residue weight is glass fibers weight. The fiber volume fraction of the composite was calculated based on the following equation [36]

$$V_f = \frac{\rho_m W_f}{\rho_f W_m + \rho_m W_f} \tag{2.9}$$

where ρ_m and ρ_f are the density of the polyester matrix and glass fibers, respectively. W_m is the matrix weight and W_f is fibers weight.

The fiber volume fraction of 3.2 mm thick composite was measured using the same method.

2.2.10 Blast resistance testing

Blast resistance tests were done at the Engineering Research and Development Center (ERDC, US Army Corps of Engineers Lab, Vicksburg, Mississippi) using a Blast Load Simulator (BLS) (Fig. 2.8). The dimensions of the tested glass panels were 890 by 590 mm. The installation of a glass panel inside the BLS is shown in Fig. 2.9.

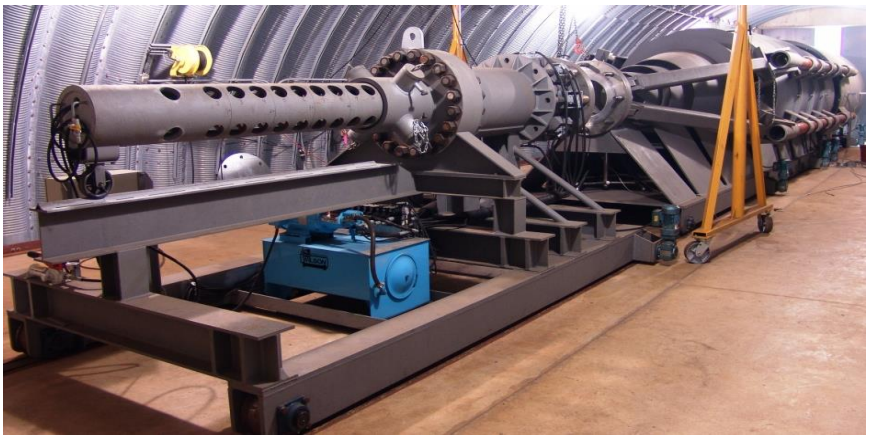

Figure 2.8 Blast Load Simulator (BLS)

Figure 2.9 Glass panel installation inside the BLS

2.3 Theoretical model for light transmission through woven glass fiber-reinforced composite

When light passes through a glass fiber, the phase of light beyond the fiber is changed (Fig. 2.10). The maximum phase difference, which is also called the maximum phase lag, can be expressed using equation (2.10) [8, 37]

$$\delta = 2kr_f \left| n_f - n_m \right| \tag{2.10}$$

where r_f is the radius of the glass fiber, k is the wavenumber of incident light and is equal to $2\pi/\lambda$ (λ is the light wavelength), n_f is the refractive index of the glass fiber, n_m is the refractive index of the surrounding matrix.

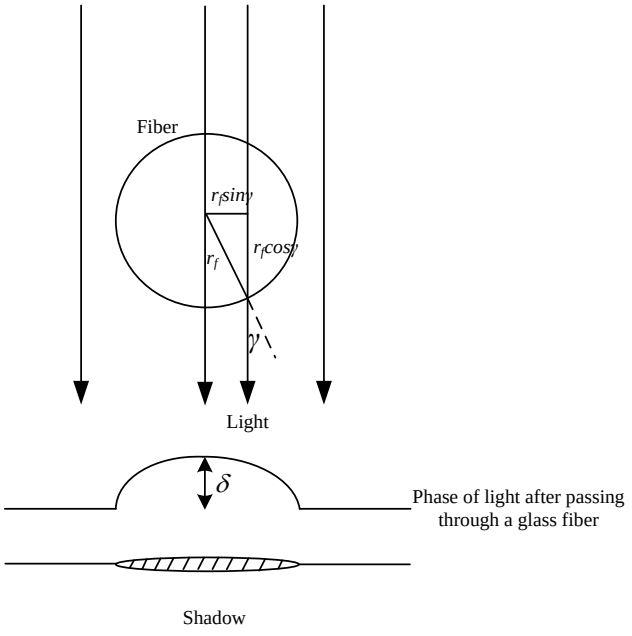

Figure 2.10 Phase of light after passing through a glass fiber

The phase lag causes the reduction of the transmitted light intensity. The intensity amplitude changes at a point at a distance of $r_f sin\gamma$ (γ is the angle between the incident light and surface of the glass fiber) from the center of the fiber is $e^{-i\delta cos\gamma}$. Based on this, the light transmittance T (ratio of transmitted light intensity to incident light intensity) of a single fiber-reinforced polymer composite can be expressed as [8]

$$T = \left[1 - G_f \left(2Re\int_0^{\pi/2}\left[1 - e^{-i\delta cos\gamma}\right]cos\gamma d\gamma\right)\right]T_m \tag{2.11}$$

$$G_f = \frac{2r_f}{w_s}$$

where w_s is the width of the composite, G_f is called shadow ratio and T_m is the light transmittance of the polymer matrix. Partial integration of equation (2.11) results in

$$T = \left[1 - G_f \left(2\left[sin\gamma\left(1 - cos\left(\delta cos\gamma\right)\right)\right]_0^{\pi/2} + \delta\int_0^{\pi/2} sin\left(\delta cos\gamma\right)sin^2\gamma d\gamma\right)\right]T_m$$

$$= \left[1 - G_f \left(2\delta\int_0^{\pi/2} sin\left(\delta cos\gamma\right)sin^2\gamma d\gamma\right)\right]T_m \tag{2.12}$$

From equation (2.12), it can be seen that light transmittance T increases with the decrease of δ. Since $\delta = 2kr_f\left|n_f - n_m\right|$, light transmittance T increases with the decrease of the refractive index difference between the glass fiber and the polymer matrix.

For woven glass fiber-reinforced polymer composite (0/90 ° woven fiber cloth, Fig. 2.11), the shadow ratio of one layer is: $G_{wf} = 2r_f\rho_t + 2r_f\rho_l$, where ρ_t is the linear density of fibers in the transverse direction, ρ_l is the linear density of fibers in the longitudinal

direction. Therefore, the light transmittance T_w of a composite with q layers of fiber cloth can be calculated as

$$T_w = \left[1 - G_{wf}\left(2\delta\int_0^{\pi/2} sin\left(\delta cos\gamma\right) sin^2\gamma d\gamma\right)\right]^q T_m \tag{2.13}$$

From equation (2.13), it can be observed that for woven glass fiber-reinforced composite, the light transmittance T_w also increases with the decrease of phase lag δ. As mentioned previously $\delta = 2kr_f\left|n_f - n_m\right|$, so light transmittance T_w increases with the decrease of the refractive index difference between glass fibers and the polymer matrix. In this research, the refractive index of glass fibers was considered as fixed (1.5595). Therefore, in order to increase the transparency of the glass fiber-reinforced composite, the refractive index of the polyester matrix was modified to reduce the refractive index difference between glass fibers and the polyester matrix. The modification was done by changing the concentrations of chemical additives in the polyester matrix.

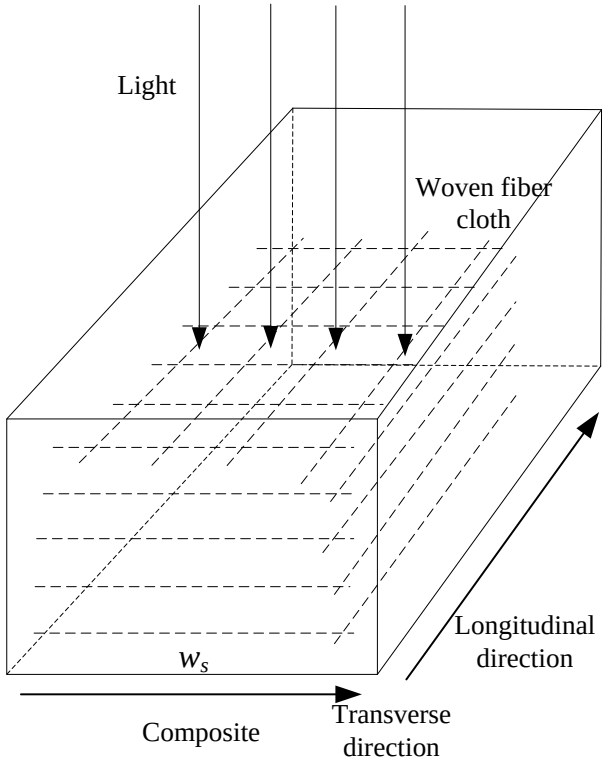

Figure 2.11 Light transmission model of woven glass fiber-reinforced composite

From equation (2.13), it can also be observed that when the refractive index difference is not zero, besides the refractive index difference, the light transmittance of the composite also depends on the shadow ratio G_{wf} and the number of fiber layers q. When the refractive index difference is zero (δ=0), the light transmittance of the composite is the same as that of the polyester matrix and in this situation, both the shadow ratio G_{wf} and the number of fiber layers q can't affect the light transmittance of the composite. In this study, the shadow ratio G_{wf} is a constant value (constant fiber radius, constant linear density in both longitudinal and transverse directions) and 5 layers of fiber cloth were used to reinforce the polyester matrix. So the effects of the shadow

ratio G_{wf} and the number of fiber layers q on light transmittance are not discussed in this study. It is worth pointing out that equation (2.13) does not explicitly incorporate the effect of fiber volume fraction on light transmittance. But from this equation, it can be inferred that the light transmittance of the composite can be affected by the change of fiber volume fraction if the change affects the number of fiber layers the light encounters. Otherwise, the light transmittance will not be affected by the change of fiber volume fraction.

2.4 Results and discussion

2.4.1 Effects of chemical additives on the refractive index of polyester

2.4.1.1 Effect of methyl ethyl ketone peroxide (MEKP) concentration on the refractive index of polyester

Fig. 2.12 shows the effect of MEKP concentration on the refractive index of polyester. With the increase of MEKP concentration, the refractive index of polyester varies around 1.5560. Increasing MEKP concentration has almost no effect on the refractive index of polyester.

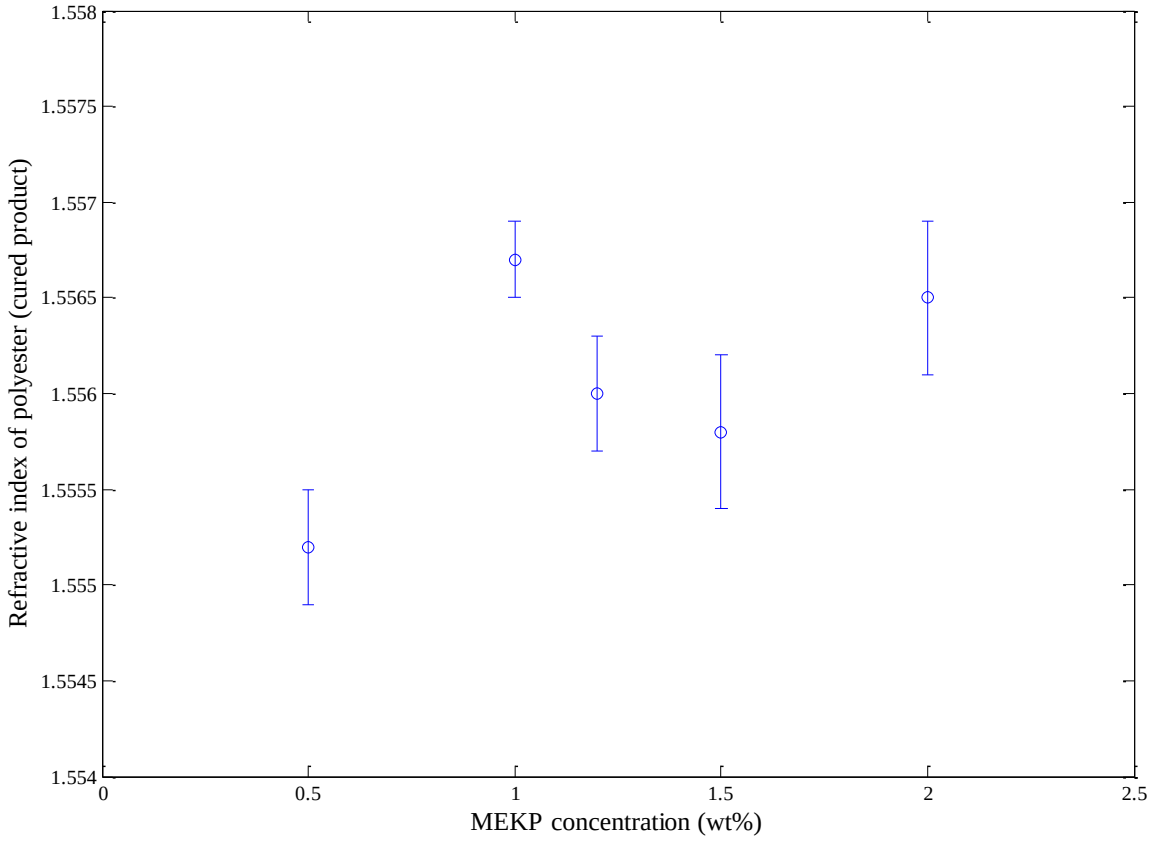

Figure 2.12 Refractive index of polyester (cured product) with different MEKP concentrations (curing condition: curing temperature 20 ℃, CE 0.03 wt%)

2.4.1.2 Effect of cobalt (II) 2-ethylhexanoate (CE) concentration on the refractive index of polyester

From Fig. 2.13, it can be seen that the refractive index of polyester increases with the increase of CE concentration. CE is used as the polymerization accelerator in this study and its color is reddish violet. More CE content in polyester means smaller gel time, less curing time and deeper color in the cured product. According to experimental

results, when CE concentration is more than 0.04 wt%, polyester cures very fast and cured product has a dark amber color. When CE concentration is less than 0.01 wt%, polyester cures very slowly. Therefore, appropriate CE concentration should be between 0.01 wt% and 0.04 wt%.

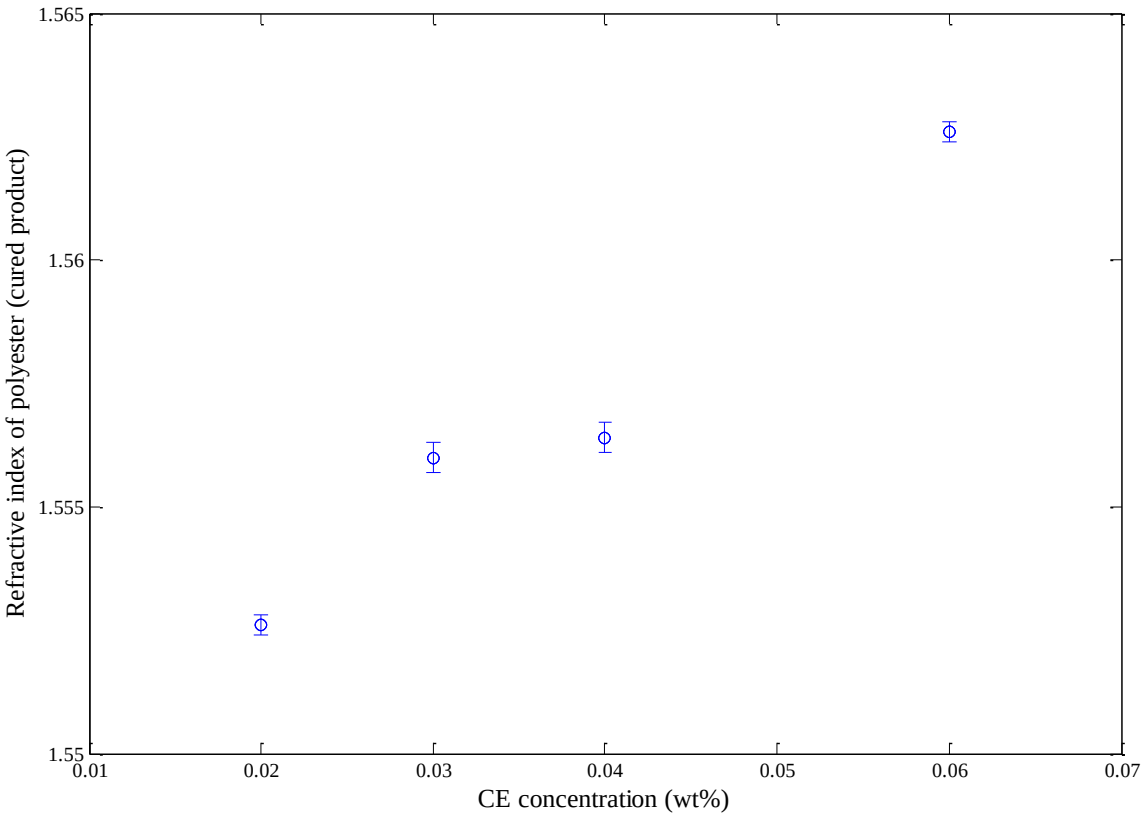

Figure 2.13 Refractive index of polyester (cured product) with different CE concentrations (curing condition: curing temperature 20 ℃, MEKP 1.2 wt%)

2.4.1.3 Effect of divinylbenzene (DV) concentration on the refractive index of polyester

Fig. 2.14 illustrates the effect of DV concentration on the refractive index of polyester. It can be seen that the refractive index of polyester increases with the increase of DV concentration. The reason for this phenomenon is that besides as a refractive index modifier, DV is also a crosslinker, with the increase of DV concentration, the crosslinking density of polyester increases which results in the increase of refractive index. Similar reports have been reported by Askadskii [38] and Murakami [39] that refractive indices of polymers can be increased by increasing the crosslinking density of polymers. When DV concentration is 3 wt%, the refractive index of polyester is 1.5581. When DV concentration is 10 wt%, the refractive index of polyester is 1.5624, which is much higher than that of glass fibers which is 1.5595. So, appropriate DV concentration is between 3 wt% and 7 wt%.

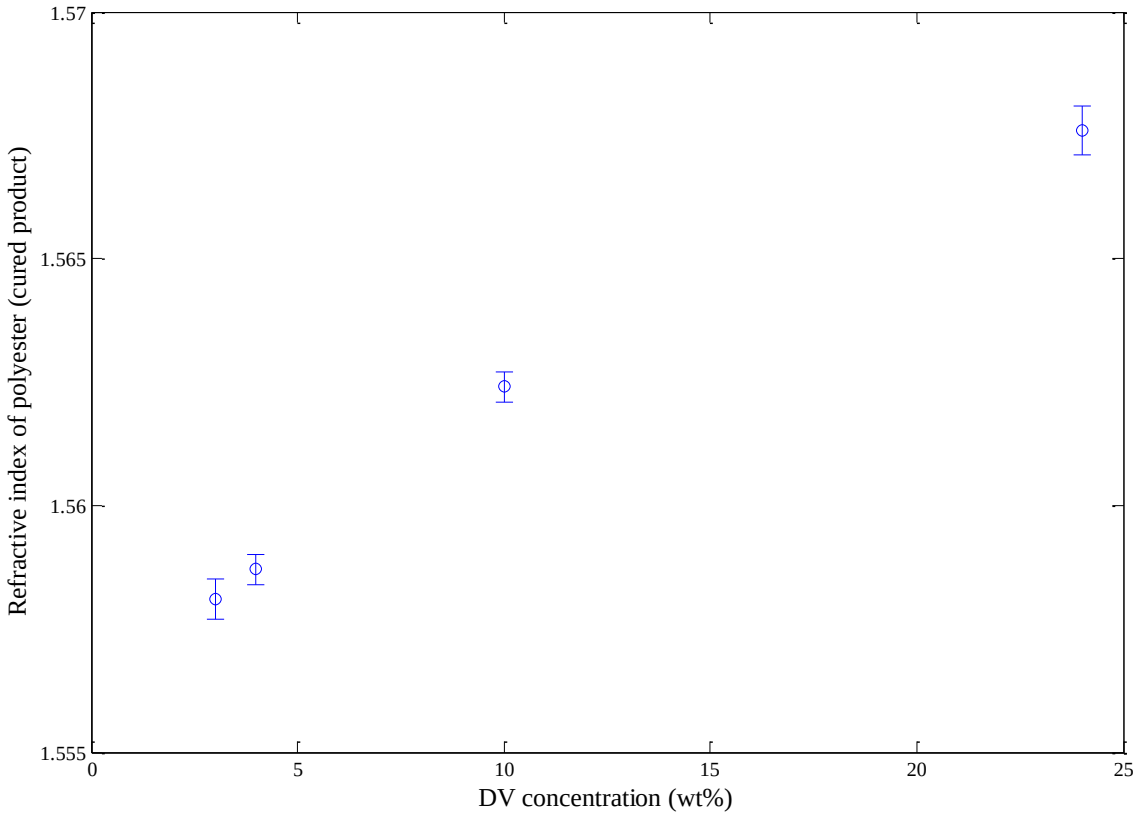

Figure 2.14 Refractive index of polyester (cured product) with different DV concentrations (curing condition: curing temperature 20 ℃, CE content 0.03 wt%, MEKP 1.2 wt%)

2.4.1.4 Effect of phenanthrene (PT) concentration on the refractive index of polyester

From Fig. 2.15, it can be seen that the refractive index of polyester increases dramatically as PT concentration increases from 0 wt% to 1.2 wt% and increases slowly with further increase in PT concentration. PT is a chemical with high refractive index (1.5943) and is used as a refractive index modifier in this research. When PT content is 0 wt%, the refractive index of polyester is 1.5560. When PT content is 1.2 wt%, the

refractive index of polyester is 1.5608. Therefore, appropriate PT concentration is between 0 wt% and 1.2 wt%.

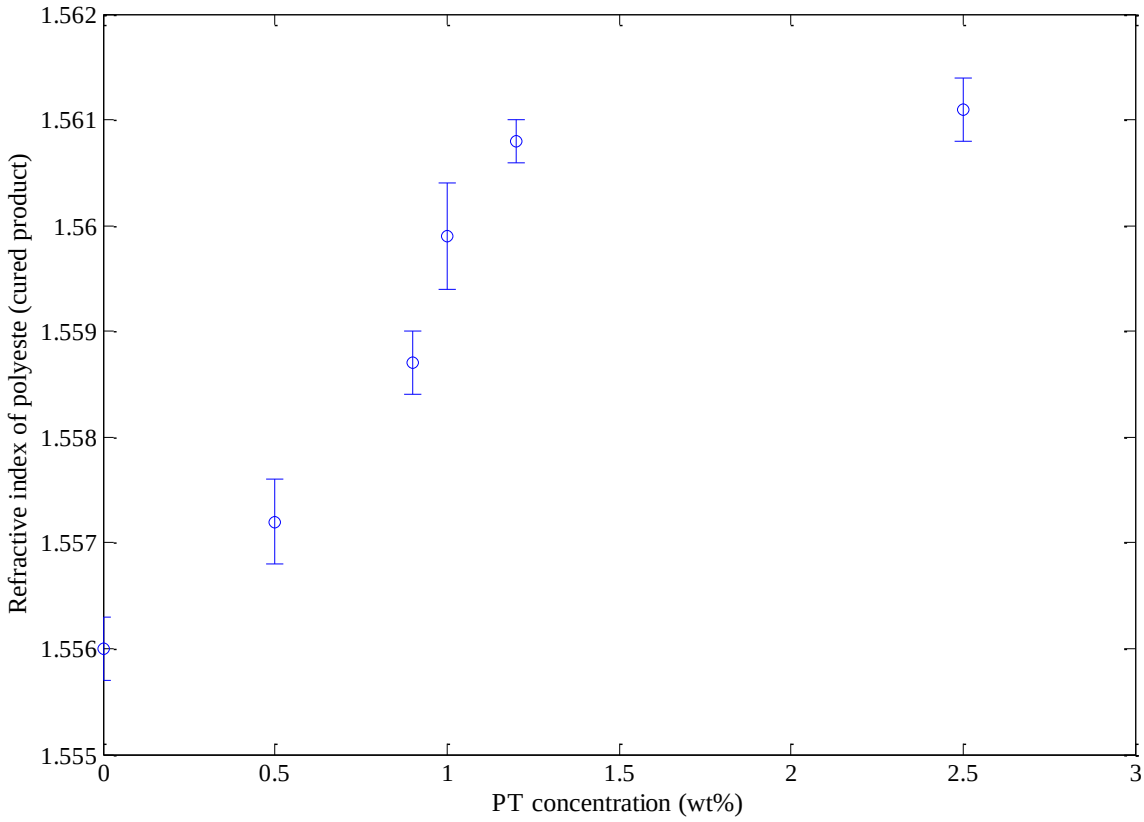

Figure 2.15 Refractive index of polyester (cured product) with different PT concentrations (curing condition: curing temperature 20 ℃, CE content 0.03 wt%, MEKP 1.2 wt%)

According to experimental results, two candidate formulations for making the transparent glass fiber-reinforced polymer composite are listed in Table 2.2. The second formulation is not recommended. Because PT is solid at room temperature, after curing, undissolved PT particles are left in the cured composite, which affects the transparency of the composite. This problem does not apply to the first formulation because DV is liquid

at room temperature. Therefore, the best formulation for making the optically transparent glass fiber-reinforced composite is: MEKP concentration=1.2 wt%, DV concentration=4 wt% and CE concentration=0.03 wt%.

Table 2.2 Candidate formulations for making the optically transparent composite

	MEKP concentration	DV concentration	PT concentration	CE concentration	Refractive index
1	1.2 wt%	4 wt%	0 wt%	0.03 wt%	1.5587
2	1.2 wt%	0 wt%	1 wt%	0.03 wt%	1.5599

2.4.2 Light transmittance

2.4.2.1 Light transmittance of the composite interlayer

Fig. 2.16 shows the light transmittance spectrum of the polyester matrix. The spectrum shows that above a wavelength of 380 nm, the light transmittance of the polyester matrix first dramatically increases to 77.5%, then slowly increases to 86.7%.

Fig. 2.16 also shows the light transmittance spectra of the composite specimens prepared using the best formulation (1.6 mm thick composite specimen with a fiber volume fraction of 24.2% and 3.2 mm thick composite specimen with a fiber volume fraction of 12.3%, both have 5 layers of fiber cloth). With the increase of light wavelength, the light transmittance of the 3.2 mm thick composite specimen first increases to 74.5%, then decreases to 65%. The light transmittance spectrum of the 1.6 mm thick composite specimen is almost the same as that of the 3.2 mm thick composite specimen. This verifies the inference derived from the theoretical analysis that the light

transmittance of the composite will not be affected by the change of fiber volume fraction if the change does not affect the number of fiber layers the light encounters.

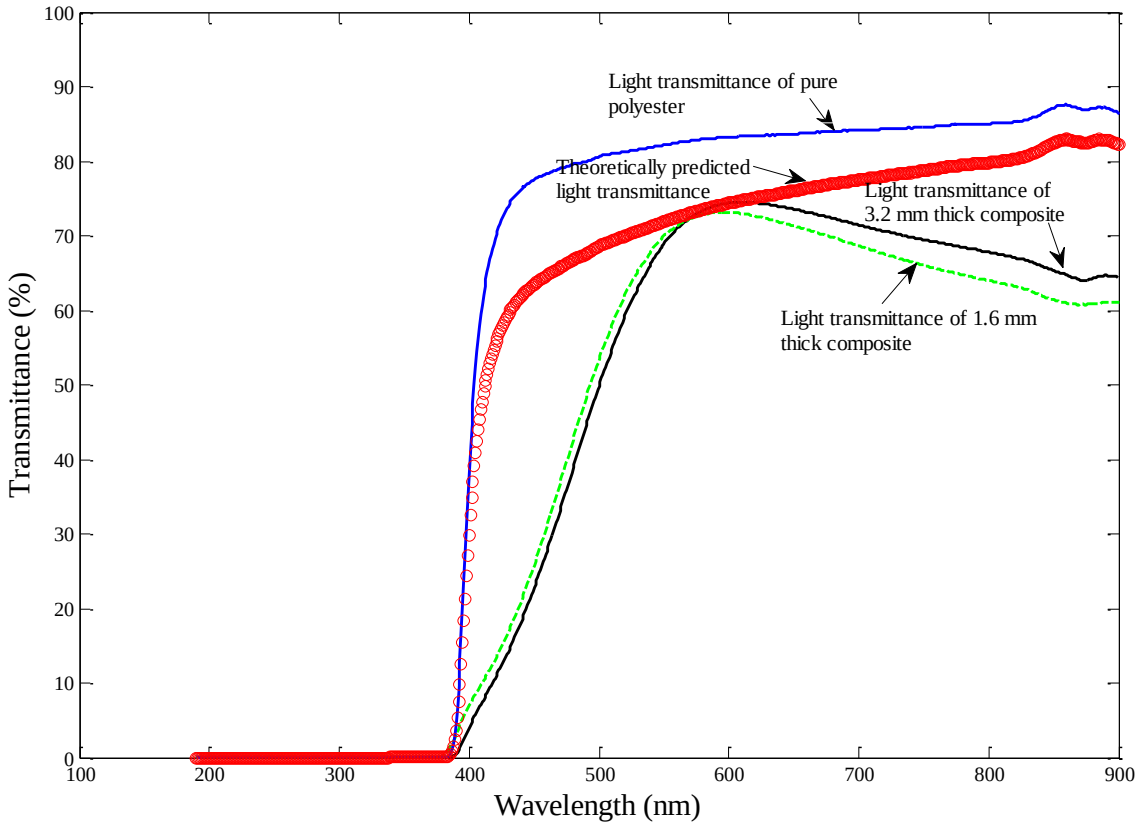

Figure 2.16 Comparison between experimentally measured light transmittance and theoretically predicted light transmittance

The light transmittance of the composite with 5 layers of fiber cloth is predicted using equation (2.13) and plotted in Fig. 2.16. It can be observed that at a wavelength of 589 nm, the theoretically calculated light transmittance coincides with the experimentally measured light transmittance of the 3.2 mm thick composite specimen and almost coincides with the light transmittance of the 1.6 mm thick composite specimen. Beyond

or below this wavelength, the theoretically calculated light transmittance curve strays from the experimentally measured light transmittance curves. The difference between the calculated result and the measured results is due to the wavelength dependence of refractive index [40]. In this study, all measured refractive indices are the refractive indices at 589 nm. Therefore at 589 nm, the refractive index difference between glass fibers and the polyester matrix is the 'real refractive index difference'. Equation (2.13) can effectively predict the light transmittance at this wavelength. Beyond or below this wavelength, because of the wavelength dependence of refractive index, the refractive indices of the polyester matrix and glass fibers both change which means the refractive index difference between them is different from the difference at 589 nm. So, except 589 nm, at other wavelengths, equation (2.13) use 'fake' refractive index difference (refractive index difference at 589 nm) to predict the light transmittance which results in the mismatch of the theoretically predicted result and the experimentally measured results. If the relationship between refractive index and wavelength of glass fibers and the polyester matrix can be obtained, the light transmittance over the whole spectrum could be predicted more precisely by the developed model.

The appearance of the glass fiber-reinforced composite prepared using the best formulation (3.2 mm thick, the appearance of the 1.6 mm thick composite is similar) and the polyester matrix is shown in Fig. 2.17. Characters underneath the composite plate and the polyester plate can be clearly read, indicating that the composite and the polyester matrix are both optically transparent.

Figure 2.17 Readability of text through the glass fiber-reinforced composite plate and the polyester plate

Besides the light wavelength, temperature may also cause the change of the refractive index difference since the polyester matrix and glass fibers have different refractive index-temperature relations. The composite plate shown above was heated to 60 ℃ (the maximum expected using temperature) for 3 h and no transparency change was noticed, which indicates that in this study, the effect of temperature on the transparency can be neglected.

2.4.2.2 Light transmittance of the laminated glass

Fig. 2.18 shows the light transmittance of the laminated glass utilizing the glass fiber-reinforced composite interlayer over a wavelength range of 190 to 900 nm. The light transmittance of the laminated glass is above 60% when the wavelength is above 482 nm. The highest transmittance is 84.4% when the wavelength is 577 nm. This result

means the fabricated laminated glass has good transparency in the visible light range. The good transparency is achieved by using the transparent composite interlayer.

Appearance of the laminated glass is shown in Fig. 2.19. Through the laminated glass, the backside view can be clearly observed, which shows the fabricated laminated glass has good transparency. This result coincides with the light transmittance spectrum analysis result shown above.

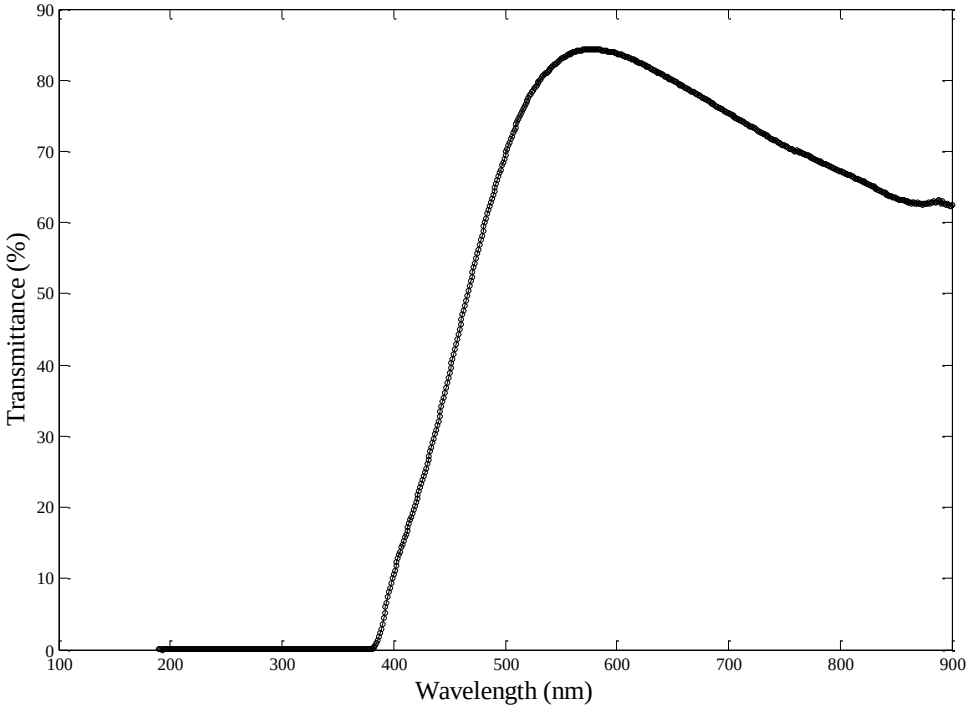

Figure 2.18 Light transmittance spectrum of the laminated glass

Figure 2.19 Appearance of the fabricated laminated glass

2.4.3 Quasi-static mechanical properties

The longitudinal stress-strain curves of the glass fiber-reinforced composite specimens (1.6 mm thick composite and 3.2 mm thick composite) are shown in Fig. 2.20, Young's modulus of the composite specimens is calculated using equation (2.1). The value of 3.2 mm thick composite is 7.67 GPa and the value of 1.6 mm thick composite is 12.33 GPa, which are both much higher than that of the neat polyester (~3 GPa) [41]. The initial linear parts of the stress-strain curves are plotted in Fig. 2.21 and the corresponding lateral stress-strain curves in the same region are also plotted in Fig. 2.21. Poisson's ratio v_{12} of the composite, which is 0.33 for 3.2 mm thick composite and 0.39 for 1.6 mm thick composite, is found by using equation (2.2) and Fig. 2.21. The shear stress-strain curves of the composite specimens in the initial loading range are plotted in Fig. 2.22. The shear

modulus of the composite is calculated using equation (2.3). For 3.2 mm thick composite, shear modulus is 2.14 GPa and for 1.6 mm thick composite, shear modulus is 3.39 GPa.

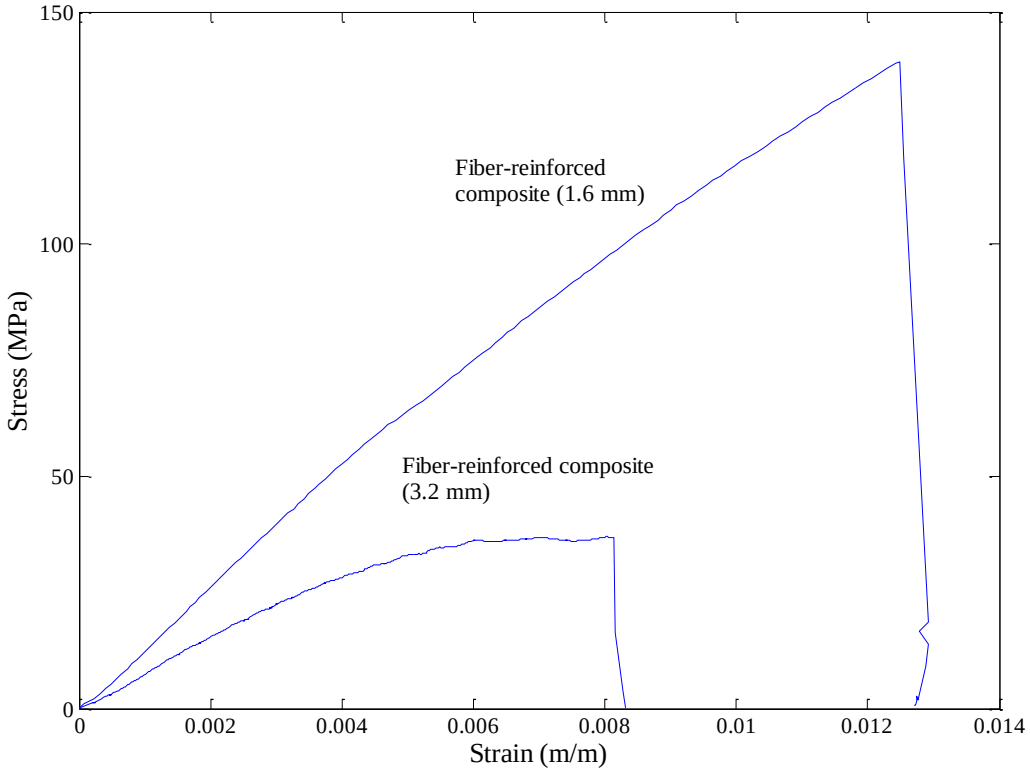

Figure 2.20 Stress-strain curves of the glass fiber-reinforced composites

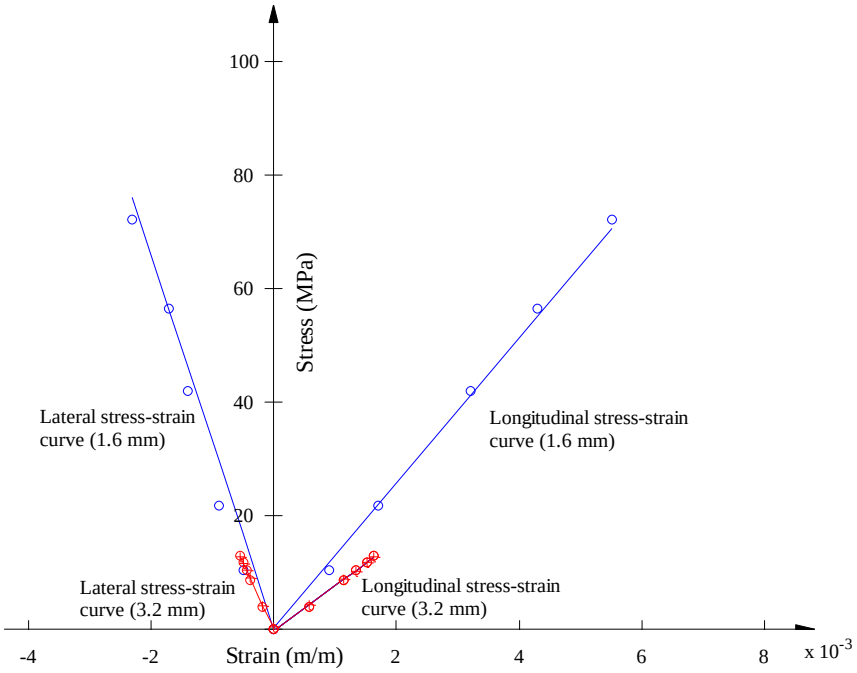

Figure 2.21 Stress vs. strain curves of the composites in the initial linear region

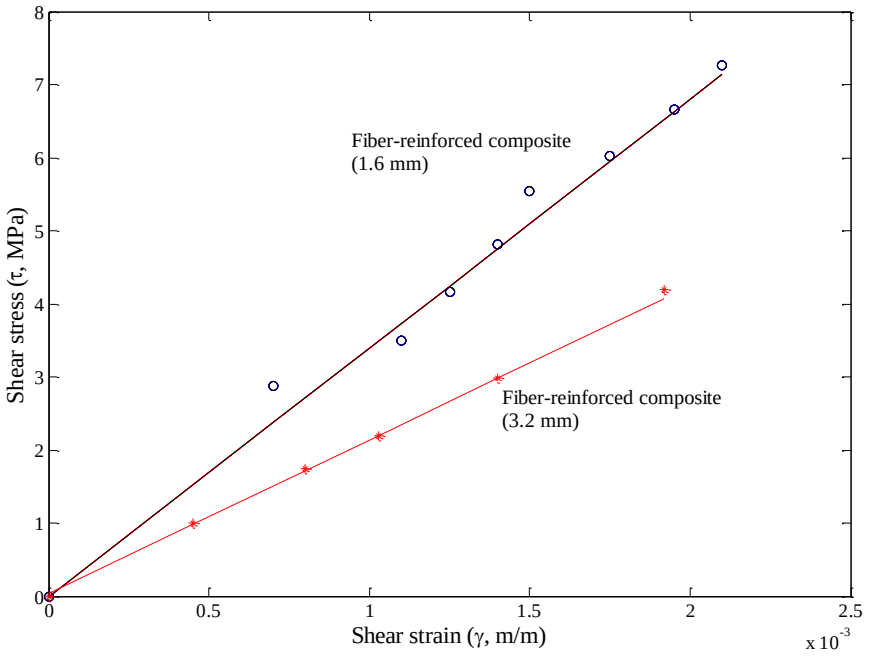

Figure 2.22 Shear stress-strain curves of the glass fiber-reinforced composites

All quasi-static mechanical properties of the composites are listed in Table 2.3.

Table 2.3 Quasi-static mechanical properties of the glass fiber-reinforced composites

	Tensile strength (σ_T, MPa)	Failure strain (ε_f)	Young's modulus (E, GPa)	Poisson's ratio (ν_{12})	Shear modulus (τ, GPa)
Fiber-reinforced composite (3.2 mm thick, fiber volume fraction 12.3%)	41.95	0.0082	7.67	0.33	2.14
Fiber-reinforced composite (1.6 mm thick, fiber volume fraction 24.2%	139.9	0.0125	12.33	0.39	3.39

2.4.4 Fracture toughness

The load-displacement curves for 0/90 º woven glass fiber-reinforced composite specimens with different initial crack lengths are shown in Fig. 2.23. From Fig. 2.23, it can be seen that for specimens with small cracks, fracture causes a sharp drop in load after the maximum load; for specimens with large cracks, fracture causes a gradual drop in load after the maximum load. The reason for this phenomenon is that the strain energy stored in specimens with small cracks is sufficient to cause sudden failure [42]. It is not the case for specimens with large cracks.

From Fig. 2.23, it can also be seen that the maximum carrying load of the composite decreases with the increase of initial crack length. The displacement at maximum load (critical displacement) decreases as initial crack length increases from 3.8 to 13.3 mm and remains nearly constant at 0.9 mm with further increase in initial crack length. The

reason for this phenomenon is that when initial crack length is longer than the critical initial crack length (13.3 mm), the fracture behavior of the composite is mainly governed by the initial crack so that the critical displacement is nearly constant. When initial crack length is less than 13.3 mm, the fracture behavior of the composite is influenced not only by the initial crack, but also by elastic and plastic deformations away from the crack plane [28]. Therefore, the critical displacement is not constant in this crack length region. It increases with the decrease of initial crack length.

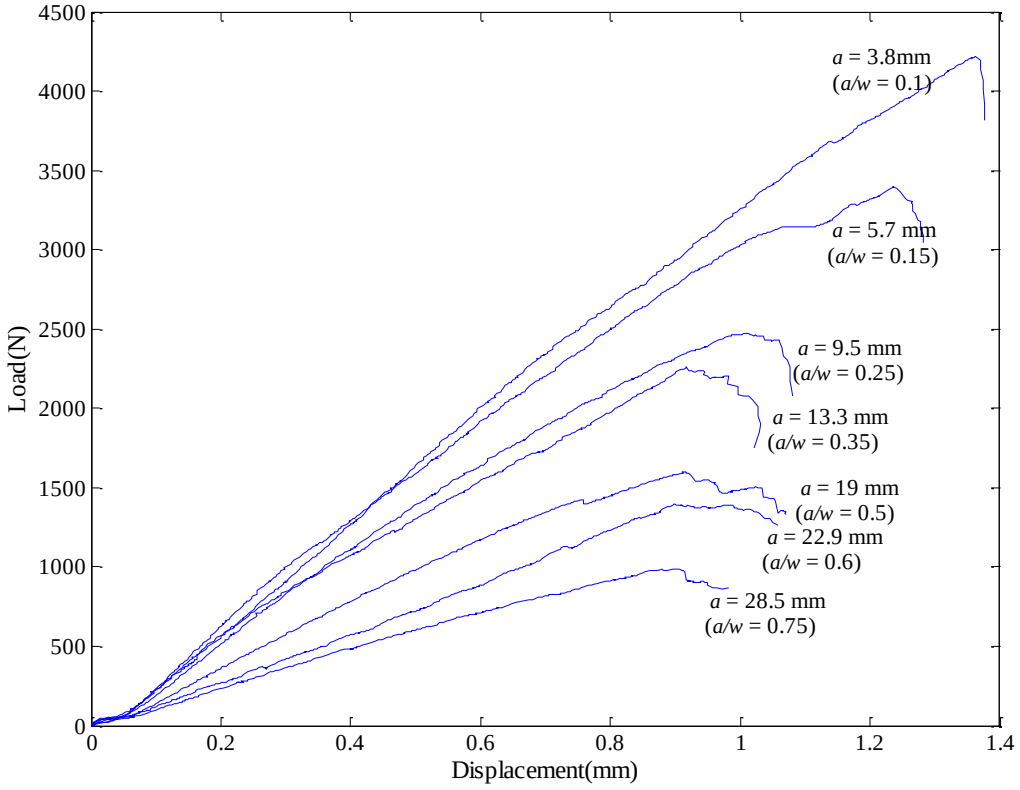

Figure 2.23 Load-displacement curves for fiber-reinforced composite specimens with different initial crack lengths (*a* is crack length and *w* is specimen's width)

The load-displacement curves shown in Fig. 2.23 are used to calculate the potential energy *U* in equation (2.5). It should be pointed out that when displacement is constant,

the potential energy U is equal to the strain energy which can be obtained by measuring the area under the load-displacement curve [31]. In order to obtain the J-integral value at different displacements, six displacements (0.18 mm, 0.36 mm, 0.54 mm, 0.72 mm, 0.90 mm and 0.95 mm) are chosen. For each displacement, the area under the load-displacement curves are measured, divided by thickness (B) and plotted against initial crack lengths (Fig. 2.24).

From Fig. 2.24, it can be seen that for a given displacement, the strain energy per unit thickness of the glass fiber-reinforced composite decreases as initial crack length increases, because the specimen with larger initial crack length has smaller load-carrying ability. For each displacement, variation of strain energy per unit thickness with initial crack length can be represented by two straight lines. Two lines intersect at a crack length of 13.3 mm, which shows a change in fracture behavior at this crack length. This result corresponds to the result observed in Fig. 2.23, which shows the fracture behavior of the composite changes at the crack length of 13.3 mm. J-integral values are obtained by calculating the slopes of the lines shown in Fig. 2.24. Based on the initial crack length ($a/w \geq 0.35$ or $a/w < 0.35$), two J-integral value versus displacement curves are obtained and plotted in Fig. 2.25. From Fig. 2.25, it can be seen that the J-integral value at the critical displacement, referred to as the critical value of J-integral (J_c), is 22.1 kJ/m^2 when $a/w \geq 0.35$. When $a/w < 0.35$, J_c can't be evaluated directly through Fig. 2.25 since the corresponding J-integral curve does not reach the critical displacements in this range. According to the reference [28], the J_c value for small initial crack length (here is $a/w <$

0.35) is close to the J_c value for large crack length (here is $a/w \geq 0.35$) . Therefore, in this research, the J_c value of glass fiber-reinforced composite is determined as 22.1 kJ/m^2.

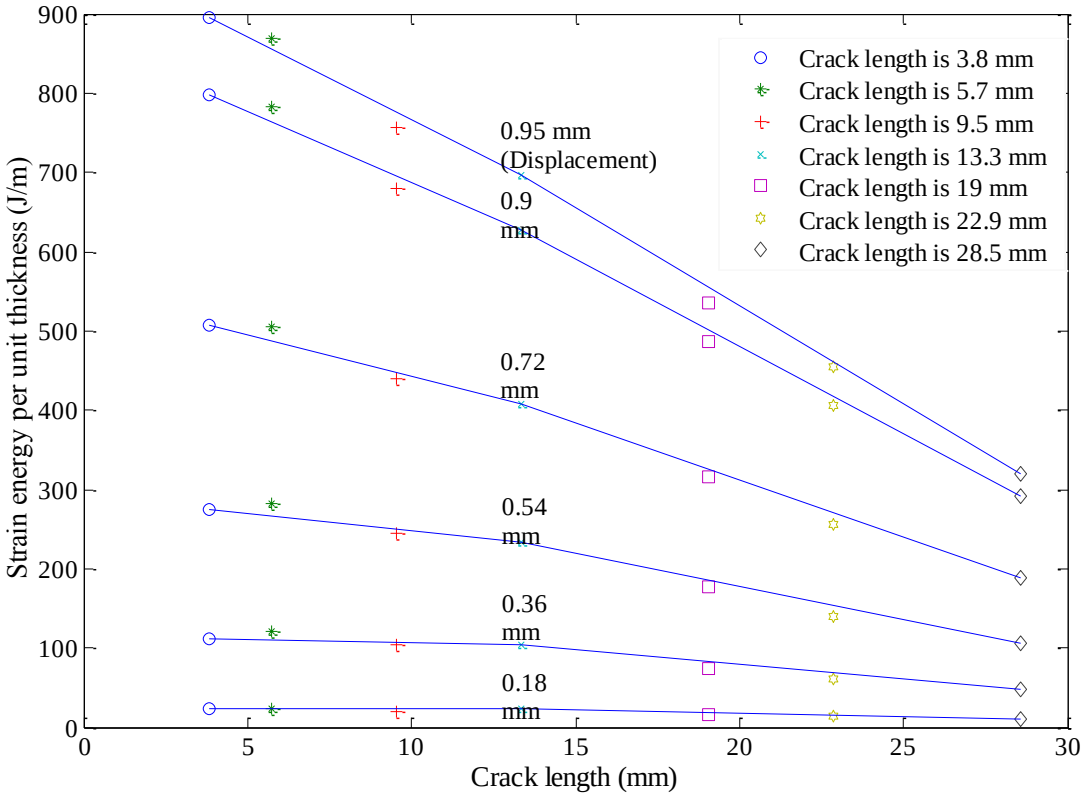

Figure 2.24 Strain energy per unit thickness versus initial crack length at different displacements

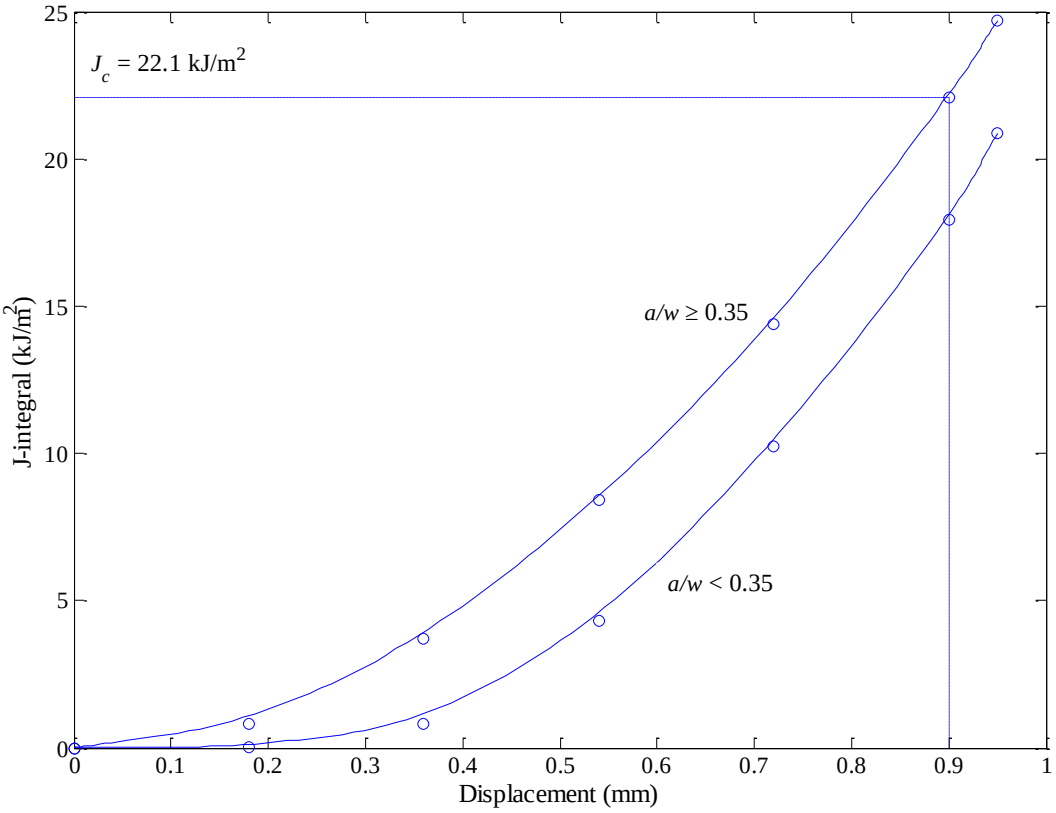

Figure 2.25 J-integral curves of the composite

2.4.5 Dynamic mechanical properties

The strain rate range studied in this research is approximately between 400-1000 s^{-1}, which is typical strain rate range for blast loading. Within this strain rate range, the valid experimental results should satisfy two required conditions of SHB test. These conditions are 1) achievement of constant strain rate and 2) achievement of stress equilibrium for duration of the incident pulse.

The effect of strain rate on the dynamic mechanical properties of the glass fiber-reinforced composite is presented in Fig. 2.26. It clearly shows that the dynamic stress-

strain curve of the composite is affected by strain rate. At different strain rates, the compressive modulus and compressive strength values of the composite are listed in Table 2.4. The compressive modulus presented in this article should be regarded as the approximate compressive modulus since there is an unavoidable uncertainty in determining the compressive modulus by using the SHB technique [16, 43]. From Table 2.4, it can be seen that the compressive modulus of the composite increases as strain rate increases. Also, it can be seen that the compressive strength of the composite increases as strain rate increases (Fig. 2.27). The compressive strength increases by about 25% as strain rate increasing from 407 s^{-1} to 960 s^{-1}. Similar trends have been reported by Li et al. [44] and Kim et al. [16]. This phenomenon may be caused by the decrease of polymer chains' molecular mobility with the increase of strain rate [45, 46]. A linear equation (2.14) is used to characterize the rate dependence of the compressive strength. The linear relationship is

$$\sigma_c = 0.099 * \dot{\varepsilon} + 174.15 \qquad (2.14)$$

where σ_c is the compressive strength, $\dot{\varepsilon}$ is the strain rate. The limitation of this relationship is that it is only applicable to the strain rate between 400 and 1000 s^{-1}.

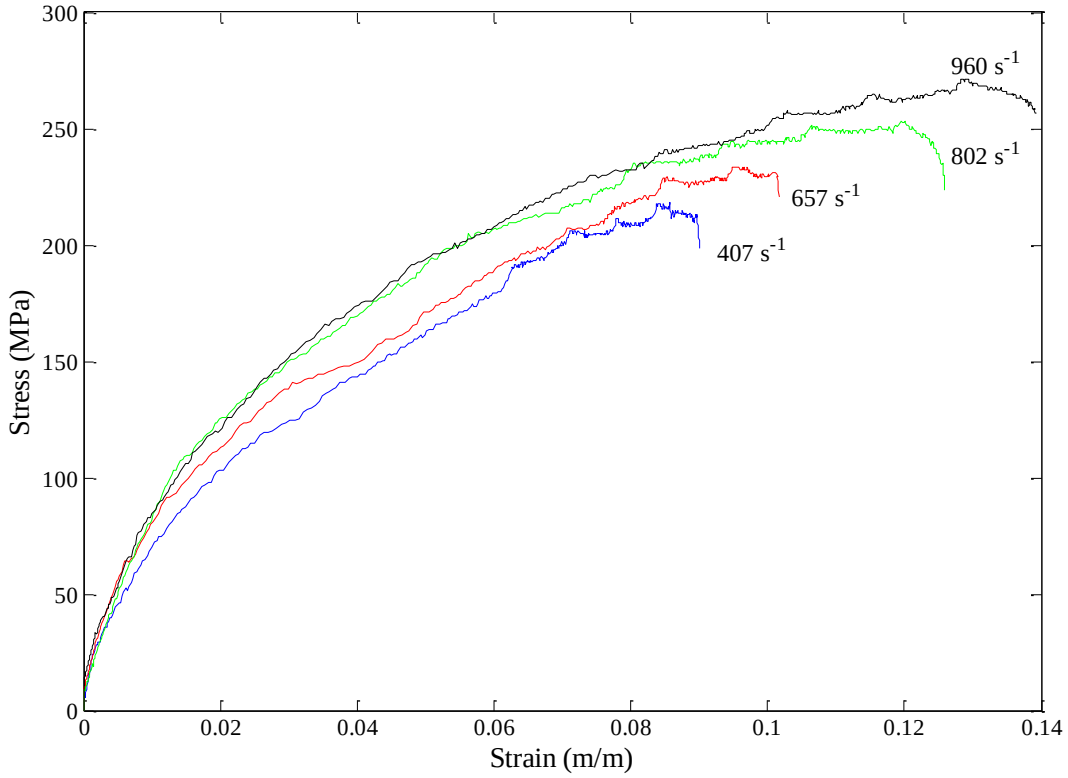

Figure 2.26 Stress-strain curves of the glass fiber-reinforced composite at different strain rates

Table 2.4 Dynamic mechanical properties of the glass fiber-reinforced composite

Strain rate (s^{-1})	Compressive modulus (GPa)	Compressive strength (MPa)
407	9.29	218.32
657	11.01	233.27
802	11.21	253.46
960	12.02	271.03

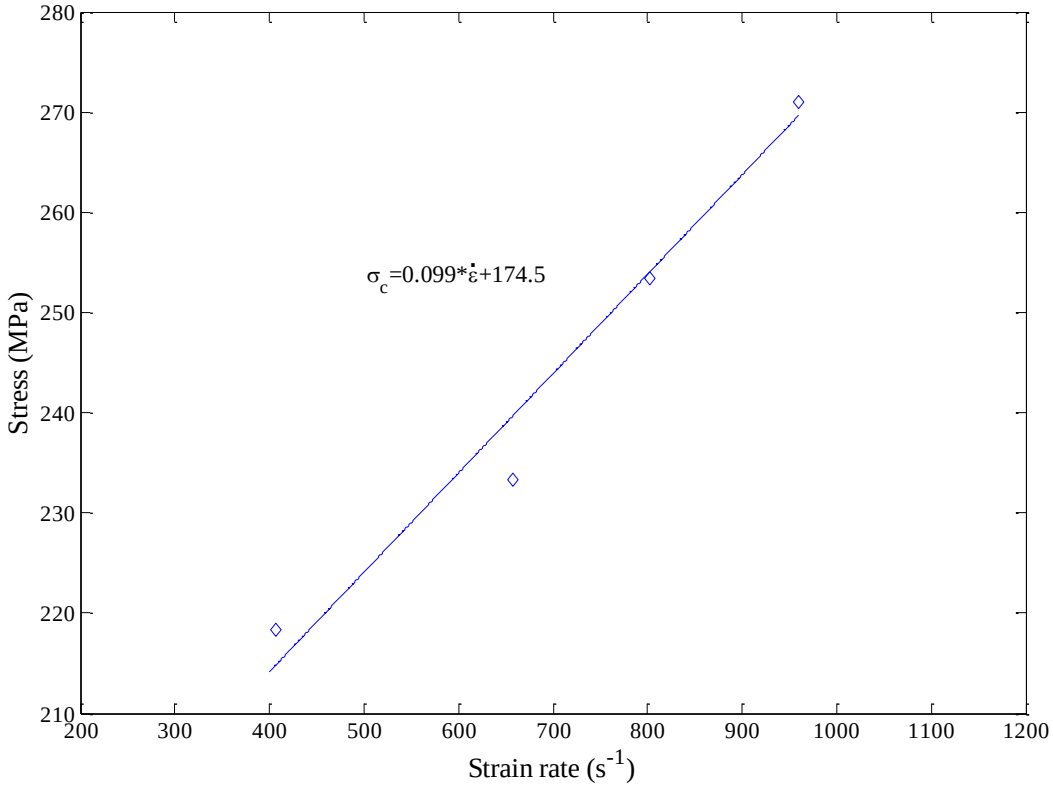

Figure 2.27 Effect of strain rate on compressive strength of the glass fiber-reinforced composite

After SHB tests, the fracture morphology of the composite was examined using an Olympus optical microscope (BX41M-LED, Olympus Co., Japan) (Fig. 2.28). When strain rate is 407 s^{-1}, there are no clearly visible cracks on the impact surface of the composite (Fig. 2.28 (a)). When strain rate is 657 s^{-1}, some fiber lines can be clearly observed on the surface, which means fibers begin to delaminate from the polyester matrix (Fig. 2.28 (b)). When strain rate is 802 s^{-1}, cracks can be observed on the surface (Fig. 2.28 (c)). When strain rate is 960 s^{-1}, a network of cracks appears on the surface ((Fig. 2.28 (d)). So, the impact-introduced failure process of the composite is as follows:

with the increase of strain rate, fibers first delaminate from the polyester matrix as a consequence of fiber/matrix interfacial debonding. Then, on further increase in strain rate, the delamination grows continuously, surface cracks tend to appear and propagate into the matrix. Specimens tested with strain rates higher than 1000 s^{-1} broke into pieces during the test.

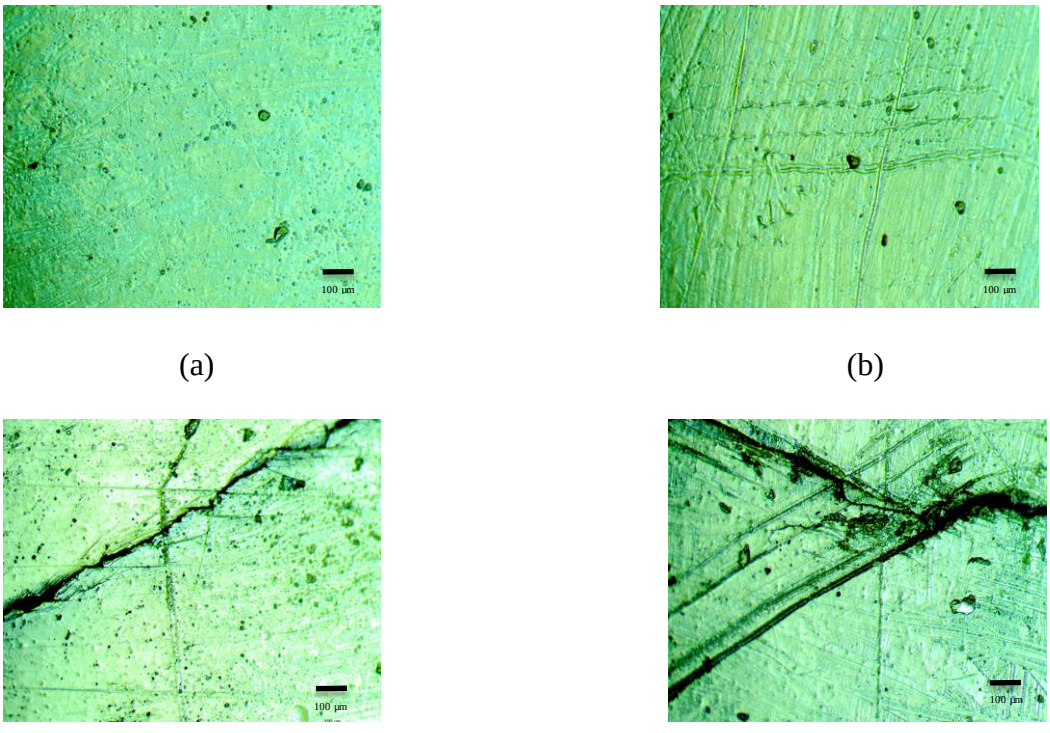

(a) (b)

(c) (d)

Figure 2.28 Surface micrographs of the glass fiber-reinforced composite at different strain rates: (a) 407 s^{-1}; (b) 657 s^{-1}; (c) 802 s^{-1}; (d) 960 s^{-1}

2.4.6 Blast resistance testing results

U.S. General Services Administration (GSA) blast loading levels C, D and E were used for tests done at ERDC. Level C specifies a minimum peak pressure of 4 psi (25.8

kPa) and impulse of 28 psi-msec (193 kPa-msec), while level D specifies a minimum peak pressure of 10 psi (69 kPa) and impulse of 89 psi-msec (614 kPa-msec). Level E is not specifically quantified by GSA but for this study we assumed level E as peak pressure greater than 20 psi (138 kPa) and impulse greater than 115 psi-msec (793 kPa-msec). Laminated window panels were tested under different blast loading levels. Window panels of 3/8 inch (9.5 mm) total thickness consisting of a 1/8 inch (3.2 mm) thick transparent composite interlayer laminated to two 1/8 inch (3.2 mm) thick tempered glass sheets were tested under level C and D with no damage to the windows. The same window construction as above but with a total thickness of 7/16 inch (11.1 mm), due to use of 1 mm thick urethane based adhesive layer on each side of the interlayer, was tested at level E, which resulted in cracks in the glass glazing with no fallout of glass and minimal damage to the composite interlayer, as shown in Fig. 2.29. A 3/8 inch thick window panel was tested under a blast condition over the minimum specified level E, which resulted in extensive damage to the window panel and it was partially dislodged from the frame as shown in Fig. 2.30. A thicker window of 5/8 inch (16 mm) total thickness consisting of two composite interlayers laminated to three glass layers (each 1/8 inch or 3.2 mm thick) was tested under blast loading well over the minimum specified level E, which resulted in cracking of the frontal and rear glass layers with no apparent damage to the composite interlayers or any fallout of glass, as seen in Fig. 2.31. The above mentioned blast testing demonstrates the viability of the novel glass window panel utilizing a transparent fiber-reinforced polymer composite interlayer under high intensity blast loading.

Field experiments are expensive and time-consuming. In order to save money and time, a numerical model is developed to predict the dynamic response of the laminated glass panel under different blast loading conditions. This model will be presented in the next chapter.

Figure 2.29 Laminated glass window panel was cracked after the GSA level E blast test. Both the outer surfaces of the glass plies were smooth to touch and minor damage to the composite interlayer

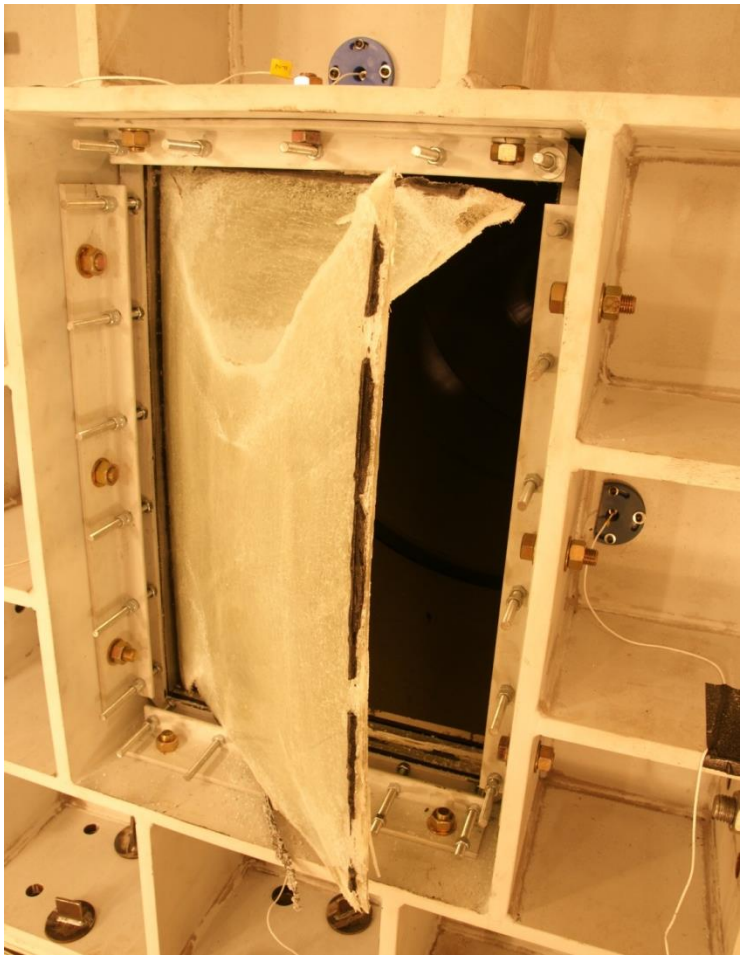

Figure 2.30 Level E blast loading resulted in severe damage to the window panel

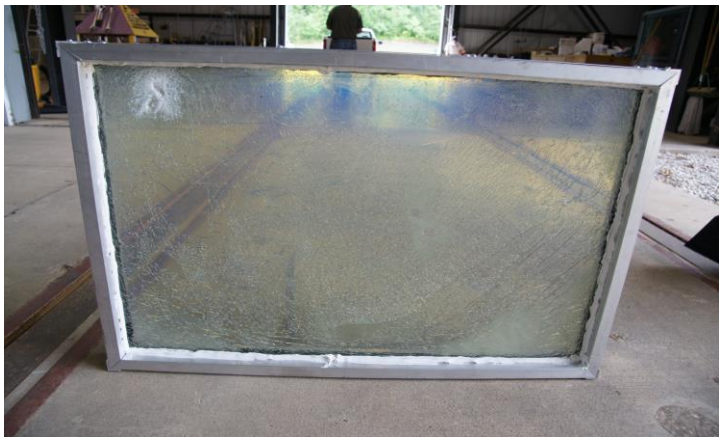

Figure 2.31 Thicker glass window panel after Level E blast loading

2.5 Summary

An optically transparent woven glass fiber-reinforced polyester matrix composite has been successfully fabricated and utilized as an interlayer in a laminated glass panel.

The properties of the composite interlayer and the laminated glass were studied. The main findings that can be inferred are as follows:

(1) A theoretical model for predicting the light transmittance of woven glass fiber-reinforced composite has been proposed. Theoretical analysis shows the transparency of the glass fiber-reinforced composite can be improved by reducing the refractive index difference between glass fibers and its matrix. In this research, the refractive index of glass fibers was considered as fixed. So the refractive index difference was minimized by chemically changing the refractive index of the polyester matrix. Effects of MEKP, CE, DV and PT concentrations on the refractive index of the polyester matrix were investigated. The best formulation for making an optically transparent composite is: MEKP concentration=1.2 wt%, DV concentration=4 wt% and CE concentration=0.03 wt%.

(2) The theoretical model also shows that besides the refractive index difference, the transparency of the glass fiber-reinforced composite also depends on the number of fiber layers the incident light encounters. This inference has been verified by experimental results.

(3) The light transmittance spectra and appearance of the composite prepared using the best formulation and the corresponding laminated glass indicate the developed glass

fiber-reinforced polymer composite and the laminated glass both have good transparency in the visible light region.

(4) Quasi-static test results show that the glass fiber-reinforced composite has much better mechanical properties than the polyester matrix.

(5) The fracture toughness of the composite based on the J-integral method is J_c= 22.1 kJ/m^2.

(6) Split Hopkinson bar test results show that the dynamic mechanical properties of the composite are strain rate sensitive. Compressive modulus and compressive strength both increase with the increase of strain rate over the range 400-1000 s^{-1}.

(7) Blast loading tests done at ERDC show the new laminated glass panels perform well under GSA specified C, D and E blast loading levels. This demonstrates the viability of the new laminated glass window panel under high intensity blast loading.

REFERENCES

[1] O'Brien, D.J., and Parquette, B., 2012, "*Polymer toughness transfer in a transparent interpenetrating glass–polymer composite*", Composites Science and Technology, **73**, pp.57-63.

[2] Brennan, R.E., and Green, W.H., 2011, "*Nondestructive characterization of low velocity impact damage in transparent laminate systems*", Hoboken, NJ: John Wiley & Sons.

[3] Iba, H., Chang, T., and Kagawa, Y., 2002, "*Optically transparent continuous glass fibre-reinforced epoxy matrix composite: fabrication, optical and mechanical properties*", Composites Science and Technology, **62**, No.15, pp.2043-2052.

[4] Olson, J.R., Day, D.E., and Stoffer, J.O., 1992, "*Fabrication and mechanical properties of an optically transparent glass fiber/polymer matrix composite*", Journal of Composite Materials, **26**, No.8, pp.1181-1192.

[5] Novak, B.M., 1993, "*Hybrid nanocomposite materials—between inorganic glasses and organic polymers*", Advanced Materials, **5**, No.6, pp.422-433.

[6] Moriwaki, T., 1996, "*Mechanical property enhancement of glass fibre-reinforced polyamide composite made by direct injection moulding process*", Composites Part A: Applied Science and Manufacturing, **27**, No.5, pp.379-384.

[7] Iba, H., Naganuma, T., Matsumura, K., and Kagawa, Y., 1999, "*Fabrication of transparent continuous oxynitride glass fiber-reinforced glass matrix composite*", Journal of Materials Science, **34**, No.23, pp.5701-5705.

[8] Iba, H., and Kagawa, Y., 1998, "*Light transmittance of continuous fibre-reinforced composites: analysis, model experiment and parametric study*", Philosophical Magazine Part B, **78**, No.1, pp.37-52.

[9] Sarva, S., Mulliken, A.D., Boyce, M.C., and Hsieh, A.J., 2004, "*Mechanics of transparent polymeric material assemblies under projectile impact: simulations and experiments*", DTIC Document.

[10] Yahya, M.Y., Cantwell, W.J., Langdon, G., and Nurick, G., 2008, "*The blast behavior of fiber reinforced thermoplastic laminates*", Journal of Composite Materials, **42**, No.21, pp.2275-2297.

[11] Avci, A., Arikan, H., and Akdemir, A., 2004, "*Fracture behavior of glass fiber reinforced polymer composite*", Cement and Concrete Research, **34**, No.3, pp.429-434.

[12] Nikpur, K., Chen, Y., and Kardos, J., 1990, "*Fracture toughness of unidirectional short-fiber reinforced epoxy composites*", Composites Science and Technology, **38**, No.2, pp.175-191.

[13] Mouritz, A., 2001, "*Ballistic impact and explosive blast resistance of stitched composites*", Composites Part B: Engineering, **32**, No.5, pp.431-439.

[14] Pankow, M., Salvi, A., Waas, A., Yen, C., and Ghiorse, S., 2011, "*Split Hopkinson pressure bar testing of 3D woven composites*", Composites Science and Technology, **71**, No.9, pp.1196-1208.

[15] Hokka, M., Kuokkala, V.T., and Ihme, S., 2009, "*Dynamic tensile testing of polyamide sheets using the HSB technique*", Proceedings of the 2009 SEM Annual Conference and Exposition on Experimental and Applied Mechanics, pp.1-7.

[16] Kim, W., Argento, A., Lee, E., Flanigan, C., Houston, D., and Harris, A., 2012, "*High strain-rate behavior of natural fiber-reinforced polymer composites*", Journal of Composite Materials, **46**, No.9, pp.1051-1065.

[17] Jiang, F., and Vecchio, K.S., 2009, "*Hopkinson bar loaded fracture experimental technique: a critical review of dynamic fracture toughness tests*", Applied Mechanics Reviews, **62**, No.6, pp.1-39.

[18] Tekalur, S.A., Shukla, A., and Shivakumar, K., 2008, "*Blast resistance of polyurea based layered composite materials*", Composite Structures, **84**, No.3, pp.271-281.

[19] Hosur, M., Alexander, J., Jeelani, S., Vaidya, U., and Mayer, A., 2003, "*High strain compression response of affordable woven carbon/epoxy composites*", Journal of Reinforced Plastics and Composites, **22**, No.3, pp.271-296.

[20] Hosur, M., Alexander, J., Vaidya, U., Jeelani, S., and Mayer, A., "*Studies on the off-axis high strain rate compression loading of satin weave carbon/epoxy composites*", Composite Structures, **63**, No.1, pp.75-85.

[21] Shokrieh, M.M., and Omidi, M.J., 2009, "*Compressive response of glass–fiber reinforced polymeric composites to increasing compressive strain rates*", Composite Structures, **89**, No.4, pp.517-523.

[22] Cao, M.S., Song, W.L., Zhou, W., Wang, D.W., Rong, J.L., and Yuan, J., 2010, "*Dynamic compressive response and failure behavior of fiber polymer composites embedded with tetra-needle-like ZnO nanowhiskers*", Composite Structures, **92**, No.12, pp.2984-2991.

[23] Shokrieh, M.M., and Omidi, M.J., 2009, "*Tension behavior of unidirectional glass/epoxy composites under different strain rates*", Composite Structures, **88**, No.4, pp.595-601.

[24] Schoßig, M., Bierögel, C., Grellmann, W., and Mecklenburg, T., 2008, "*Mechanical behavior of glass-fiber reinforced thermoplastic materials under high strain rates*", Polymer Testing, **27**, No.7, pp.893-900.

[25] Song, B., Chen, W., and Weerasooriya, T., 2003, "*Quasi-static and dynamic compressive behaviors of a S-2 glass/SC15 composite*", Journal of Composite Materials, **37**, No.19, pp.1723-1743.

[26] ASTM, "*Standard test method for tensile properties of polymer matrix composite materials*", West Conshohocken, PA: ASTM International.

[27] ASTM, "*Standard test method for in-plane shear response of polymer matrix composite materials by tensile test of a ±45° laminate*", West Conshohocken, PA: ASTM International.

[28] Agarwal, B., Kumar, P., and Khanna, S.K., 1986, "*Determination of the fracture toughness of fabric reinforced composites by the J-integral approach*", Composites Science and Technology, **25**, No.4, pp.311-323.

[29] Cherepanov, G., 1967, "*Crack propagation in continuous media PMM*", Journal of Applied Mathematics and Mechanics, **31**, No.3, pp.503-512.

[30] Rice, J.R., 1967, "*A path independent integral and the approximate analysis of strain concentration by notches and cracks*", Journal of Applied Mechanics, **35**, No.2, 379-386.

[31] Landes, J., and Begley, J., 1972, "*The effect of specimen geometry on J/c. fracture toughness*", Proceedings of the 1971 National Symposium on Fracture Mechanics, pp.24-39.

[32] Gama, B.A., Lopatnikov, S.L., and Gillespie, J.W., 2004, "*Hopkinson bar experimental technique: A critical review*", Applied Mechanics Reviews, **57**, No.4, pp.223-250.

[33] Phan, H.T., 2012, "*High strain rate behavior of graphene reinforced polyurethane composites*", Columbia, MO: University of Missouri.

[34] Woldesenbet, E., and Vinson, J.R., 1999, "*Specimen geometry effects on high-strain-rate testing of graphite/epoxy composites*", AIAA Journal, **37**, No.9, pp.1102-1106.

[35] ASTM, "*Standard test method for ignition loss of cured reinforced resins*", West Conshohocken, PA: ASTM International.

[36] Aditi, C., 2012, "*On-orbit assessment of satellite structural properties via robust structural health monitoring*", Tempe, AZ: Arizona State University.

[37] Van, D.H.H.C., 1981, "*Light scattering by small particles*", Mineola, NY: Dover Publications.

[38] Askadskii, A.A., 1990, "*Influence of crosslinking density on the properties of polymer networks*", Polymer Science USSR, **32**, No.10, pp.2061-2069.

[39] Murakami, K., and Ando, S., 2011, "*Effects of UV crosslinking under high temperature on the refractive indices and aggregation structures of benzophenone-containing polyimides*", Journal of Photopolymer Science and Technology, **24**, No.3, pp.277-282.

[40] Jenkins, F.A., and White, H.E., 1957, 3rd ed., "*Fundamentals of optics*", New York, NY: McGraw-Hill.

[41] Pothan, L.A., Mai, Y., Thomas, S., and Li, R., 2008, "*Tensile and flexural behavior of sisal fabric/polyester textile composites prepared by resin transfer molding technique*", Journal of Reinforced Plastics and Composites, **27**, No.16-17, pp.1847-1866.

[42] Agarwal, B.D., Patro, B.S., and Kumar, P., 1984, "*J integral as fracture criterion for short fibre composites: An experimental approach*", Engineering Fracture Mechanics, **19**, No.4, pp.675-684.

[43] Al-Mousawi, M., Reid, S., and Deans, W., 1997, "*The use of the split Hopkinson pressure bar techniques in high strain rate materials testing*", Proceedings of the Institution of Mechanical Engineers, Part C: Journal of Mechanical Engineering Science, **211**, No.4, pp.273-292.

[44] Li, Y., Lin, Z., Jiang, A., and Chen, G., 2004, "*Experimental study of glass-fiber mat thermoplastic material impact properties and lightweight automobile body analysis*", Materials & Design, **25**, No.7, pp.579-585.

[45] Guo, Y., and Li, Y., 2007, "*Quasi-static/dynamic response of SiO_2–epoxy nanocomposites*", Materials Science and Engineering: A, **458**, No.1, pp.330-335.

[46] Omar, M.F., Md, A.H., Ahmad, Z.A., Mazuki, A.A.M, and Yokoyama, T., 2010, "*Dynamic properties of pultruded natural fibre reinforced composites using Split Hopkinson Pressure Bar technique*", Materials & Design, **31**, No.9, pp.4209-4218.

CHAPTER 3 A STUDY OF THE DYNAMIC RESPONSE OF THE NOVEL LAMINATED GLASS UNDER BLAST LOADING

3.1. Introduction

In this chapter, a numerical model is proposed to characterize the dynamic response of the fabricated laminated glass under blast loading. The validity of the proposed numerical model has been proven by experimental results. Laminated glass's failure analysis is also performed in this chapter using the stress analysis approach.

3.2. Blast resistance testing

Field experiments were done at the Engineering Research and Development Center (ERDC, US Army Corps of Engineers Lab, Vicksburg, Mississippi) using a Blast Load Simulator (BLS). The thickness of the tested laminated glass was around 9.5 mm (consisting of a 1/8 inch (3.2 mm) thick transparent composite interlayer laminated to two 1/8 inch (3.2 mm) thick tempered glass sheets). Sample gages were attached to the laminated glass to record the pressure loading history and the midpoint deflection history during the blast.

3.3 Blast resistance testing results

Both medium and high intensity blast loading tests were done at ERDC. The pressure-time curve of the medium intensity blast is shown in Fig. 3.1. The key parameters of the blast are obtained by curve fitting the initial pressure phase using equation (1.1). The result of fitting is: peak overpressure P_o=5.14 psi (35.4 kPa), constant α=0.1011, and positive pressure duration time t_p=11.3 ms.

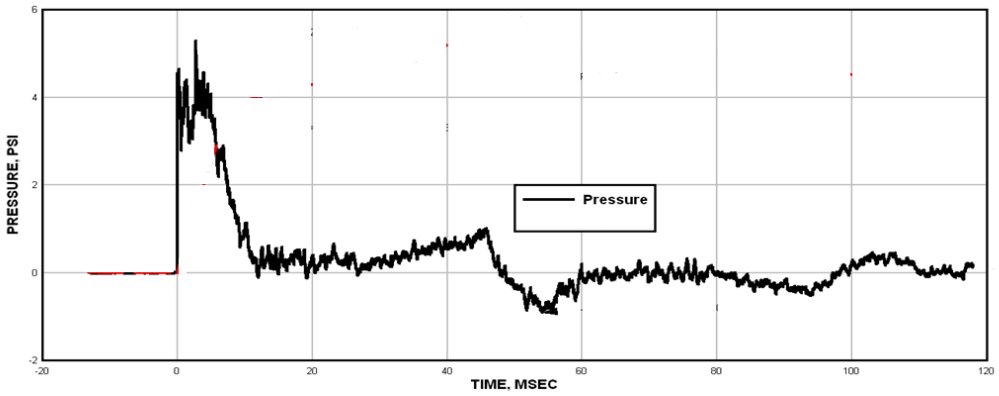

Figure 3.1 Pressure-time curve of the medium intensity blast

Fig. 3.2 shows the midpoint deflection of the laminated glass under the medium intensity blast shown in Fig. 3.1. It can be seen that the maximum deflection is about 0.415 inch (10.5 mm) and appears in the first deflection peak region.

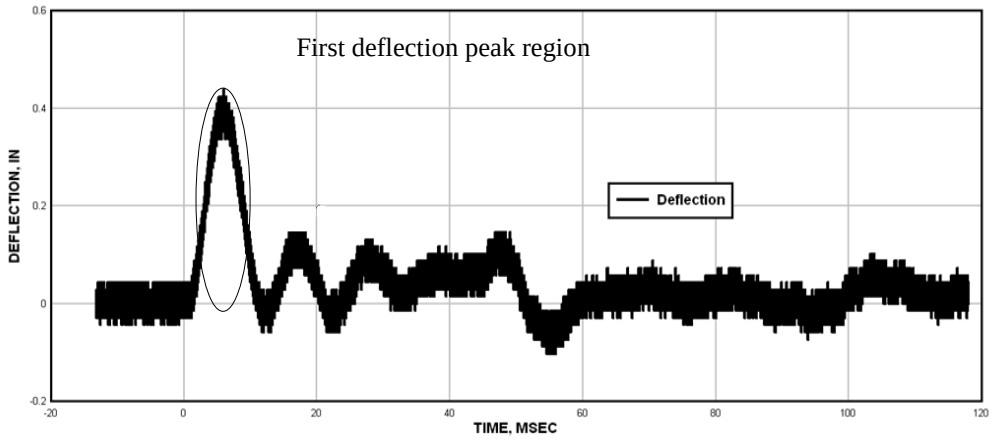

Figure 3.2 Midpoint deflection of the laminated glass under the medium intensity blast

The pressure-time curve of the high intensity blast is shown in Fig. 3.3. The key parameters of the blast are: peak overpressure P_o=13.22 psi (91.1 kPa), constant α = 0.2744, positive pressure duration time t_p =15.4 ms.

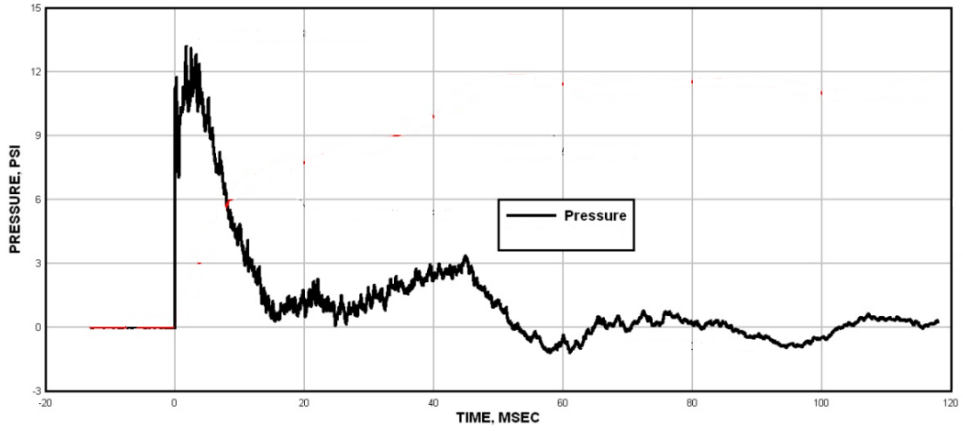

Figure 3.3 Pressure-time curve of the high intensity blast

Fig. 3.4 shows the midpoint deflection of the laminated glass under the high intensity blast shown in Fig. 3.3. The maximum deflection is around 0.99 inch (25.1 mm) and also appears in the first deflection peak region.

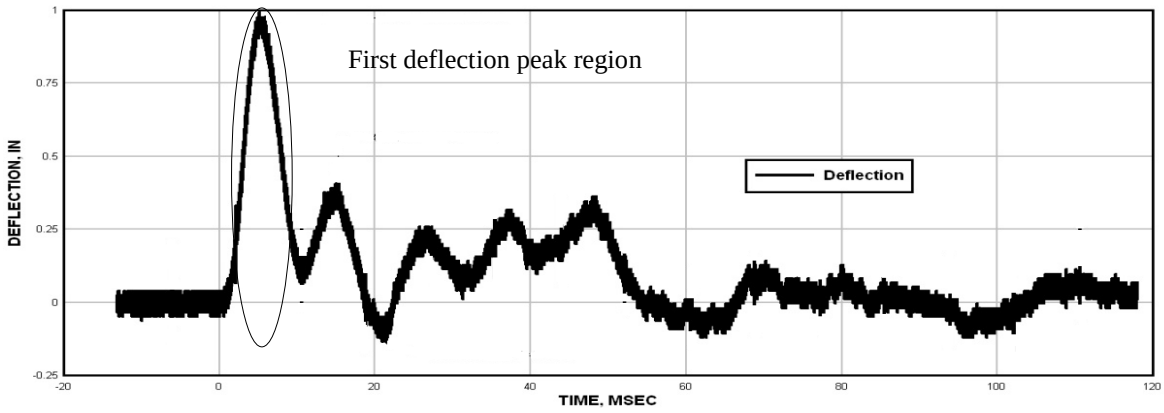

Figure 3.4 Midpoint deflection of the laminated glass under the high intensity blast

Field experiments are important for understanding the dynamic response of the laminated glass under blast loading. Besides field testing, model-based analysis can also be used to study the dynamic response of the laminated glass under blast loading. In this study, a numerical model is proposed to characterize the dynamic response of the fabricated laminated glass under blast loading.

3.4 Numerical modeling of the dynamic response of the fabricated laminated glass under blast loading

According to Hamilton's principle [1]

$$\int_{t_1}^{t_2} \left(\delta T - \delta \Pi + \delta W \right) dt = 0 \tag{3.1}$$

where T is the kinetic energy of the laminated glass, Π is the strain energy of the laminated glass and W is the work done by external load(s).

For the laminated glass, kinetic energy T can be calculated using the following equation [2]

$$T = \frac{1}{2} M \int_0^a \int_0^b \left(\frac{\partial w}{\partial t} \right)^2 dxdy \tag{3.2}$$

where M is the unit area mass of the laminated glass and is equal to $\rho_o h_o + \rho_c h_c + \rho_i h_i$. ρ_o , ρ_c and ρ_i are the density of the outer glass sheet, the composite interlayer and the inner glass sheet, respectively. $\rho_o = \rho_i = 2600\,\text{kg/m}^3$ and $\rho_c = 1200\,\text{kg/m}^3$. h_o , h_c , and h_i are the thickness of the outer glass sheet, the composite interlayer and the inner glass sheet, respectively. In this study, $h_o = h_c = h_i = 3.2\,\text{mm}$. w is the transverse (thickness direction) deflection of the laminated glass.

Strain energy Π can be calculated using the following equation [2]

$$\Pi = \frac{1}{2} \iiint_V \left(\sigma_x \varepsilon_x + \sigma_y \varepsilon_y + \tau_{xy} \gamma_{xy} \right) dxdydz \tag{3.3}$$

According to the classical plate theory [3], the strain components in the x-y plane (Fig. 3.5) can be expressed by the transverse deflection, *w*, as

$$\varepsilon_x = -z \frac{\partial^2 w}{\partial x^2}, \qquad \varepsilon_y = -z \frac{\partial^2 w}{\partial y^2}, \qquad \gamma_{xy} = -2z \frac{\partial^2 w}{\partial x \partial y} \tag{3.4}$$

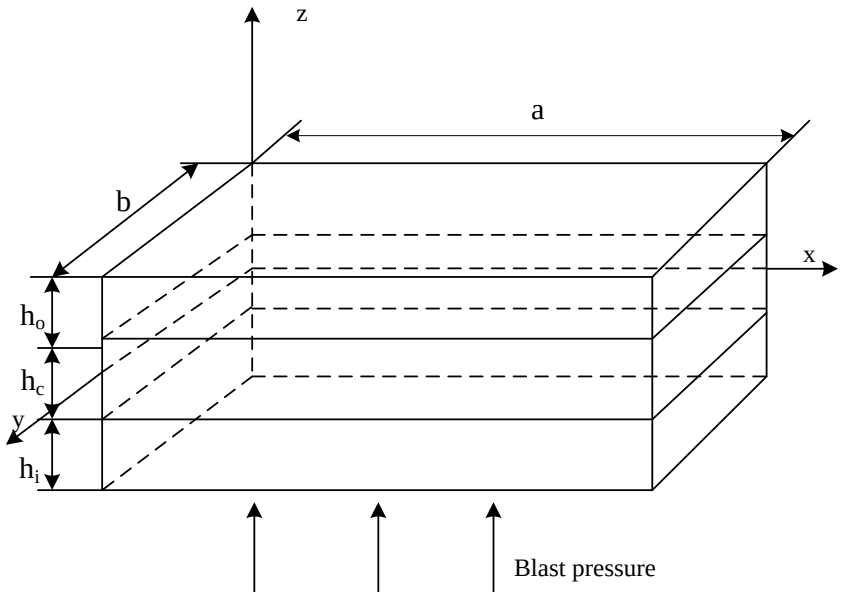

Figure 3.5 Schematic diagram of the laminated glass

For the orthotropic composite interlayer, $\sigma_x = \frac{E_c}{1-v_c^2}\varepsilon_x + \frac{v_c E_c}{1-v_c^2}\varepsilon_y$, $\sigma_y = \frac{v_c E_c}{1-v_c^2}\varepsilon_x + \frac{E_c}{1-v_c^2}\varepsilon_y$ and $\tau_{xy} = G_c\gamma_{xy}$, where E_c, G_c and v_c are Young's modulus, shear modulus and Poisson's ratio of the composite interlayer, respectively. It should be noted that the mechanical properties of the glass fiber-reinforced composite, such as Young's modulus and shear modulus, are influenced by strain rate [4]. However, in this analysis, since strain rate was not measured in field testing, the strain rate effect is not considered. So E_c, G_c and v_c values used here are the values obtained from previous quasi-static mechanical tests (Table 2.3). Substituting σ_x, σ_y and τ_{xy} expressions into equation (3.3), the strain energy of the composite interlayer is

$$\Pi_{comp} = \frac{1}{2}\iiint_V \left(\frac{E_c \varepsilon_x \varepsilon_x}{1-\nu_c^{\,2}} + \frac{\nu_c E_c \varepsilon_y \varepsilon_x}{1-\nu_c^{\,2}} + \frac{\nu_c E_c \varepsilon_x \varepsilon_y}{1-\nu_c^{\,2}} + \frac{E_c \varepsilon_y \varepsilon_y}{1-\nu_c^{\,2}} + G_c \gamma_{xy} \gamma_{xy} \right) dxdydz \qquad (3.5)$$

Integrating equation (3.5) through the transverse direction (thickness direction, z direction) results in

$$\Pi_{comp} = \frac{1}{2}\int_0^a \int_0^b \left[\begin{array}{l} \dfrac{E_c h_c^3}{12(1-\nu_c^{\,2})}\left(\dfrac{\partial^2 w}{\partial x^2}\right)^2 + \dfrac{E_c h_c^3}{12(1-\nu_c^{\,2})}\left(\dfrac{\partial^2 w}{\partial y^2}\right)^2 \\ + \dfrac{2\nu_c E_c h_c^3}{12(1-\nu_c^{\,2})}\left(\dfrac{\partial^2 w}{\partial x^2}\right)\left(\dfrac{\partial^2 w}{\partial y^2}\right) + \dfrac{4G_c h_c^3}{12}\left(\dfrac{\partial^2 w}{\partial x \partial y}\right)^2 \end{array} \right] dxdy \qquad (3.6)$$

where a is the length of the laminated glass, b is width of the laminated glass. In this study, a = 0.89 m and b = 0.59 m.

Similarly, the strain energy of the outer and inner glass sheets is

$$\Pi_{glass} = \frac{1}{2}\left\{ \frac{2E_g}{3(1-\nu_g^{\,2})}\left[h_g^3 + \frac{3h_c^2 h_g}{4} + \frac{3h_g^2 h_c}{2} \right] \right\}$$
$$\int_0^a \int_0^b \left[\left(\frac{\partial^2 w}{\partial x^2}\right)^2 + \left(\frac{\partial^2 w}{\partial y^2}\right)^2 + 2\nu_g \frac{\partial^2 w}{\partial x^2}\frac{\partial^2 w}{\partial y^2} + 2\left(1-\nu_g\right)\left(\frac{\partial^2 w}{\partial x \partial y}\right)^2 \right] dxdy \qquad (3.7)$$

where h_g is the thickness of one glass sheet (inner or outer layer glass sheet), E_g is Young's modulus of glass, ν_g is Poisson's ratio of glass, In this study, tempered glass is used, for which E_g = 68 GPa , ν_g = 0.2. Summing the strain energy of the composite interlayer and glass sheets, the total strain energy of the laminated glass is

$$\Pi = \frac{1}{2}\int_0^a \int_0^b \left[A\left(w_{xx}\right)^2 + A\left(w_{yy}\right)^2 + Bw_{xx}w_{yy} + C\left(w_{xy}\right)^2 \right] dxdy \tag{3.8}$$

$$A = \frac{2E_g}{3\left(1-\nu_g{}^2\right)}\left[h_g^3 + \frac{3h_c^2 h_g}{4} + \frac{3h_g^2 h_c}{2} \right] + \frac{E_c h_c^3}{12\left(1-\nu_c{}^2\right)}$$

$$B = 2\nu\left\{ \frac{2E_g}{3\left(1-\nu_g{}^2\right)}\left[h_g^3 + \frac{3h_c^2 h_g}{4} + \frac{3h_g^2 h_c}{2} \right] \right\} + \frac{2\nu_c E_c h_c^3}{12\left(1-\nu_c{}^2\right)}$$

$$C = 2\left(1-\nu\right)\left\{ \frac{2E_g}{3\left(1-\nu_g{}^2\right)}\left[h_g^3 + \frac{3h_c^2 h_g}{4} + \frac{3h_g^2 h_c}{2} \right] \right\} + \frac{4G_c h_c^3}{12}$$

where w_{kl} means a differentiation with respect to variable *k* and variable *l*.

For blast loading, the work done by external load is given by [2]

$$W = \int_0^a \int_0^b P\left(t\right) w dxdy \tag{3.9}$$

where $P(t)$ is the instantaneous blast pressure and can be described by equation (1.1).

Substituting T, Π, W into equation (3.1), it can be rewritten as

$$\int_t^{t_2} \int_0^a \int_0^b \left\{ -M\ddot{w}\delta w - \left(Aw_{xxxx} + Aw_{yyyy} + \left(B+C\right) w_{xxyy} \right) \delta w + P\left(t\right)\delta w \right\} dxdydt = 0 \tag{3.10}$$

where $\ddot{w}$ means a second-order derivative of *w* with respect to time. From equation (3.10), the equation of motion of the laminated glass is obtained as

$$M\ddot{w} + A\left(w_{xxxx} + w_{yyyy} \right) + \left(B+C\right) w_{xxyy} = P\left(t\right) \tag{3.11}$$

The laminated glass in this study is considered as simply supported. So the boundary conditions are

$$w = 0, \;\; w_{xx} = 0, \qquad at \; x = 0, a,$$

$$w = 0, \;\; w_{yy} = 0, \qquad at \; y = 0, b,$$

The initial condition is

$$w(x, y, 0) = 0, \quad \dot{w}(x, y, 0) = 0$$

In order to solve equation (3.11), an approximate function is chosen for w by considering the simply supported boundary conditions [5, 6]

$$w(x, y, t) = \sum_{m=1}^{\infty} \sum_{n=1}^{\infty} \psi \sin\left(\frac{m\pi x}{a}\right) \sin\left(\frac{n\pi y}{b}\right) \tag{3.12}$$

where ψ is a unknown time dependent function. Here, for calculation convenience, m and n are both simplified to 1. Substituting equation (3.12) into equation (3.11) and applying Galerkin method, the equation of motion of the laminated glass is changed to

$$\frac{\left(a\left(\frac{A\pi^6\psi}{4} - 4b^4 P_o\left(1\text{-}t/t_p\right)\mathrm{e}^{\text{-}\alpha t/t_p} + \frac{M\pi^2\ddot{\psi}b^4}{4}\right)\right)}{\pi^2 b^3} + \frac{a^2\left(\frac{B\pi^6\psi b^2}{4} + \frac{C\pi^6\psi b^2}{4}\right) + \frac{A\pi^6\psi b^4}{4}}{\pi^2 a^3 b^3} = 0 \tag{3.13}$$

Rearranging equation (3.13) and the following equation is obtained

$$\ddot{\psi} = \frac{4}{M\pi^2 b^4}\left(-\frac{A\pi^6\psi}{4} + 4b^4 P_o\left(1\text{-}t/t_p\right)\mathrm{e}^{-\alpha t/t_p} - \frac{a^2\left(\frac{B\pi^6\psi b^2}{4} + \frac{C\pi^6\psi b^2}{4}\right) + \frac{A\pi^6\psi b^4}{4}}{a^4} \right) \quad (3.14)$$

Equation (3.14) is a nonlinear ordinary differential equation and can be solved using MATLAB. After obtaining function ψ, the transverse deflection w can be calculated using equation (3.12).

Besides the method shown above, equation (3.11) can also be solved by the following procedures:

1) Equation (3.11) is converted to a second-order ordinary differential equation using double Fourier expansion.

2) The obtained ordinary differential equation is solved by Euler's method.

The procedures for converting equation (3.11) to a second-order ordinary differential equation using double Fourier expansion are given in the Appendix A.

3.5 Comparison between numerical and experimental results

Fig. 3.6 shows the predicted maximum deflection state of the laminated glass under the medium intensity blast loading. Fig. 3.7 shows the predicted maximum deflection state of the laminated glass under the high intensity blast loading. In Fig. 3.6 and 3.7, the laminated glass is simplified to a zero-thickness plate. From Fig. 3.6 and 3.7, it can be seen that the maximum deflection occurs at the midpoint. At the position close to the

edge of the laminated glass, the deflection decreases. This prediction correspnds fairly well with the experimental results.

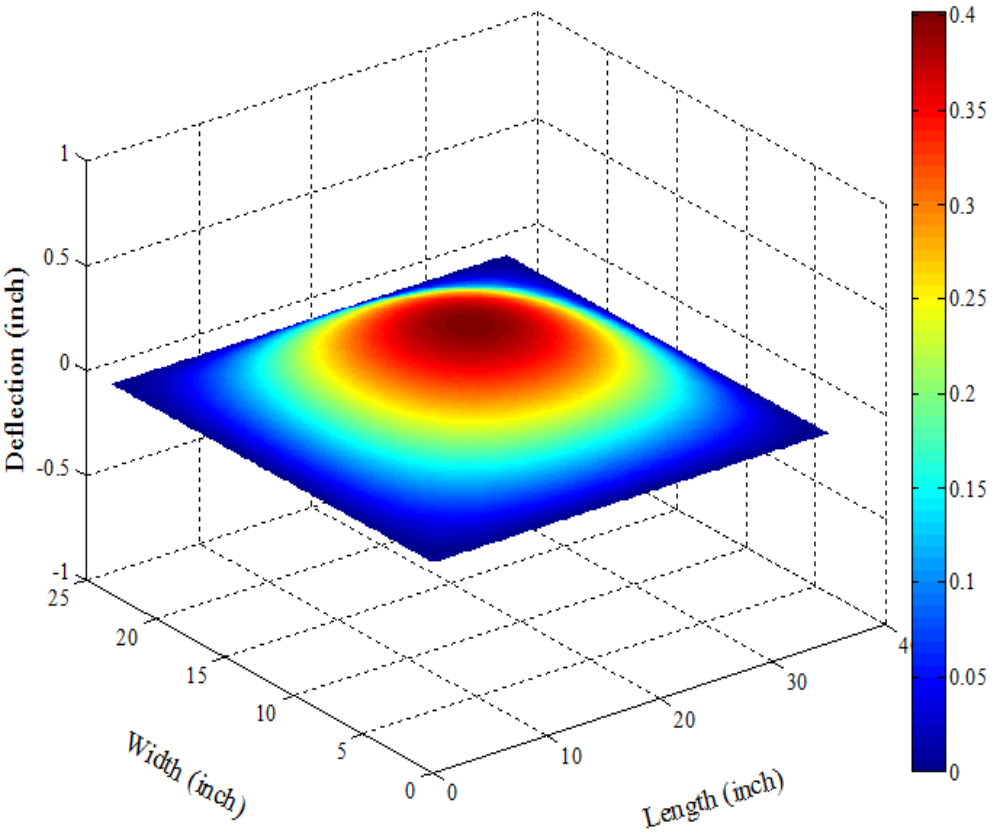

Figure 3.6 The maximum deflection state of the laminated glass under the medium intensity blast loading

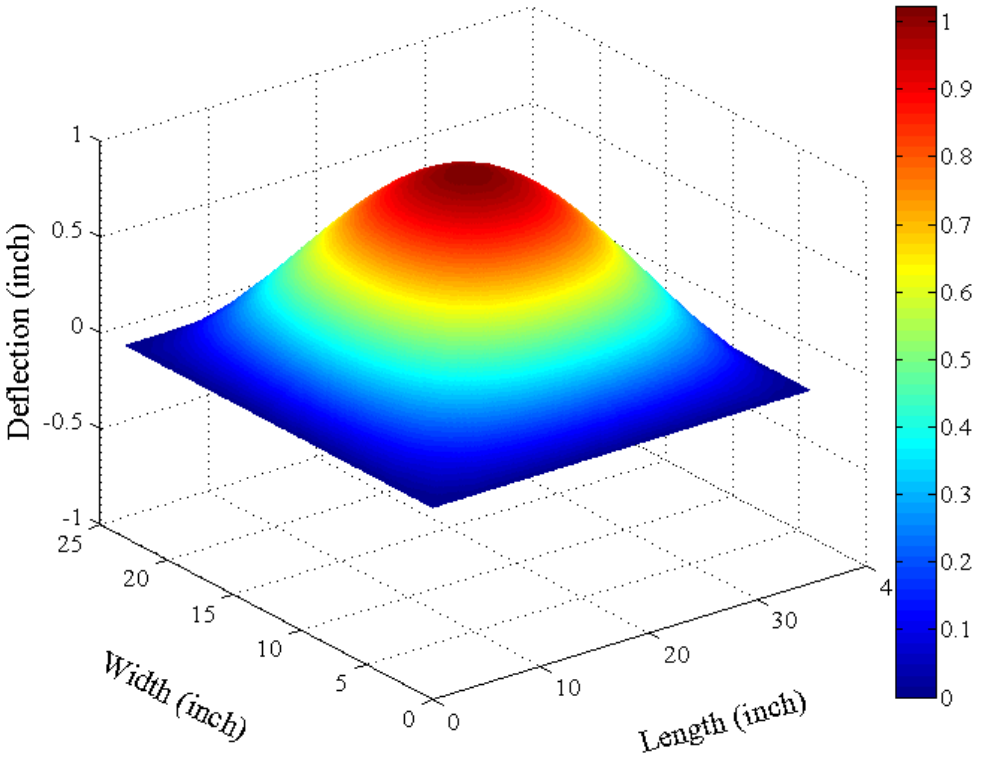

Figure 3.7 The maximum deflection state of the laminated glass under the high intensity blast loading

From Fig. 3.2 and 3.4, it can be seen that the maximum deflection, which is an important criterion for evaluating the blast resistance of the fabricated laminated glass, occurs in the first deflection peak region. Therefore, the knowledge of the deflection history in the first peak region is important and is simulated by the developed numerical model. Fig. 3.8 shows the predicted midpoint deflection history in the first deflection peak region. The predicted maximum deflection is 0.42 inch (10.6 mm) and the predicted positive deflection duration time is 7.8 ms. The experimentally measured midpoint

deflection history (the circled region in Fig. 3.2) is also plotted in Fig. 3.8. The experimentally measured maximum deflection value is 0.415 inch (10.5 mm) and the meausred duration time is 8.3 ms. The discrepancy between the numerical result and the experimental result may be caused by the neglect of the composite interlayer's plastic deformation and the strain rate effect on mechanical properties in the modeling. It can be observed from Fig. 3.8 that for the medium intensity blast loading, the predicted result matches well with the experimentally measured result.

Similarly, for the high intensity blast loading, the predicted midpoint deflection history in the first deflection peak region is compared in Fig. 3.9 with the experimentally measured result. The predicted maximum deflection is 1.03 inch (26.1 mm) and the predicted positive deflection duration time is 8.1 ms. The experimentally measured maximum deflection value is 0.99 inch (25.2 mm) and the measured duration time is 9.4 ms. Fig. 3.9 shows that for the high intensity blast loading, the predicted result also matches fairly well with the experimentally measured result. Considering the good match of the numerically predicted results and the experimentally measured results under medium and high intensity blast loading, it can be concluded that the developed numerical model is valid for predicting the dynamic reponse of the laminated glass under both medium and high intensity blast loading.

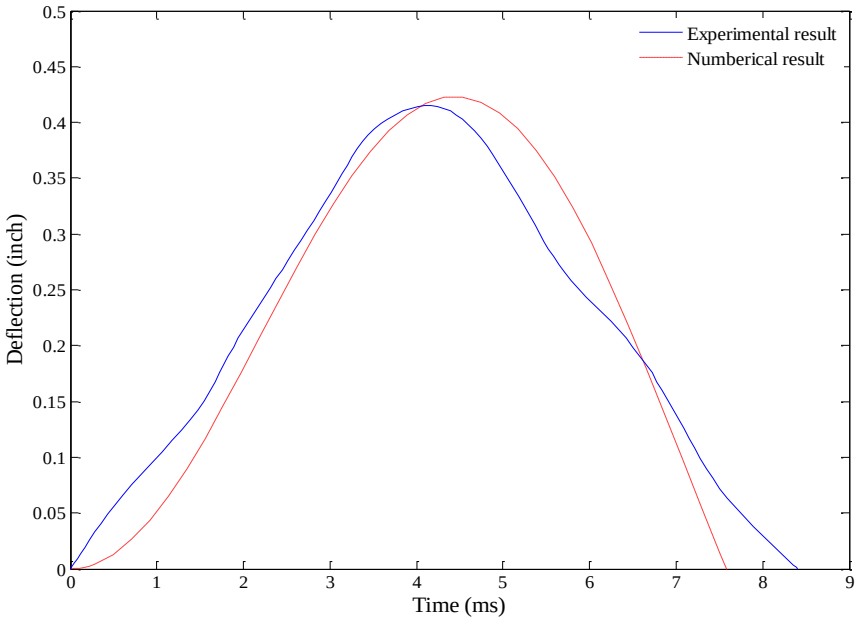

Figure 3.8 Midpoint deflection of the laminated glass under the medium intensity blast loading in the first deflection peak region

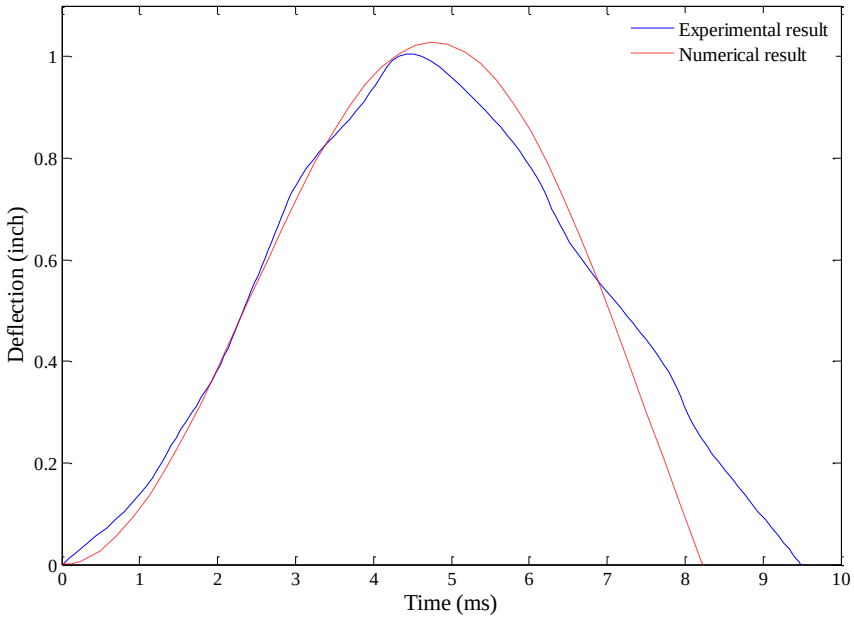

Figure 3.9 Midpoint deflection of the laminated glass under the high intensity blast loading in the first deflection peak region

3.6 Laminated glass failure analysis

Based on the stress-strain relationship, the stresses of the laminated glass under blast loading can be expressed as following equations

$$\sigma_x = \frac{E_{avg}}{1-\nu_{avg}^2}\left(\varepsilon_x + \nu_{avg}\varepsilon_y\right) \tag{3.15}$$

$$\sigma_y = \frac{E_{avg}}{1-\nu_{avg}^2}\left(\nu_{avg}\varepsilon_x + \varepsilon_y\right)$$

$$\tau_{xy} = G_{avg}\gamma_{xy}$$

Substituting equation (3.4) into equation (3.15) results in

$$\sigma_x = -\frac{E_{avg}z}{1-\nu_{avg}^2}\left(\frac{\partial^2 w}{\partial x^2} + \nu_{avg}\frac{\partial^2 w}{\partial y^2}\right) \tag{3.16}$$

$$\sigma_y = -\frac{E_{avg}z}{1-\nu_{avg}^2}\left(\nu_{avg}\frac{\partial^2 w}{\partial x^2} + \frac{\partial^2 w}{\partial y^2}\right)$$

$$\tau_{xy} = -2G_{avg}z\frac{\partial^2 w}{\partial x \partial y}$$

where E_{avg}, ν_{avg} and G_{avg} are the average Young's modulus, Poisson's ratio and shear modulus of the laminated glass, respectively. These parameters can be calculated using the following equations [7]

$$E_{avg} = \frac{E_g h_g + E_c h_c + E_g h_g}{h_g + h_c + h_g}$$

$$v_{avg} = \frac{v_g h_g + v_c h_c + v_g h_g}{h_g + h_c + h_g}$$

$$G_{avg} = \frac{E_g h_g + 2\left(1+v_g\right) G_c h_c + E_g h_g}{2\left(1+v_g\right)\left(h_g + h_c + h_g\right)}$$

After obtaining the values of the deflection *w*, the stresses of the laminated glass can be calculated using equation (3.16). And then the principal stresses of the laminated glass can be calculated. According to the literature [6], the maximum principal stress always occurs at the midpoint of the laminated glass. So the midpoint maximum principal stress history in the first and second deflection peak regions (the first positive deflection peak region and the first negative deflection peak region) is calculated and compared with the tensile strength of tempered glass to determine whether the laminated glass can survive when subjected to blast loading. This criterion is proposed by Wei et al. and used in their research [6]. The reason for studying the principal stress history in the first two deflection peak regions only is that according to equation (3.16), stresses varies directly with the deflection *w*. From Fig. 3.2 and 3.4, it can be observed that compared with the maximum deflection (the first deflection peak), the deflection after the first two deflection peak regions is small, which means corresponding stresses/principal stresses are small. Therefore, in this study, the principal stress history after the first two deflection peak regions is not discussed. When subjected to the medium intensity blast loading, the midpoint maximum principal stress histories of the inner glass surface (pressure impact

surface) and the outer glass surface (pressure non-impact surface) in the first two deflection peak regions are calculated and plotted in Fig. 3.10.

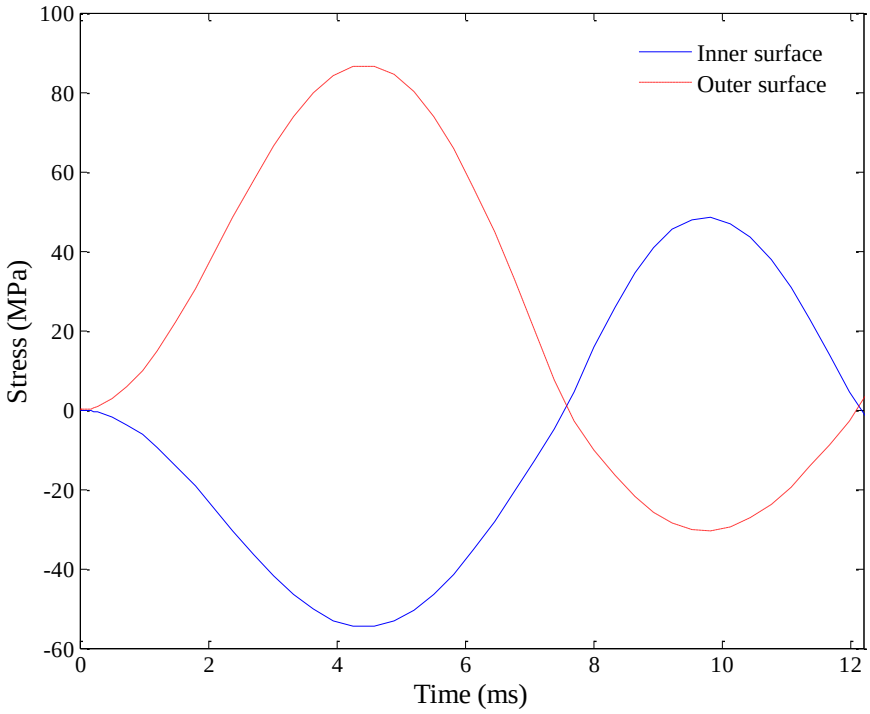

Figure 3.10 Midpoint maximum principal stress history
under the medium intensity blast loading

Fig. 3.10 illustrates that for the inner surface, the maximum compression stress is about 55 MPa and the maximum tensile stress is about 50 MPa; for the outer surface, the maximum compression stress is about 31 MPa and the maximum tensile stress is about 85 MPa. The tensile strength of tempered glass is usually above 175 MPa (sometimes above 200 MPa), and its compressive strength is much higher than its tensile strength [8-11]. Therefore, according to the stress analysis, the laminated glass will survive when

subjected to the medium intensity blast loading. This result has been proven by the experimental result.

When subjected to the high intensity blast loading, the midpoint maximum principal stress histories of the inner surface and the outer surface in the first two deflection peak regions are shown in Fig. 3.11. From Fig. 3.11, it can be observed that the outer layer glass first experiences its maximum tensile stress (around 200 MPa), which is close to but not beyond the tensile strength of tempered glass. Then, the inner layer glass experiences its maximum tensile stress (~95 MPa), which is lower than the tensile strength of tempered glass. So, the laminated glass will survive after exposing to the high intensity blast loading. This result corresponds with the experimentally observed result.

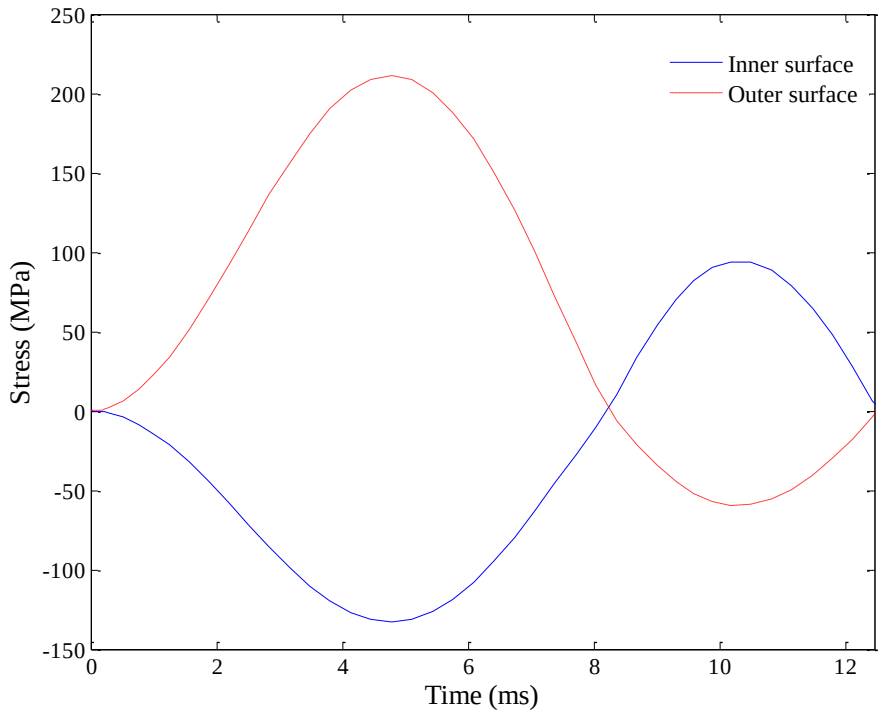

Figure 3.11 Midpoint maximum principal stress history under the high intensity blast loading

3.7 Summary

The dynamic response of the fabricated laminated glass under blast loading has been investigated by field testing and model-based analysis. The predicted response, in terms of the midpoint deflection, agrees fairly well with the experimentally measured results under medium and high intensity blast loading. Stress analysis and experimental results both show that the fabricated laminated glass can survive under medium and high intensity blast loading.

REFERENCES

[1] Pai, P.F., 2007, "*Highly flexible structures: modeling, computation, and experimentation*", Reston, VA: American Institute of Aeronautics & Astronautics.

[2] Wei, J., 2004, "*Dynamics and failure analysis of architectural glazing subjected to blast loading*", Rolla, MO: University of Missouri.

[3] Ugural, A.C., 1981, "*Stresses in plates and shells*", New York, NY: McGraw-Hill.

[4] Barre, S., Chotard, T., and Benzeggagh, M., 1996, "*Comparative study of strain rate effects on mechanical properties of glass fibre-reinforced thermoset matrix composite*", Composites Part A: Applied Science and Manufacturing, **27**, No.12, pp.1169-1181.

[5] Kazancı, Z., 2011, "*Dynamic response of composite sandwich plates subjected to time-dependent pressure pulses*", International Journal of Non-Linear Mechanics, **46**, No.5, pp.807-817.

[6] Wei, J., and Dharani, L.R., 2006, "*Response of laminated architectural glazing subjected to blast loading*", International Journal of Impact Engineering, **32**, No.12, pp.2032-2047.

[7] Vinson, J.R., 1999, "*The Behavior of Sandwich Structures of Isotropic and Composite Materials*", Lancaster, PA: Technomic Publishing Company, Inc.

[8] Kalluri, R.S., 2007, "*Failure of transparent polymer composite laminated glass panels under impact loading*", Columbia, MO: University of Missouri.

[9] Mencik, J., 1992, "*Strength and fracture of glass and ceramics*", New York, NY: Elsevier.

[10] Veer, F., Zuidema, J., Bos, F., and Romein, T., 2005, "*The strength and fracture behaviour of annealed and tempered float glass*", Proceedings of the 9th International Conference on Architectural and Automotive Glass (GPD), pp.1-6.

[11] National Glass, "*Glass Manufacture*", http://www.nationalglass.com.au/catalogues/NGP_Section_20.pdf.

CHAPTER 4 NONLINEAR DYNAMIC ANALYSIS OF THE NOVEL LAMINATED GLASS UNDER BLAST LOADING

4.1 Introduction

In this chapter, the dynamic response of the fabricated laminated glass under a medium intensity blast loading of peak pressure=5.14 psi (the same medium blast loading as described in Chapter 3) is investigated using a new numerical model and a finite element model. The numerical model analysis result and the finite element model analysis result are compared with the experimentally measured result. Based on the new numerical model, the blast resistance of the fabricated laminated glass is compared with that of the same configuration laminated glass with PVB interlayer.

4.2 Numerical modeling and finite element modeling of the dynamic response the fabricated laminated glass under blast loading

4.2.1 Numerical modeling

The schematic diagram of the laminated glass is shown in Fig. 4.1. It consists of a 1/8 inch (3.2 mm) thick transparent composite interlayer and two 1/8 inch (3.2 mm) thick tempered glass sheets. The origin of the coordinate system of the laminated glass is set at the corner of the midplane. The midplane (x-y plane) is in the middle of the laminated glass panel, with respect to the thickness direction.

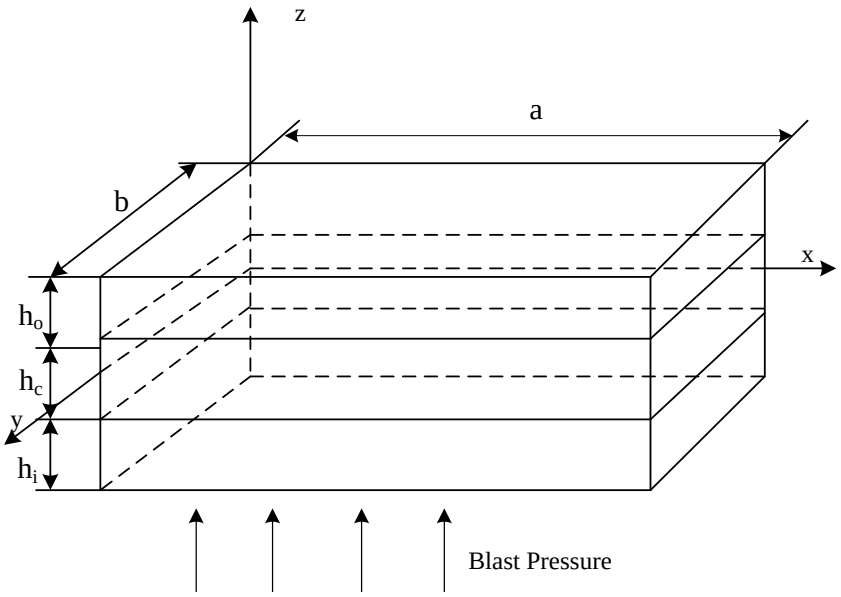

Figure 4.1 Schematic diagram of the laminated glass
(top and bottom layers are glass sheets, middle layer is the composite interlayer)

The strain-displacement relationship for a plate is [1, 2]

$$\varepsilon_x = \frac{\partial u}{\partial x} + \frac{1}{2}\left(\frac{\partial w}{\partial x}\right)^2 - z\frac{\partial^2 w}{\partial x^2} \tag{4.1}$$

$$\varepsilon_y = \frac{\partial v}{\partial y} + \frac{1}{2}\left(\frac{\partial w}{\partial y}\right)^2 - z\frac{\partial^2 w}{\partial y^2} \tag{4.2}$$

$$\gamma_{xy} = 2\varepsilon_{xy} = \frac{\partial u}{\partial y} + \frac{\partial v}{\partial x} + \frac{\partial w}{\partial x}\frac{\partial w}{\partial y} - 2z\frac{\partial^2 w}{\partial x \partial y} \tag{4.3}$$

where ε_x, ε_y and γ_{xy} are strain components and *u*, *v* and *w* are displacement components (in *x*, *y* and *z* directions, respectively).

The moments of a plate are [3]

$$M_x = \int_{-\frac{h}{2}}^{\frac{h}{2}} z\sigma_x dz \qquad M_y = \int_{-\frac{h}{2}}^{\frac{h}{2}} z\sigma_y dz \qquad M_{xy} = -\int_{-\frac{h}{2}}^{\frac{h}{2}} z\tau_{xy} dz \qquad (4.4)$$

where h is the thickness of the plate. For the glass fiber-reinforced orthotropic composite interlayer, σ_{xc} , σ_{yc} and τ_{xyc} are $\frac{E_c}{1-v_c^2}\varepsilon_x + \frac{v_c E_c}{1-v_c^2}\varepsilon_y$, $\frac{v_c E_c}{1-v_c^2}\varepsilon_x + \frac{E_c}{1-v_c^2}\varepsilon_y$, and $G_c\gamma_{xy}$, respectively. E_c , G_c and v_c are Young's modulus, shear modulus and Poisson's ratio of the composite interlayer, respectively. The values of E_c , G_c and v_c are obtained from Table 2.3. In this research, glass is considered as an isotropic material, σ_{xg} , σ_{yg} and τ_{xyg} of the glass sheets are $\frac{E_g}{1-v_g^2}\varepsilon_x + \frac{v_g E_g}{1-v_g{}^2}\varepsilon_y$, $\frac{E_g v_g}{1-v_g{}^2}\varepsilon_x + \frac{E_g}{1-v_g{}^2}\varepsilon_y$, and $\frac{E_g}{2(1+v_g)}\gamma_{xy}$, respectively. E_g and v_g are Young's modulus and Poisson's ratio of glass sheets, respectively. In this study, E_g is 68 GPa and v_g is 0.2.

First, substitute equations (4.1)-(4.3) into σ_{xc}, σ_{yc}, τ_{xyc} expressions, then substitute the resultant σ_{xc}, σ_{yc}, τ_{xyc} into equation (4.4) and integrate this equation through the thickness direction. The moments of the composite interlayer (M_{xc}, M_{yc}, M_{xyc}) can be expressed as

$$M_{xc} = -\frac{E_c h_c^3}{12\left(1-\nu_c^{\,2}\right)}\left(\frac{\partial^2 w}{\partial x^2}+\nu_c\frac{\partial^2 w}{\partial y^2}\right) \tag{4.5}$$

$$M_{yc} = -\frac{E_c h_c^3}{12\left(1-\nu_c^{\,2}\right)}\left(\nu_c\frac{\partial^2 w}{\partial x^2}+\frac{\partial^2 w}{\partial y^2}\right)$$

$$M_{xyc} = \frac{G_c h_c^3}{6}\frac{\partial^2 w}{\partial x \partial y}$$

where h_c is the thickness of the composite interlayer, in this study, h_c = 3.2 mm.

Similarly, the moments of the glass sheets (M_{xg}, M_{yg}, M_{xyg}) can be expressed as

$$M_{xg} = -\frac{E_g}{3\left(1-\nu_g^2\right)}\left(h_g^3+\frac{3h_g^2 h_c}{2}+\frac{3h_g h_c^2}{4}\right)\left(\frac{\partial^2 w}{\partial x^2}+\nu_g\frac{\partial^2 w}{\partial y^2}\right)$$

$$M_{yg} = -\frac{E_g}{3\left(1-\nu_g^2\right)}\left(h_g^3+\frac{3h_g^2 h_c}{2}+\frac{3h_g h_c^2}{4}\right)\left(\nu_g\frac{\partial^2 w}{\partial x^2}+\frac{\partial^2 w}{\partial y^2}\right) \tag{4.6}$$

$$M_{xyg} = \frac{E_g}{3\left(1+\nu_g\right)}\left(h_g^3+\frac{3h_g^2 h_c}{2}+\frac{3h_g h_c^2}{4}\right)\frac{\partial^2 w}{\partial x \partial y}$$

where h_g stands for the thickness of a glass sheet (inner or outer glass sheet), in this study, $h_g = h_{outer} = h_{inner}$= 3.2 mm. It should be pointed out that for simplicity, only the effect of the higher-order derivative component on moments is considered in this study.

The total moments of the laminated glass are

$$M_x = -\frac{E_c h_c^3}{12\left(1-\nu_c^{\,2}\right)}\left(\frac{\partial^2 w}{\partial x^2}+\nu_c\frac{\partial^2 w}{\partial y^2}\right)-\frac{E_g}{3\left(1-\nu_g^2\right)}\left(h_g^3+\frac{3h_g^2h_c}{2}+\frac{3h_gh_c^2}{4}\right)\left(\frac{\partial^2 w}{\partial x^2}+\nu_g\frac{\partial^2 w}{\partial y^2}\right)$$
$$-\frac{E_g}{3\left(1-\nu_g^2\right)}\left(h_g^3+\frac{3h_g^2h_c}{2}+\frac{3h_gh_c^2}{4}\right)\left(\frac{\partial^2 w}{\partial x^2}+\nu_g\frac{\partial^2 w}{\partial y^2}\right)$$

$$M_y = -\frac{E_c h_c^3}{12\left(1-\nu_c^{\,2}\right)}\left(\nu_c\frac{\partial^2 w}{\partial x^2}+\frac{\partial^2 w}{\partial y^2}\right)-\frac{E_g}{3\left(1-\nu_g^2\right)}\left(h_g^3+\frac{3h_g^2h_c}{2}+\frac{3h_gh_c^2}{4}\right)\left(\nu_g\frac{\partial^2 w}{\partial x^2}+\frac{\partial^2 w}{\partial y^2}\right) \quad (4.7)$$
$$-\frac{E_g}{3\left(1-\nu_g^2\right)}\left(h_g^3+\frac{3h_g^2h_c}{2}+\frac{3h_gh_c^2}{4}\right)\left(\nu_g\frac{\partial^2 w}{\partial x^2}+\frac{\partial^2 w}{\partial y^2}\right)$$

$$M_{xy} = \frac{G_c h_c^3}{6}\frac{\partial^2 w}{\partial x\partial y}+\frac{E_g}{3\left(1+\nu_g\right)}\left(h_g^3+\frac{3h_g^2h_c}{2}+\frac{3h_gh_c^2}{4}\right)\frac{\partial^2 w}{\partial x\partial y}$$
$$+\frac{E_g}{3\left(1+\nu_g\right)}\left(h_g^3+\frac{3h_g^2h_c}{2}+\frac{3h_gh_c^2}{4}\right)\frac{\partial^2 w}{\partial x\partial y}$$

According to references [3, 4], the equilibrium equation for the laminated glass is

$$\frac{\partial Q_x}{\partial x}+\frac{\partial Q_y}{\partial y}+q+q^*=m\frac{\partial^2 w}{\partial t^2} \quad (4.8)$$

where

$$Q_x = \frac{\partial M_x}{\partial x}+\frac{\partial M_{yx}}{\partial y} \quad (4.9)$$

$$Q_y = \frac{\partial M_y}{\partial y}-\frac{\partial M_{xy}}{\partial x}$$

m is the unit area mass of the laminated glass and $m=\rho_g h_g+\rho_c h_c+\rho_g h_g$, where ρ_g is the density of the glass and is 2600 kg/m^3. ρ_c is the density of the composite interlayer and is

1200 kg/m^3, q^* is the resultant force caused by deflection and q is the external load acting on the laminated glass which can be expressed using equation (1.1). Substituting equation (4.9) into equation (4.8), and since $M_{xy} = -M_{yx}$, a new equilibrium equation is obtained

$$\frac{\partial^2 M_x}{\partial x^2} + \frac{\partial^2 M_y}{\partial y^2} - 2\frac{\partial^2 M_{xy}}{\partial x \partial y} + q + q^* = m\frac{\partial^2 w}{\partial t^2} \tag{4.10}$$

Substituting equation (4.7) and equation (1.1) into equation (4.10) results in

$$\left(A\frac{\partial^4 w}{\partial x^4} + B\frac{\partial^4 w}{\partial x^2 \partial y^2}\right) + \left(B\frac{\partial^4 w}{\partial x^2 \partial y^2} + A\frac{\partial^4 w}{\partial y^4}\right) + 2C\frac{\partial^4 w}{\partial x^2 \partial y^2} + m\frac{\partial^2 w}{\partial t^2} = P_o\left(1 - t/t_p\right)e^{-\alpha t/t_p} + q^* \tag{4.11}$$

where

$$A = \frac{E_c h_c^3}{12\left(1-\nu_c^2\right)} + \frac{2E_g}{3\left(1-\nu_g^2\right)}\left(h_g^3 + \frac{3}{2}h_g^2 h_c + \frac{3}{4}h_g h_c^2\right)$$

$$B = \frac{E_c h_c^3 \nu_c}{12\left(1-\nu_c^2\right)} + \frac{2E_g \nu_g}{3\left(1-\nu_g^2\right)}\left(h_g^3 + \frac{3}{2}h_g^2 h_c + \frac{3}{4}h_g h_c^2\right)$$

$$C = \frac{G_c h_c^3}{6} + \frac{2E_g}{3\left(1+\nu_g\right)}\left(h_g^3 + \frac{3}{2}h_g^2 h_c + \frac{3}{4}h_g h_c^2\right)$$

Equation (4.11) can be rearranged to

$$D\left(\frac{\partial^4 w}{\partial x^4} + \frac{\partial^4 w}{\partial y^4}\right) + F\frac{\partial^4 w}{\partial x^2 \partial y^2} + m\frac{\partial^2 w}{\partial t^2} = P_o\left(1 - t/t_p\right)e^{-\alpha t/t_p} + q^* \tag{4.12}$$

where

$$D=\frac{E_c h_c^3}{12\left(1-\nu_c^2\right)}+\frac{2E_g}{3\left(1-\nu_g^2\right)}\left(h_g^3+\frac{3}{2}h_g^2 h_c+\frac{3}{4}h_g h_c^2\right)$$

$$F=\frac{E_c h_c^3 \nu_c}{6\left(1-\nu_c^2\right)}+\frac{G_c h_c^3}{3}+\frac{4E_g}{3\left(1-\nu_g^2\right)}\left(h_g^3+\frac{3}{2}h_g^2 h_c+\frac{3}{4}h_g h_c^2\right)$$

q^* can be expressed as [3]

$$q^*=h\left(\frac{\partial^2\phi}{\partial y^2}\frac{\partial^2 w}{\partial x^2}+\frac{\partial^2\phi}{\partial x^2}\frac{\partial^2 w}{\partial y^2}-2\frac{\partial^2\phi}{\partial x\partial y}\frac{\partial^2 w}{\partial x\partial y}\right) \tag{4.13}$$

where ϕ is called Airy's stress function and is used to represent stresses: $\sigma_x=\frac{\partial^2\phi}{\partial y^2}$, $\sigma_y=\frac{\partial^2\phi}{\partial x^2}$, $\sigma_{xy}=-\frac{\partial^2\phi}{\partial x\partial y}$, h is the thickness of the whole laminated glass and is equal to $h_g+h_c+h_g$. Substituting equation (4.13) into equation (4.12), equation (4.12) can be rewritten as

$$D\left(w_{xxxx}+w_{yyyy}\right)+Fw_{xxyy}+m\ddot{w}=P_o\left(1-t/t_p\right)e^{-\alpha t/t_p}+h\left(\phi_{yy}w_{xx}+\phi_{xx}w_{yy}-2\phi_{xy}w_{xy}\right) \tag{4.14}$$

where $(\,)_l$ means a differentiation with respect to variable l and $\ddot{w}$ means a second-order derivative of w with respect to time. Equation (4.14) cannot be solved by itself. In order to solve it, a St. Venant's compatibility equation is introduced [3, 5], as listed below

$$\frac{\partial^2\varepsilon_x}{\partial y^2}+\frac{\partial^2\varepsilon_y}{\partial x^2}=2\frac{\partial^2\varepsilon_{xy}}{\partial x\partial y} \tag{4.15}$$

Rearranging equation (4.15) and substituting equations (4.1)-(4.3) into equation (4.15), results in equation (4.16)

$$\frac{\partial^2 \varepsilon_x}{\partial y^2} + \frac{\partial^2 \varepsilon_y}{\partial x^2} - 2\frac{\partial^2 \varepsilon_{xy}}{\partial x \partial y} = \left(\frac{\partial^2 w}{\partial x \partial y} \right)^2 - \frac{\partial^2 w}{\partial x^2} \frac{\partial^2 w}{\partial y^2} \tag{4.16}$$

The strains shown in equation (4.16) can first be expressed in terms of stresses and then in terms of Airy's stress function. After substituting Airy's function into equation (4.16), a new compatibility equation is obtained as

$$N\phi_{yyyy} + N\phi_{xxxx} + P\phi_{xxyy} = \left(w_{xy} \right)^2 - w_{xx} w_{yy} \tag{4.17}$$

where

$$N = \frac{h_g + h_c + h_g}{E_g h_g + E_c h_c + E_g h_g}$$

$$P = \frac{h_g + h_c + h_g}{E_g h_g + \dfrac{G_c E_c}{E_c - 2\nu_c G_c} h_c + E_g h_g}$$

Equation (4.14) and (4.17) constitute a solvable system of nonlinear partial differential equations, which are also the equations of motion for the fabricated laminated glass.

In this study, the laminated glass is considered as simply supported. So the boundary conditions are

$$w = 0, \quad w_{xx} = 0, \qquad \text{at } x = 0, a \tag{4.18}$$

$$w = 0, \quad w_{yy} = 0, \qquad \text{at } y = 0, b$$

The initial condition is

$$w = 0, \quad \dot{w} = 0, \qquad \text{at } t = 0 \tag{4.19}$$

where a is the length of the laminated glass, which is 0.89 m and b is the width of the laminated glass, which is 0.59 m.

Based on the boundary conditions, the following deflection mode shape is assumed [6, 7],

$$w(x, y, t) = \sum_{m=1}^{\infty}\sum_{n=1}^{\infty}\varphi(t)\sin\left(\frac{\pi x}{a}\right)\sin\left(\frac{\pi y}{b}\right) \tag{4.20}$$

where $\varphi(t)$ is an unknown function. For simplicity, equation (4.20) is approximated to its first term. Substituting equation (4.20) into equation (4.17) results in

$$N\phi_{yyyy} + N\phi_{xxxx} + P\phi_{xxyy} = \frac{\varphi^2\pi^4}{2a^2b^2}\left(\cos\left(\frac{2\pi x}{a}\right) + \cos\left(\frac{2\pi y}{b}\right)\right) \tag{4.21}$$

The solution for this equation can be assumed as [6]

$$\phi = \frac{1}{N}\varphi^2\left[f_1\cos\left(\frac{2\pi x}{a}\right) + f_2\cos\left(\frac{2\pi y}{b}\right)\right] \tag{4.22}$$

Substituting equation (4.22) into the left part of equation (4.21) results in

$$N\phi_{yyyy} + N\phi_{xxxx} + P\phi_{xxyy} = \varphi^2\left(f_1\frac{16\pi^4}{a^4}\cos\left(\frac{2\pi x}{a}\right) + f_2\frac{16\pi^4}{b^4}\cos\left(\frac{2\pi y}{b}\right)\right) \tag{4.23}$$

Therefore, equation (4.21) can be rewritten as

$$\varphi^2\left(f_1\frac{16\pi^4}{a^4}\cos\left(\frac{2\pi x}{a}\right)+f_2\frac{16\pi^4}{b^4}\cos\left(\frac{2\pi y}{b}\right)\right)=\frac{\varphi^2\pi^4}{2a^2b^2}\left(\cos\left(\frac{2\pi x}{a}\right)+\cos\left(\frac{2\pi y}{b}\right)\right) \quad (4.24)$$

From equation (4.24), it can be inferred that $f_1=\frac{a^2}{32b^2}$ and $f_2=\frac{b^2}{32a^2}$, so the solution for equation (4.24) is obtained. Introducing the solution and equation (4.20) into equation (4.14) and applying Galerkin method to equation (4.14), the nonlinear partial differential equation (4.14) is changed to a nonlinear ordinary differential equation with respect to time

$$\frac{abm}{4}\ddot{\varphi}-\frac{4abP_o}{\pi^2}\left(1-\frac{t}{t_p}\right)e^{-\frac{\alpha t}{t_p}}+\frac{\pi^4\varphi\left(Da^4+Fa^2b^2+Db^4\right)}{4a^3b^3}+\frac{\pi^4\varphi^3h\left(a^4+b^4\right)}{64a^3b^3N}=0 \quad (4.25)$$

where $\ddot{\varphi}$ is the second-order derivative of φ with respect to time. Equation (4.25) can be solved using MATLAB. After obtaining the function φ, the transverse deflection *w* can be calculated using equation (4.20).

Besides the transverse deflection, the principal stresses of the laminated glass under blast loading can also be obtained through this model by the following procedures:

1) After obtaining the transverse deflection, since the strain-displacement relationships are known from equations (4.1)-(4.3), so the strains of the laminated glass can be calculated (ignore the displacements in x and y directions).

2) According to the stress-strain relationships of the laminated glass [6, 8], the bending stresses of the laminated glass can be calculated. The membrane stresses of the laminated glass can be calculated using Airy's stress function [9].

3) By adding the bending and membrane stresses together, the total stresses of the laminated glass are obtained

$$\sigma_x = \frac{E_{avg}}{1-v_{avg}^2}\left(\frac{1}{2}\left(\frac{\partial w}{\partial x}\right)^2 - z\left(\frac{\partial^2 w}{\partial x^2}\right) + v_{avg}\left(\frac{1}{2}\left(\frac{\partial w}{\partial y}\right)^2 - z\frac{\partial^2 w}{\partial y^2}\right)\right) + \frac{\partial^2 \phi}{\partial y^2} \tag{4.26}$$

$$\sigma_y = \frac{E_{avg}}{1-v_{avg}^2}\left(v_{avg}\left(\frac{1}{2}\left(\frac{\partial w}{\partial x}\right)^2 - z\left(\frac{\partial^2 w}{\partial x^2}\right)\right) + \frac{1}{2}\left(\frac{\partial w}{\partial y}\right)^2 - z\frac{\partial^2 w}{\partial y^2}\right) + \frac{\partial^2 \phi}{\partial x^2}$$

$$\tau_{xy} = G_{avg}\left(\frac{\partial w}{\partial x}\frac{\partial w}{\partial y} - 2z\frac{\partial^2 w}{\partial x \partial y}\right) - \frac{\partial^2 \phi}{\partial x \partial y}$$

where E_{avg}, v_{avg} and G_{avg} are the average Young's modulus, Poisson's ratio and shear modulus of the laminated glass, respectively.

4) The principal stresses of the laminated glass can be calculated based on the total stresses.

4.2.2 Finite element modeling

In this research, the dynamic response of the laminated glass is also studied using the finite element software ANSYS. The laminated glass is discretized by the four-node shell element SHELL181. 280 elements are used for discretization.

SHELL181 element is suitable for analyzing thin to moderately shell structures, including composite shells and sandwich constructions [10, 11].

The following figure shows the geometry of this element.

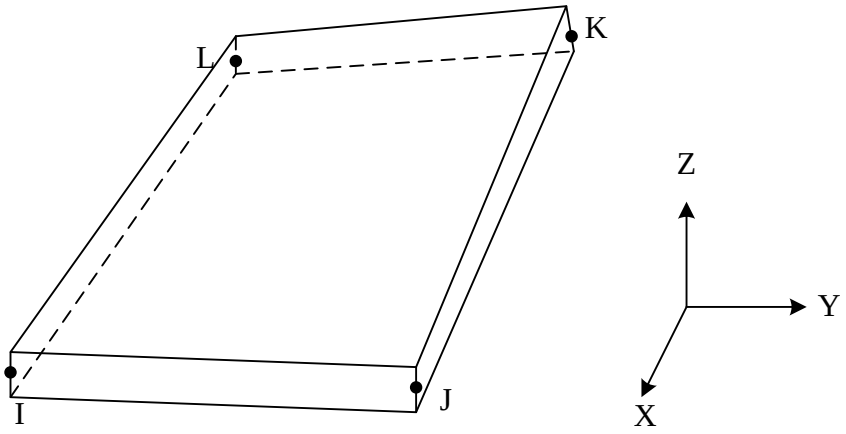

Figure 4.2 SHELL181 geometry [10]
(I, J, K and L are nodes)

The shell section commands of the SHELL181 element allow for sandwich structure definition. Options are available for specifying the thickness, material, orientation and number of integration points through the thickness of sandwich structure layers (Fig. 4.3).

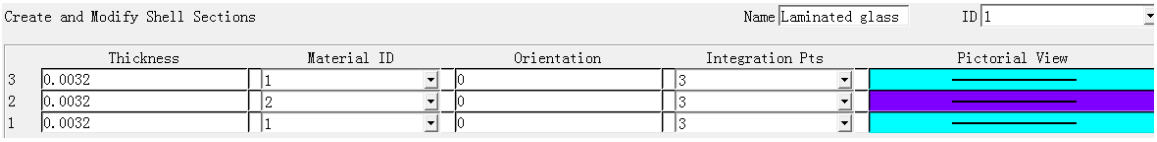

Figure 4.3 Shell section page

Materials properties obtained from mechanical tests and blast constants (P_o, α and t_p) obtained from blast curve fitting are used as inputs in the finite element modeling.

4.3 Results and discussions

4.3.1 Midpoint deflection

The dynamic response, in terms of the midpoint deflection, of the laminated glass under the medium intensity blast loading is predicted using the new numerical mode and the finite element model, respectively. The experimentally measured result is compared with the numerical modeling result and the finite element modeling result (Fig. 4.4). From this figure, it can be seen that both the numerical modeling result and the finite element modeling result match well with the experimentally measured result, especially in predicting the peak deflection. However, the discrepancy is more apparent during the unloading phase. The discrepancy between the experimentally measured result and the analytically predicted results (finite element modeling result and numerically modeling result) may be caused by the neglect of the composite interlayer's plastic deformation and the strain rate effect on mechanical properties in the modeling.

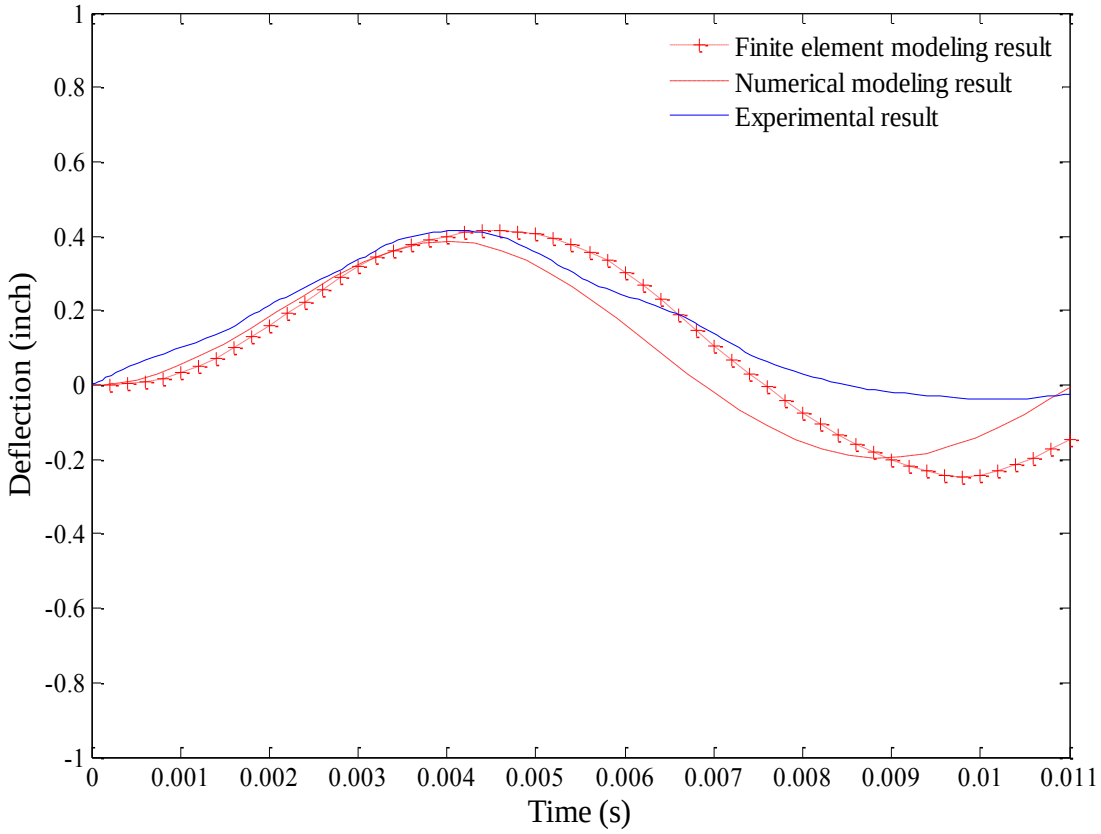

Figure 4.4 Midpoint deflection comparison

Since both the numerical model and the finite element model can describe the dynamic response of the laminated glass, both models are used to study the midpoint maximum principal stress history of the laminated glass as it is an important criterion for determining whether a laminated glass fails when subjected to a blast loading [6].

4.3.2 Midpoint maximum principal stress history

Fig. 4.5 and Fig. 4.6 demonstrate the midpoint maximum principal stress history of the inner glass surface (pressure impact surface) and outer glass surface (pressure non-

impact surface), respectively. The blue line in these figures represents the finite element model calculated result and the red line represents the numerical model calculated result. From Fig. 4.5, it can be observed that for the inner glass surface, the maximum compression stresses calculated using the finite element model and the new numerical model are close and approximately 45 MPa. But the calculated maximum tensile stresses are a little different. The result calculated using the finite element model is around 60 MPa and the result calculated using the numerical model is around 45 MPa. From Fig. 4.6, it can be observed that for the outer glass surface, the maximum tensile stress calculated using the finite element model is around 105 MPa and the tensile stress calculated using the numerical model is around 95 MPa. The maximum compression stress calculated using the finite element method is around 45 MPa and the compression stress calculated using the numerical model is around 25 MPa. On the whole, the numerical modeling results match with the basic variation of the finite element modeling results. However, there is a variation of about 10-20% in the prediction of the peak principle stress values between the two methods. Since the tensile strength of tempered glass is usually higher than 175 MPa and its compressive strength is much higher than its tensile strength [12-15], the fabricated laminated glass is expected to survive when subjected to the medium intensity blast loading. This has been proven by the field testing result.

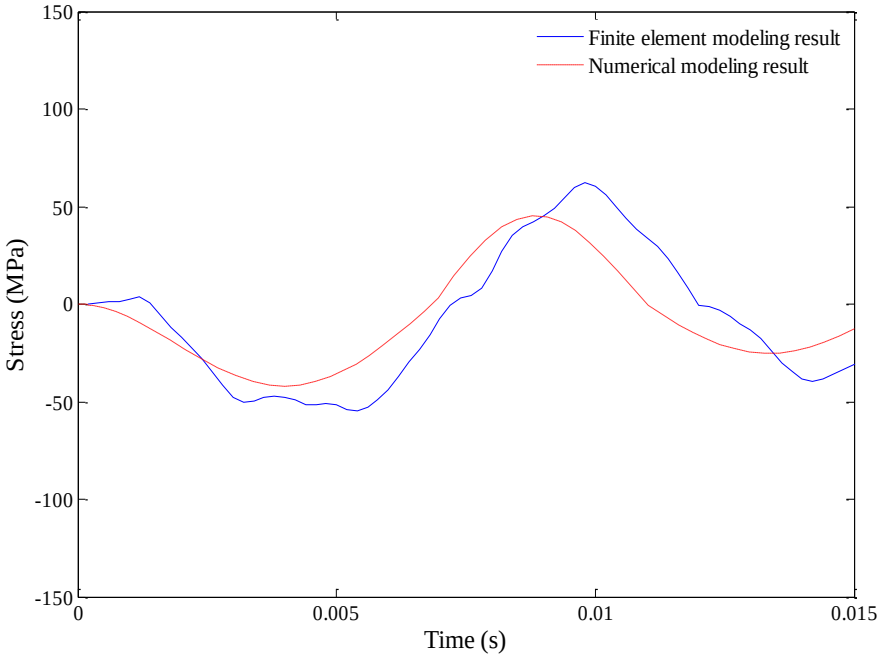

Figure 4.5 Midpoint maximum principal stress history of the inner glass surface

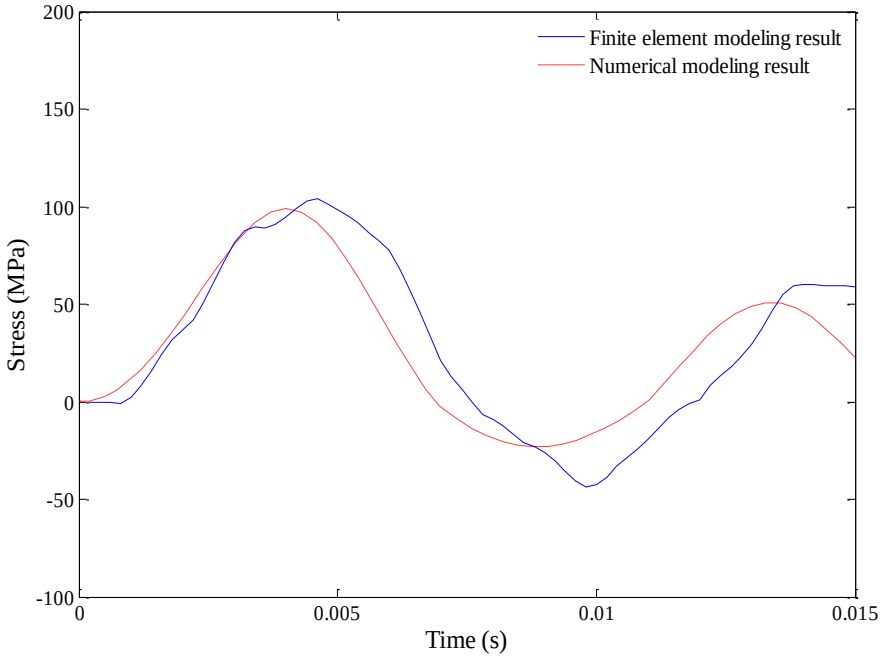

Figure 4.6 Midpoint maximum principal stress history of the outer glass surface

The midpoint deflection and maximum principle stresses of the laminated glass with PVB interlayer can also be predicted using the new numerical model and the finite element model by setting the interlayer properties to the properties of PVB. Young's modulus and Poisson's ratio of PVB are 100 MPa and 0.448, respectively [16]. When subjected to the medium intensity blast loading used in this chapter, the midpoint deflections of the laminated glass with the composite interlayer and the laminated glass with PVB interlayer are plotted in Fig. 4.7 (results obtained from the new numerical model. Results obtained from the finite element model are similar, so not shown here). From Fig. 4.7, it can be observed that compared with the same configuration laminated glass with the composite interlayer, the maximum deflection of the laminated glass with PVB interlayer is larger. The midpoint maximum principal stresses of the inner surface and the outer surface are plotted in Fig. 4.8 and Fig. 4.9, respectively. These figures demonstrate that the midpoint maximum principal stresses (inner surface and outer surface) of the laminated glass with PVB interlayer are larger than those of the laminated glass with the composite interlayer. These results means the laminated glass with PVB interlayer is more likely to fail when both laminated glasses subjected to the same intensity blast loading.

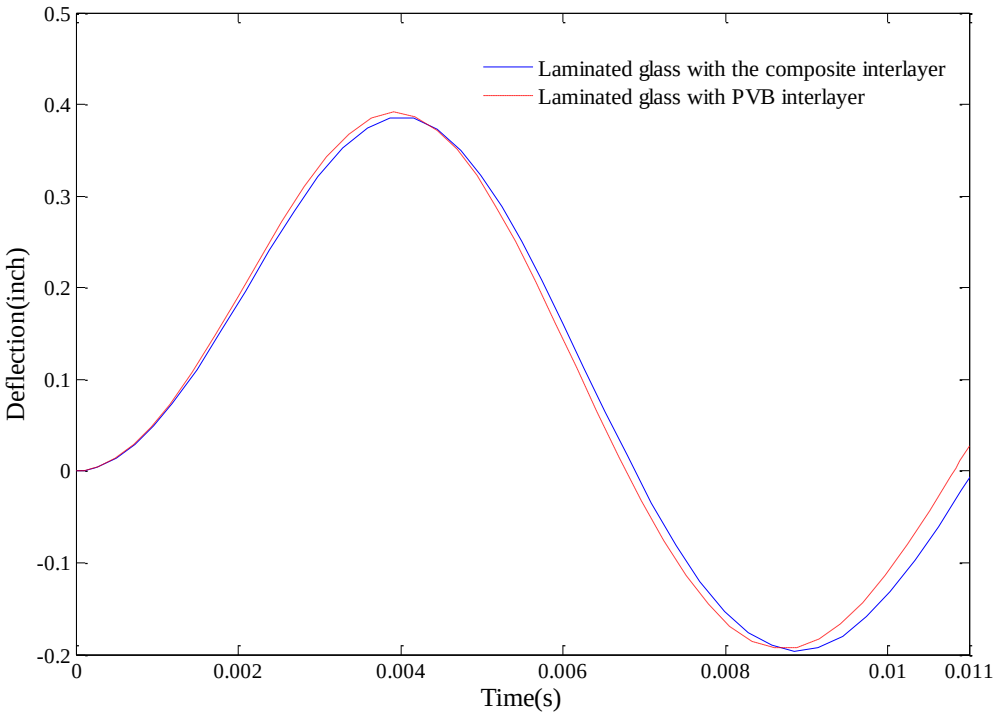

Figure 4.7 Comparison of midpoint deflections under the medium intensity blast loading

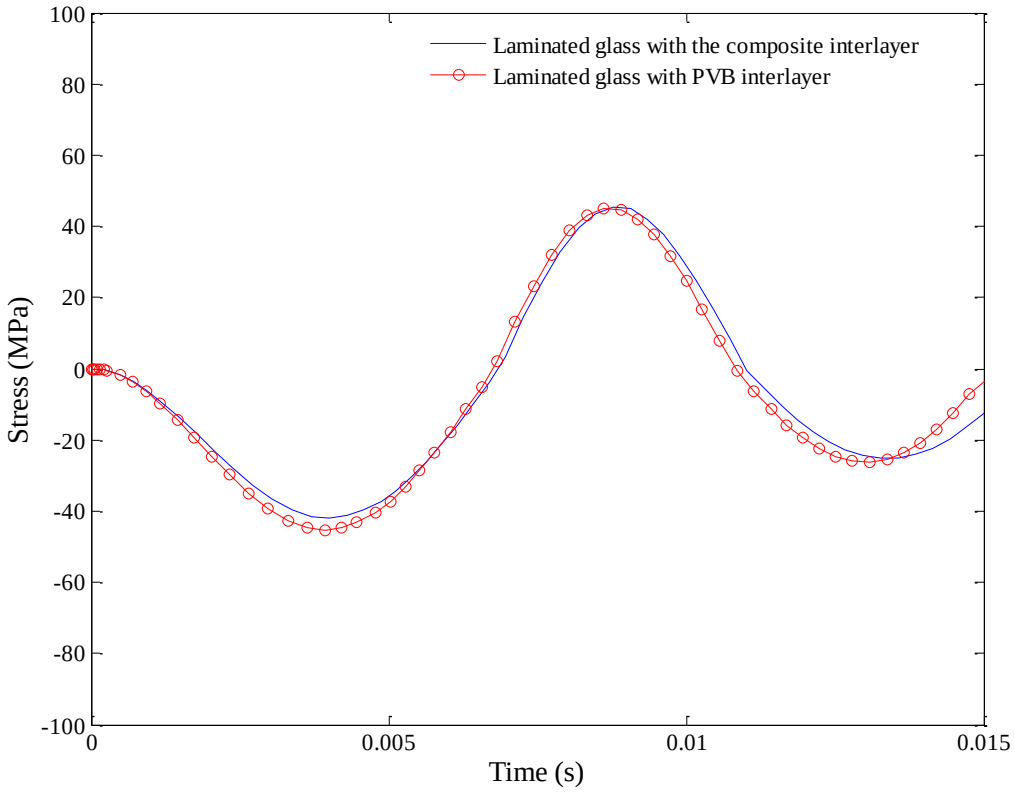

Figure 4.8 Comparison of midpoint maximum principal stresses (inner surface)

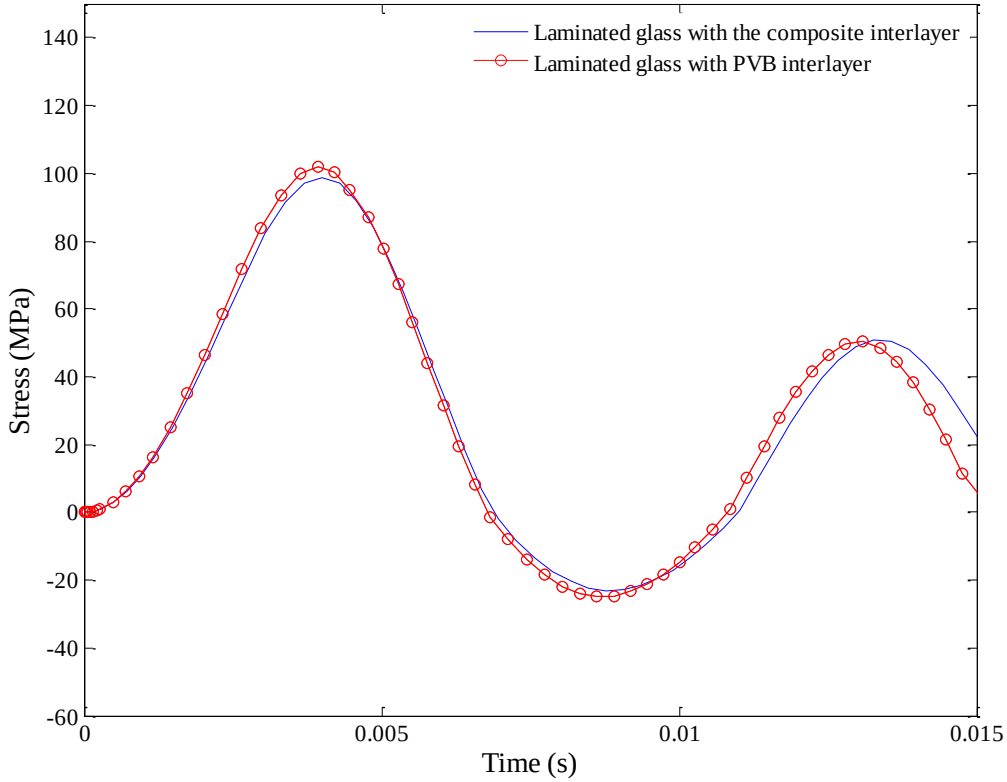

Figure 4.9 Comparison of midpoint maximum principal stresses (outer surface)

4.4 Summary

The dynamic response of the fabricated laminated glass under a medium intensity blast loading is studied using a new numerical model and a finite element model. The predicted result, either using the numerical model or the finite element model, agrees well with experimentally measured result.

Stress analysis shows the fabricated laminated glass can survive when subjected to the medium intensity blast loading. This has been proven by the field experimental result. Dynamic response analysis and stress analysis both show that under the same intensity

blast, the laminated glass with fiber-reinforced composite interlayer performs better than the same configuration laminated glass with PVB interlayer. In other words, to reach the same protection effect, the laminated glass with the composite interlayer can be fabricated thinner and lighter.

REFERENCES

[1] Kazancı Z., 2011, "*Dynamic response of composite sandwich plates subjected to time-dependent pressure pulses*", International Journal of Non-Linear Mechanics, **46**, No.5, pp.807-817.

[2] Kazanci, Z., and Mecitoglu, Z., 2006, "*Nonlinear damped vibrations of a laminated composite plate subjected to blast load*", AIAA Journal, **44**, No.9, pp.2002-2008.

[3] Nishawala, V., 2011, "*A study of large deflection of beams and plates*", New Brunswich, NJ: Rutgers University.

[4] Riber, H.J., 1997, "*Non-linear analytical solutions for laterally loaded sandwich plates*", Composite Structures, **39**, No.1, pp.63-83.

[5] Ugural, A.C., 1981, "*Stresses in plates and shells*", New York, NY: McGraw-Hill.

[6] Wei, J., and Dharani, L.R., 2006, "*Response of laminated architectural glazing subjected to blast loading*", International Journal of Impact Engineering, **32**, No.12, pp.2032-2047.

[7] Teng, T.L., Liang, C.C., and Liao, C.C., 1996, "*Transient dynamic large-deflection analysis of panel structure under blast loading*", JSME International Journal Series A, Mechanics and Material Engineering, **39**, No.4, pp.591-597.

[8] Vinson, J.R., 1999, "*The behavior of sandwich structures of isotropic and composite materials*", Lancaster, PA: Technomic Publishing Company.

[9] Brubak, L., Hellesland, J., Steen, E., and Byklum, E., 2004, "*Approximate buckling strength analysis of plates with arbitrarily oriented stiffeners*", Proceedings of the 17th Nordic Seminar on Computational Mechanics (NSCM-17), pp.50-53.

[10] ANSYS, "*ANSYS Help*", Canonsburg, PA: ANSYS.

[11] ANSYS, "*SHELL181*", http://mostreal.sk/html/elem_55/chapter4/ES4-181.htm.

[12] Kalluri, R.S., 2007, "*Failure of transparent polymer composite laminated glass panels under impact loading*", Columbia, MO: University of Missouri.

[13] Mencik, J., 1992, "*Strength and fracture of glass and ceramics*", New York, NY: Elsevier.

[14] Veer, F., Zuidema, J., Bos, F., and Romein, T., 2005, "*The strength and fracture behaviour of annealed and tempered float glass*", Proceedings of the 9th International Conference on Architectural and Automotive Glass (GPD), pp.1-6.

[15] National Glass, "*Glass Manufacture*", http://www.nationalglass.com.au/catalogues/NGP_Section_20.pdf.

[16] Bennison, S.J., Qin, M.H., and Davies, P.S., 2008, "*High-performance laminated glass for structurally efficient glazing*", Innovative Light-Weight Structures and Sustainable Facades, pp.1-12.

CHAPTER 5 CONCLUSIONS AND FUTURE WORK

In this research, a transparent glass fiber-reinforced polyester composite has been developed. The transparent glass fiber-reinforced composite was fabricated by matching the refractive index of the polyester matrix with that of glass fibers. The light transmittance of the composite varies with light wavelength and can reach up to a maximum of 74.5% for a wavelength of 600 nm. Different tests have been used to determine the properties of the composite. Tensile test was used to find Young's modulus, Poisson's ratio and Shear modulus. J-integral test was used to find the fracture toughness.

The transparent composite developed was used to fabricate a novel blast-resistant laminated glass. The dynamic response of the fabricated laminated glass under blast loading was tested using a Blast Load Simulator. The dynamic response is also analytically investigated using model-based method and finite element method. The model-based analysis is conducted based on two numerical models. The equations of motion of two models are partial differential equations. In order to solve these equations, Galerkin method is used to change these equations to nonlinear ordinary differential equations and these nonlinear ordinary differential equations are solved using Runge-Kutta method in MATLAB. After obtaining the solutions of these equations, the dynamic response of the fabricated laminated glass is characterized. The finite element analysis is performed using the commercial finite element software ANSYS. The analytically calculated results (results obtained from the model-based analysis and the finite element

analysis) are compared with the experimentally measured results. Comparison results show that analytically calculated results match well with the experimentally measured results, which proves the validity of the developed numerical models and the finite element model. Stress analysis of the fabricated laminated glass shows that a 3/8 inch thick laminated glass panel can survive when subjected to both medium and high intensity blast loading and compared with the same configuration laminated glass with PVB interlayer, it has better blast resistance.

To sum up, a novel laminated glass has been fabricated. The dynamic response of the fabricated laminated glass under blast loading has been investigated. Though a lot of work has been devoted to the fabrication and study of this laminated glass, this laminated glass could be further improved through some modifications and further study as suggested below:

1) More transparent composite interlayer. Though the developed glass fiber-reinforced composite interlayer has good transparency, the transparency of the composite interlayer can be further increased, like increasing to more than 80% at any wavelength in the visible light region. One possible way to further increase the transparency of the composite interlayer is to find new chemical additives to further reduce the refractive index difference between glass fibers and the polyester matrix.

2) Better laminated glass fabrication method. Presently, the laminated glass panels are fabricated using the hand lay-up technique. This technique is the simplest one to fabricate the laminated glass. This technique requires minimal investment in molds but is not suitable for mass production. Also this technique may introduce air bubbles at the

interfaces between the composite interlayer and glass sheets during lamination, which can reduce the transparency of the laminated glass. Therefore, a better technique is needed for the potential mass production.

3) More precise numerical model. The numerical models developed are good for predicting the dynamic response of the fabricated laminated glass under blast loading. But there are still gaps between the experimentally measured results and the predicted results. The discrepancy may be caused by the neglect of the composite interlayer's plastic deformation and the strain rate effect on mechanical properties in the modeling. If the plastic deformation and the strain rate effect are considered in the modeling, a more precise numerical model can be established and thereby, the dynamic response of the laminated glass under blast loading can be predicted more precisely.

APPENDIX A

The procedures for converting equation (3.11) to a second-order ordinary differential equation are shown below

$$M\ddot{w} + A\left(w_{xxxx} + w_{yyyy}\right) + \left(B + C\right) w_{xxyy} = P\left(t\right) \tag{A.1}$$

$$P\left(t\right) = P_o\left(1\text{-}t/t_p\right)\mathrm{e}^{-\alpha t/t_p}$$

where M is the unit area mass of the laminated glass, *A*, *B* and *C* are constants, P_o is the peak pressure of a blast loading, α is a constant and t_p is the positive pressure duration time of the blast. By using double Fourier expansion, P_o can be expanded as $\sum_{m=1}^{\infty}\sum_{n=1}^{\infty} P_{mn} \sin\left(\frac{m\pi x}{a}\right)\sin\left(\frac{n\pi y}{b}\right)$, where P_{mn} is an unknown function, *m* and *n* are positive integers, *a* and *b* are the length and width of the laminated glass, respectively [1]. Similarly, *w*, which is the thickness direction displacement component, can be expanded as $\sum_{m=1}^{\infty}\sum_{n=1}^{\infty} W_{mn}\left(t\right)\sin\left(\frac{m\pi x}{a}\right)\sin\left(\frac{n\pi y}{b}\right)$, where $W_{mn}\left(t\right)$ is an unknown time function. Therefore,

$$w_{xxxx} = \left(\frac{m\pi}{a}\right)^4 \sum_{m=1}^{\infty}\sum_{n=1}^{\infty} W_{mn}\left(t\right)\sin\left(\frac{m\pi x}{a}\right)\sin\left(\frac{n\pi y}{b}\right)$$

$$w_{yyyy} = \left(\frac{n\pi}{b}\right)^4 \sum_{m=1}^{\infty}\sum_{n=1}^{\infty} W_{mn}\left(t\right)\sin\left(\frac{m\pi x}{a}\right)\sin\left(\frac{n\pi y}{b}\right)$$

$$w_{xxyy} = \left(\frac{m\pi}{a}\right)^2\left(\frac{n\pi}{b}\right)^2 \sum_{m=1}^{\infty}\sum_{n=1}^{\infty} W_{mn}\left(t\right)\sin\left(\frac{m\pi x}{a}\right)\sin\left(\frac{n\pi y}{b}\right)$$

$$\ddot{w} = \sum_{m=1}^{\infty}\sum_{n=1}^{\infty} W_{mn}^{"}\left(t\right)\sin\left(\frac{m\pi x}{a}\right)\sin\left(\frac{n\pi y}{b}\right)$$

where $W_{mn}^{"}(t)$ is the second-order derivative of $W_{mn}(t)$ in respect of time *t*.

Substitute $P_o, w_{xxxx}, w_{yyyy}, w_{xxyy}, \ddot{w}$ into equation (A.1), equation (A.1) can be rewritten as

$$M\left\{\sum_{m=1}^{\infty}\sum_{n=1}^{\infty}W_{mn}^{"}(t)\sin\left(\frac{m\pi x}{a}\right)\sin\left(\frac{n\pi y}{b}\right)\right\}+\left\{A\left(\frac{m\pi}{a}\right)^4\sum_{m=1}^{\infty}\sum_{n=1}^{\infty}W_{mn}(t)\sin\left(\frac{m\pi x}{a}\right)\sin\left(\frac{n\pi y}{b}\right)\right\}$$

$$+\left\{A\left(\frac{n\pi}{b}\right)^4\sum_{m=1}^{\infty}\sum_{n=1}^{\infty}W_{mn}(t)\sin\left(\frac{m\pi x}{a}\right)\sin\left(\frac{n\pi y}{b}\right)\right\} \quad \text{(A.2)}$$

$$+\left\{(B+C)\left(\frac{m\pi}{a}\right)^2\left(\frac{n\pi}{b}\right)^2\sum_{m=1}^{\infty}\sum_{n=1}^{\infty}W_{mn}(t)\sin\left(\frac{m\pi x}{a}\right)\sin\left(\frac{n\pi y}{b}\right)\right\}$$

$$=\left\{\sum_{m=1}^{\infty}\sum_{n=1}^{\infty}P_{mn}\sin\left(\frac{m\pi x}{a}\right)\sin\left(\frac{n\pi y}{b}\right)\right\}\left(1-\frac{t}{t_p}\right)e^{-\alpha t/t_p}$$

Simplify equation (A.2) and get

$$\left\{A\left(\frac{m\pi}{a}\right)^4+(B+C)\left(\frac{m\pi}{a}\right)^2\left(\frac{n\pi}{b}\right)^2+A\left(\frac{n\pi}{b}\right)^4\right\}W_{mn}(t)+MW_{mn}^{"}(t)=P_{mn}\left(1-\frac{t}{t_p}\right)e^{-\alpha t/t_p} \quad \text{(A.3)}$$

Let $J=A\left(\frac{m\pi}{a}\right)^4+(B+C)\left(\frac{m\pi}{a}\right)^2\left(\frac{n\pi}{b}\right)^2+A\left(\frac{n\pi}{b}\right)^4$

Equation (A.3) can be rewritten as,

$$JW_{mn}(t)+MW_{mn}^{"}(t)=P_{mn}\left(1-\frac{t}{t_p}\right)e^{-\alpha t/t_p} \quad \text{(A.4)}$$

In equation (A.4), P_{mn} is the only unknown coefficient. If the value of P_{mn} can be obtained, equation (A.4) can be solved using Euler's method. The unknown coefficient P_{mn} can be obtained through following procedures proposed by Timoshenko [1, 2]:

Since,

$$P_o = \sum_{m=1}^{\infty}\sum_{n=1}^{\infty} P_{mn} \sin\left(\frac{m\pi x}{a}\right)\sin\left(\frac{n\pi y}{b}\right)$$

Multiply each side of above equation by $\int_0^b \sin\frac{n_0\pi y}{b}$ where n_0 is an arbitrary integer, obtains

$$\int_0^b P_o \sin\frac{n_0\pi y}{b}\,dy = \sum_{m=1}^{\infty}\sum_{n=1}^{\infty} P_{mn} \sin\frac{m\pi x}{a}\int_0^b \sin\frac{n_0\pi y}{b}\sin\frac{n\pi y}{b}\,dy \qquad \text{(A.5)}$$

According to identity principle [1],

$$\int_0^b \sin\frac{n_0\pi y}{b}\sin\frac{n\pi y}{b}dy = \begin{cases} 0 & \text{if } n \neq n_0 \\ \dfrac{b}{2} & \text{if } n=n_0 \end{cases}$$

So,

$$\sum_{n=1}^{\infty}\int_0^b \sin\frac{n_0\pi y}{b}\sin\frac{n\pi y}{b}\,dy = \frac{b}{2}$$

Equation (A.5) can be rewritten as

$$\int_0^b P_o \sin\frac{n_0\pi y}{b}\,dy = \frac{b}{2}\sum_{m=1}^{\infty} P_{mn} \sin\frac{m\pi x}{a} \qquad \text{(A.6)}$$

Similarly, multiply equation (A.6) by $\int_0^a \sin\frac{m_0\pi x}{a}$, where m_0 is an arbitrary integer number, obtains

$$\int_0^a P_o \sin\frac{m_0\pi x}{a}dx\int_0^b \sin\frac{n_0\pi y}{b}dy = \frac{b}{2}\sum_{m=1}^{\infty} P_{mn}\int_0^a \sin\frac{m\pi x}{a}\sin\frac{m_0\pi x}{a}dx \qquad \text{(A.7)}$$

Still according to the identity principle,

$$\int_0^a \sin\frac{m_0\pi x}{a}\sin\frac{m\pi x}{a}dx = \begin{cases} 0 & \text{if } m \neq m_0 \\ \frac{a}{2} & \text{if } m=m_0 \end{cases}$$

So,

$$\int_0^a P_o \sin\frac{m_0\pi x}{a}dx\int_0^b \sin\frac{n_0\pi y}{b}dy = \frac{ab}{4}P_{mn} \qquad \text{(A.8)}$$

P_{mn} can be expressed as

$$P_{mn} = \frac{4}{ab}\int_0^a \sin\frac{m\pi x}{a}dx\int_0^b P_o \sin\frac{n\pi y}{b}dy \qquad \text{(A.9)}$$

Integrate equation (A.9) and get the value of P_{mn}

$$P_{mn}=\frac{4}{ab}\int_0^a \sin\left(\frac{m\pi x}{a}\right)dx\int_0^b P_o \sin\left(\frac{n\pi y}{b}\right)dy=\frac{4P_o}{ab}\int_0^a\left\{\left[\sin\left(\frac{m\pi x}{a}\right)dx\right]\frac{b}{n\pi}\int_0^b \sin\left(\frac{n\pi y}{b}\right)d\frac{n\pi y}{b}\right\}$$

$$=\frac{4P_o}{ab}\int_0^a\left\{\left[\sin\left(\frac{m\pi x}{a}\right)dx\right]\left(-\frac{b}{n\pi}\left[\cos\left(\frac{n\pi y}{b}\right)\right]_0^b\right)\right\}=\frac{4P_o}{ab}\int_0^a\left\{-\frac{b}{n\pi}\sin\left(\frac{m\pi x}{a}\right)\left[\cos(n\pi)-1\right]\right\}$$

$$=\frac{8P_o b}{abn\pi}\int_0^a \sin\frac{m\pi x}{a}dx=\frac{8P_o b}{abn\pi}\left[\frac{a}{m\pi}\int_0^a \sin\frac{m\pi x}{a}d\frac{m\pi x}{a}\right]=\frac{8P_o}{nm\pi^2}\left[-\cos(\frac{m\pi x}{a})\right]_0^a=\frac{16P_o}{nm\pi^2}$$

when *m*, *n*=1, 3, 5....

Substitute the value of P_{mn} into equation (A.4),

$$JW_{mn}(t)+MW_{mn}^{"}(t)=\frac{16P_o}{nm\pi^2}\left(1-\frac{t}{t_p}\right)e^{-\alpha t/t_p} \qquad \text{(A.10)}$$

As mentioned previously, equation (A.10) can be solved using Euler's method. After getting the values of time function $W_{mn}(t)$, *w*, the thickness direction displacement component, can be calculated using the equation $\sum_{m=1}^{\infty}\sum_{n=1}^{\infty}W_{mn}(t)\sin\left(\frac{m\pi x}{a}\right)\sin\left(\frac{n\pi y}{b}\right)$.

REFERENCES

[1] Auburn University, "*Plates Subjected to Transverse Loads*".

[2] Timoshenko, S., Woinowsky, K.S., and Woinowsky, S., 1959, "*Theory of plates and shells*", New York, NY: McGraw-Hill.

VITA

Hua Zhu was born on November 9th, 1982 in Yantai, Shandong, China. He got his Bachelor's degree in Polymer Science and Engineering from Yantai University (Yantai, China) in 2005. After that, he studied at Nanjing University of Technology (Nanjing, China), where he graduated with his Master's degree in Materials Science in 2008. At the same year, he came to the United States and studied at University of Massachusetts-Lowell for one year. Then he transferred to University of Missouri-Columbia and started his Ph.D. study under the supervision of Dr. Sanjeev K. Khanna. He is married to Tianyi Qiu, who is studying physiology in Physiology and Pharmacology Department at University of Missouri-Columbia.